University of Tennessee, Knoxville
Trace: Tennessee Research and Creative Exchange

Masters Theses | Graduate School

5-2008

Numerical Analysis of Piling Framed Tie-Down Concrete Retaining Wall

Eli L. Branch IV
University of Tennessee - Knoxville

Recommended Citation

Branch IV, Eli L., "Numerical Analysis of Piling Framed Tie-Down Concrete Retaining Wall. " Master's Thesis, University of Tennessee, 2008.
https://trace.tennessee.edu/utk_gradthes/336

This Thesis is brought to you for free and open access by the Graduate School at Trace: Tennessee Research and Creative Exchange. It has been accepted for inclusion in Masters Theses by an authorized administrator of Trace: Tennessee Research and Creative Exchange. For more information, please contact trace@utk.edu.

To the Graduate Council:

I am submitting herewith a thesis written by Eli L. Branch IV entitled "Numerical Analysis of Piling Framed Tie-Down Concrete Retaining Wall." I have examined the final electronic copy of this thesis for form and content and recommend that it be accepted in partial fulfillment of the requirements for the degree of Master of Science, with a major in Civil Engineering.

Richard Bennett, Major Professor

We have read this thesis and recommend its acceptance:

Eric Drumm, Edwin Burdette

Accepted for the Council:
Dixie L. Thompson

Vice Provost and Dean of the Graduate School

(Original signatures are on file with official student records.)

To the Graduate Council:

I am submitting herewith a thesis written by Eli Lawrence Branch IV entitled "Numerical Analysis of Piling Framed Tie-Down Concrete Retaining Wall." I have examined the final electronic copy of this thesis for form and content and recommend that it be accepted in partial fulfillment of the requirements for the degree of Master of Science, with a major in Civil Engineering.

Dr. Richard Bennett, Major Professor

_____

We have read this thesis and recommend its acceptance:

Dr. Eric Drumm

_____

Dr. Edwin Burdette

_____

Accepted for the Council:

Carolyn R. Hodges, Vice Provost and
Dean of the Graduate School

_____

(Original signatures are on file with official student records)

Numerical Analysis of Piling Framed Tie-Down Concrete Retaining Wall

A Thesis Presented for the

Master of Science Degree in Civil Engineering

The University of Tennessee, Knoxville

Eli Lawrence Branch IV

May 2008

Copyright © 2008 by Eli L. Branch IV

All rights reserved.

ACKNOWLEDGEMENTS

I would like to express my sincere gratitude to Dr. Eric Drumm and Dr. Richard Bennett for their assistance as my graduate advisors. Dr. Drumm has made considerable contributions to this research particularly in the geotechnical aspects of the project and through the writing process. Dr. Bennett initially recruited me for this project, so without him I would not have been a part of this research. I would also like to thank Dr. Edwin Burdette for assistance in reviewing the text along with Dr. Drumm and Dr. Bennett.

In addition, I would like to thank Nikola Zisi and Feng Chen as well as Dr. Drumm and Dr. Bennett for helping me learn to use ADINA. Their suggestions and assistance is greatly appreciated.

I wish to thank my family for their support and encouragement during my studies. I also want to thank all my friends especially Wes Macdonald and Qiao Dong, who have been great friends through it all.

Most importantly, I would like to thank the Graduate College for awarding me the Black Graduate Fellowship and the Institute for Geotechnology which funded portions of my graduate studies and this research.

ABSTRACT

The behavior of a novel pile framed retaining wall developed by the Tennessee Department of Transportation (TDOT) is investigated using a 2D non-linear finite element (FE) analysis for. The wall design eliminates the need for a construction right of way behind the wall; thus it is ideal for urban areas. The design concept consists of vertical and battered H pile sections as the structural frame, and a concrete facing that is installed as the soil is excavated during top-down construction. Vertical tie-down anchors and a concrete cap and facing are used to counteract overturning moments. A 2-D FE analysis of the wall system was conducted to understand how the earth pressures are applied to the sloped wall, and how the loads are distributed throughout the piling frame. An increased understanding of the performance of this new system will lead to more economic pile sections and spacing under service loads. In addition, the construction sequence was modeled to investigate the non-linear response of the wall system. Parametric studies were conducted to investigate wall performance for different soil conditions, boundary conditions, wall heights, and tie-down forces. The results show that active earth pressures are adequate for design and that TDOT's original design was conservative.

TABLE OF CONTENTS

LIST OF TABLES

LIST OF FIGURES

Figure Page

CHAPTER I

INTRODUCTION AND LITERATURE REVIEW

1.1 Introduction

The construction of conventional retaining walls in urban settings is often difficult due to right-of-way restraints and/or cost restrictions. Conventional retaining walls include concrete cantilever walls, soldier piles with lagging, pile secant drilled cantilever walls, and walls using tie-back anchors for lateral support. Numerous authors have written on the subject of wall types and their construction (Macnab, 2002). Property adjacent to proposed walls is often unavailable or too expensive, prohibiting the construction of cantilever-type retaining walls which require ample space behind the wall for construction. Walls utilizing tie-backs anchors have the same restrictions but instead of above ground, they require underground easements behind the wall to avoid buried utilities or adjacent building foundations.

1.1.1 Wall System Description

To overcome the challenges of building traditional retaining walls in urban environments, the Tennessee Department of Transportation (TDOT) has developed a new concept for a retaining wall. The concept consists of battered and vertical piles as the structural frame of the wall, and vertical anchors to provide additional stability against overturning, (Pate

and Haddad, 2007). The battered and vertical piles are attached to a horizontal whaler the spans between frames in the longitudinal direction along the wall. After the frames are connected, two vertical tie-down anchors per frame, attached the horizontal whalers, are anchored to rock to hold down the wall against overturning. To complete the wall and transmit the soil forces to the frame, a concrete facing is poured spanning the frames so they act as a wall. In their paper, Pate and Haddad outline the details of the wall's design as well as a description of the construction of the first pile framed wall built in Knoxville, TN in 2005. Figure 1.1-1 is a photograph of the first implementation of the pile-framed wall system at the eastbound West Hills exit of I-40/I-75 in West Knoxville. Figure 1.1-2 shows a cross-section view of the pile framed wall system along with a 3D schematic of the framing system and anchors. .

Figure 1.1-1 Completed Pile Framed Wall (Pate and Haddad, 2007)

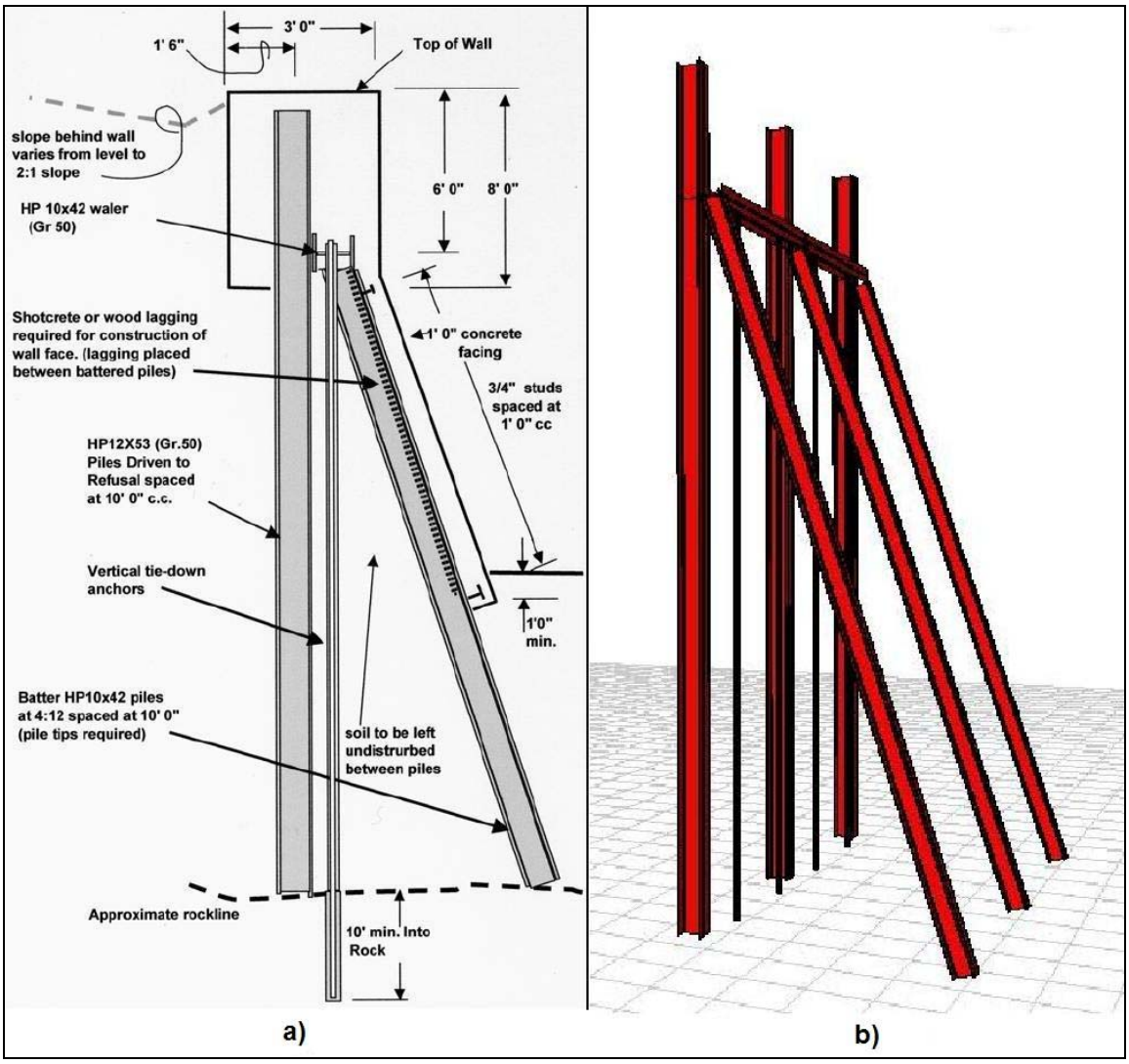

Figure 1.1-2 a) Cross Section of Wall (Pate and Haddad, 2007) b) 3D Schematic

The proximity of the adjacent buildings along the West Hills exit made this site an ideal application of the pile framed system because it is constructed from the top-down, avoiding excavation behind the wall. A cantilever-type wall was not suitable because it is built from the bottom-up, and a significant easement behind the proposed wall is excavated to the elevation of roadway grade. Then the wall is built, and the soil

backfilled to the desired height. Construction on the pile framed system begins by driving the piles, and then only the soil in front of the wall is excavated down to the elevation of roadway grade. The concrete facing and cap are poured to complete the wall. Figure 1.1-3 illustrates the difference between conventional walls and the pile framed system, and how existing buildings prevent the use of conventional walls. Table 1 provides a description of the construction sequence.

Table 1 Construction Sequence of Pile Framed Wall System

1	Excavate soil in preparation of pile driving
2	Drive battered HP 10x42 piles to refusal, cut and prepare end of piles for attachment to whaler
3	Drill and case 6 inch holes for tie-down anchors into competent rock
4	Install and attach HP 10x42 whaler to battered pile with welds
5	Drive vertical piles, cut tops to required elevation and attach whaler
6	Cut holes in web of whaler for tie-down anchors
7	Install, grout, and load test tie-down anchors (10 ft. minimum embedment in rock)
8	Excavate soil in 7 ft. lifts, place timber lagging between batter piles as excavation proceeds.
9	Clean top flange of battered piles and weld on shear studs
10	Place forms and reinforcing bars in both directions along batter face
11	Pour concrete facing full height
12	Place forms and reinforcing bars for concrete cap, then pour concrete
13	Reslope initially excavated soil at top of wall

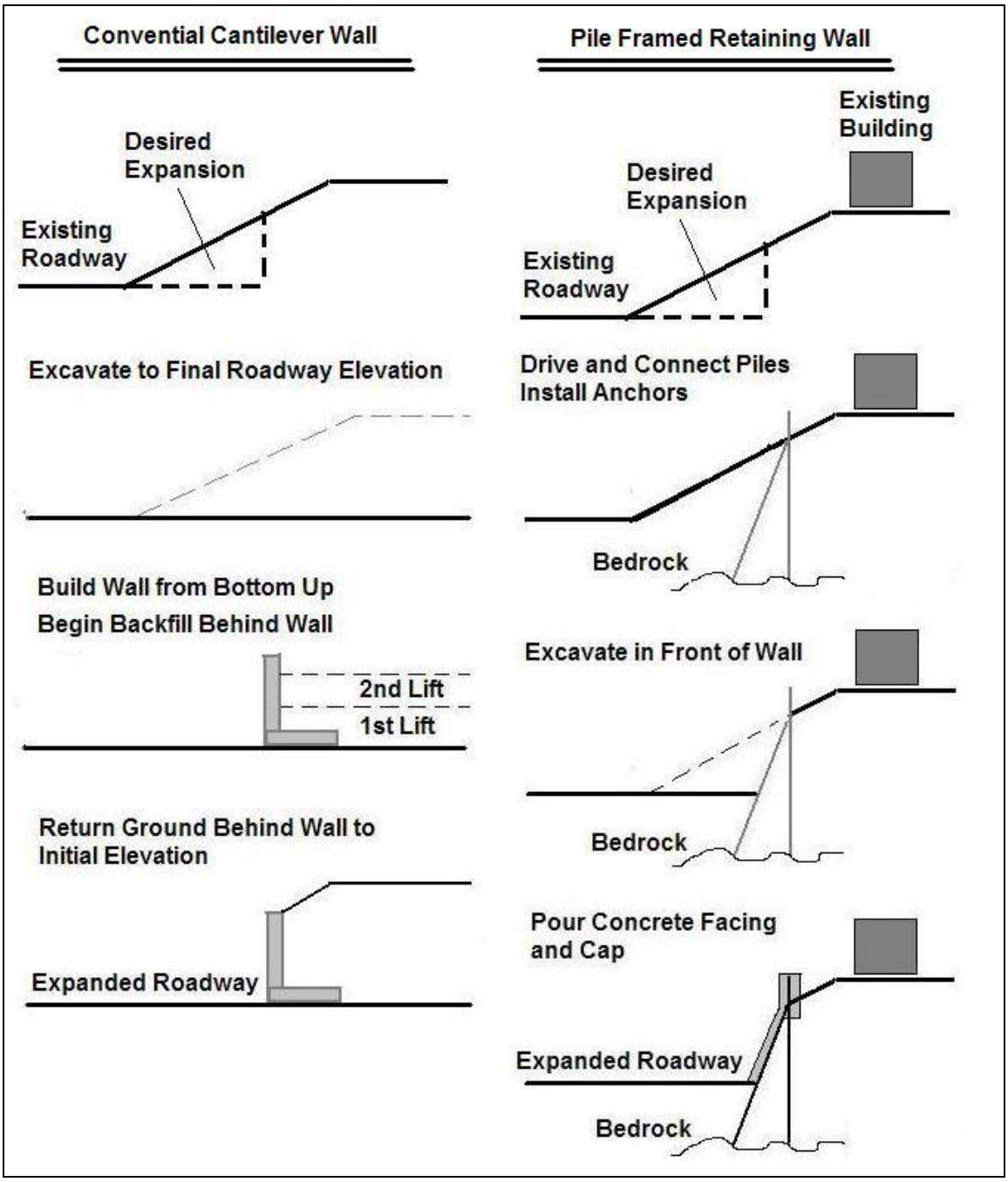

Figure 1.1-3 Conventional Cantilever vs. Pile Framed Wall Construction

The soil parameters for the initial wall were obtained from laboratory tests, Standard Penetration Test (SPT) N values, and soil sample observations. The designers then followed conventional methods for the analysis of earth pressures, such as the Rankine and Coulomb models. These models are widely used and include cases for wall inclination and backfill slope conditions (Lambe and Whitman, 1969, Coduto, 2001). From the various methods, the designers made a well calculated assumption of the magnitude and distribution earth pressures for their design.

A key feature of the wall design was the vertical anchor that acts to resist overturning as well as aiding in the construction process of the wall. The anchor gave the wall adequate overturning resistance to keep it stable while the soil in front of the wall is excavated prior to pouring the concrete facing. The installation of the anchors commanded much attention during construction, and as a result it was one of the most costly features of the design. However, the designers were very pleased with the wall‘s performance and cost savings. Building the first wall with the new pile-framed design saved the State of Tennessee approximately $13 million, primarily because expensive properties behind the wall did not have to be purchased.

Since the pile framed retaining wall is a novel concept, this research is one part of a multi-part project intended to better understand the behavior of the wall to create a more economical design. In this thesis, a two-dimensional numerical analysis was performed. The objectives of the numerical analysis are to understand how the earth pressures are

being transferred to the pile frame, make recommendations for optimizing the design, and provide numerical results to compare with field instrumentation data that will be collected on a second wall being constructed in 2007-08.

1.1.2 Site Descriptions

Prior to the start of this research, TDOT had constructed the first pile framed wall system in Knoxville, TN. At the time this thesis was completed, the construction of the second pile-framed wall was underway in Knoxville. Detailed soil investigations reports were completed by independent consultants for TDOT as part of the construction contracts (Wilbur Smith and Associates, 2002 and 2006). Thus, this section provides a brief summary of the soil conditions at the two sites. In later sections, an explanation of the selected soil parameters for the numerical analysis is provided

1.1.2.1 Site 1: West Hills

As stated before, the first wall was built along the West Hills (WH) exit of I-40/I-75 in West Knoxville. There is no geotechnical investigation at the exact location of the project; therefore the results of an investigation of a nearby project have been used to give a general description of the pile-framed wall site. The project site is underlain by two geologic formations, Copper Ridge Dolomite at the West end, and Chepultepec dolomite at the East end. Since the Copper Ridge and Chepultepec dolomites consist of carbonate rock, the site is susceptible to the typical carbonate hazards of karst

topography, which includes sinkholes, pinnacled rock, caverns and caves (WSA 2002). The geotechnical investigation conducted at the project site included 87 soil test borings which indicated two distinct soil strata (fill and residual soils) uniform over the project area. The fill soil was characterized as firm to stiff Clay (CH) and the residual soils were characterized as stiff to very stiff Clay (CH). Laboratory analysis for strength properties of the project soils was limited to an unconsolidated-undrained (UU) triaxial compression test. Groundwater was not present at the site.

1.1.2.2 Site 2: SmartFix Project

The second application of the pile-framed wall system was along an exit for I-40 as part of a major construction project, called SmartFix (SF), to expand and improve I-40 through central Knoxville. The retaining wall will be along the westbound exit onto James White Parkway. The project site is underlain by the Chapman Ridge sandstone formation, which generally consists of calcareous sandstone interbedded with shale, silty shale and limestone in some areas (Wilbur Smith and Associates, 2006). Wilbur Smith and Associates suggested that although sinkholes and voids are common to surrounding formations, there is a relatively low risk of sinkhole development within the Chapman Ridge formation and no surface signs of sinkhole activity were observed. The geotechnical investigation conducted at the project site included 20 soil test borings indicating two distinct soil strata (fill, and residuum) which were further divided into fine grained residuals and coarse grained residuals. The fill soil was characterized as clay (CH, CL). The residual soils varied widely across the site in both grain-size distribution

and density/stiffness (Wilbur Smith and Associates, 2006). The depth of the residuum varied as well with an average of 7.62 m (25 ft) and maximum of 18.29 m (60ft). The fine grained residuals varied between clays (CH, CL) and silts (MH, ML), whereas the coarse grained residuals consisted of silty sand (SM) of clayey sand (SC). Laboratory analysis for the project soils included consolidated undrained (CU) triaxial tests on 14 Shelby tube samples.

1.2 Literature Review

1.2.1 Earth Pressures

The first step in the design of retaining walls is the determination of the magnitude and direction of forces from the soil acting on the wall. The soil pressure acting on the back of the retaining wall is typically the most important, because it acts horizontally to overturn the wall; thus, it is called the lateral earth pressure. When discussing pressures or stresses in soil important the differentiation between effective and total stresses must be addressed. If one considers soil to be a matrix of soil, air, and water, then effective stress analysis considers the strength of the soil particles only. Things become more complicated when the pore water in the soil matrix is considered. When pore water is present some of the stress is carried by the soil particles and some is carried by the pore water; the latter is often referred to as pore pressure. In effective stress analysis soil

parameters are typically written with an apostrophe or prime to denote it as an effective parameter, i.e. c' for effective cohesion.

Lateral earth pressures come from horizontal stresses, σ_h' in the soil which are proportional to the vertical stresses, σ_z' by a ratio, K, which is commonly called the coefficient of lateral earth pressure where:

$$K = \frac{\sigma_h'}{\sigma_v'}$$

K is a constant in terms of effective stress parameters. In addition, K is dependent on three important soil conditions: the at-rest condition, the active condition, and the passive condition.

The at-rest condition represents soil stresses in the ground in an undisturbed state. In terms of a retaining wall, the at-rest condition assumes that a wall does not experience any lateral movement so that the soil behind the wall is undisturbed and at-rest. According to Michalowski, 2005, the coefficient of earth pressure at rest proposed by Jaky is accepted as the horizontal-to-vertical stress ratio in loose deposits and normally consolidated clays, is written as

$$K_o = 1\text{-}\sin\phi$$

where ϕ is the internal friction angle. The friction angle is a measure of the forces that resist particles from sliding against one another. It depends on the frictional properties between particles and the interlocking of individual particles. Various authors have

written about the at-rest earth pressure coefficient, and its more complex forms (Michalowski 2005, Mesri and Hayat 1993, Lambe and Whitman 1969).

In order to explain the active and passive conditions, the concept of the Mohr-Coulomb (MC) failure envelope, as it applies to the stress state of a point in soil, must be addressed. When a soil mass is disturbed by construction or natural changes, the shear stresses are changed. If the shear stresses in the soil exceed the shear strength of the soil, the soil fails. In terms of the MC failure envelope, shear failure will occur whenever the stress states at a point in the soil meets or exceeds this envelope. The failure envelope, or shear strength of a soil depends on the cohesion, the stress acting on the shear surface, and the internal friction angle. Shear strength is often written in equation form as:

$$\tau = c + \sigma \tan \phi$$

where τ = shear strength, c=cohesion, σ = stress acting on the shear surface, and ϕ = internal friction angle. Cohesion is the shear strength of the soil when the normal stress acting on the shear surface is zero. Cohesion can be further separated into true cohesion, or true bonding of soil grains, and apparent cohesion, or frictional strength between grains, not true cohesive forces. The MC failure criterion is the same for effective and total stress analysis as long as all the soil parameters are consistent with the type of analysis. From this point on, the discussion is in terms of effective stress for simplicity.

The normal stress acting on the shear surface is perpendicular to the shear stresses which act parallel to the shear surface. Normal and shear stresses can be computed for any direction if the magnitude and direction of the principal stresses are known. There exist at any stressed point three orthogonal (i.e. mutually perpendicular) planes on which there are zero shear stresses (Lambe and Whitman, 1969). In the ground, the soil stresses are static; thus the horizontal stress, σ_h' and the vertical stress, σ_v' are principal stresses. Therefore, the stress acting on the shear surface and thus the shear strength of soil can be determined if certain soil properties and the stresses in the vertical and horizontal directions are known.

Returning to the discussion of active and passive conditions, the active condition occurs when there is sufficient wall movement away from the soil to cause shear failure. Compared to a rigid wall, if the wall moves away from the soil, the horizontal stress will decrease. The passive condition occurs when there is sufficient wall movement toward the soil to cause shear failure. In this case the wall movement will increase horizontal stresses. There only needs to be small lateral movements in either direction to generate the corresponding condition as shown in Table 2.

Table 2. Wall Movement Required to Reach Active or Passive Condition (CGS, 1992)

	Horizontal Movement Required For:	
Soil Type	**Active Condition**	**Passive Condition**
Dense Sand	0.001H	0.020H
Loose Sand	0.004H	0.060H
Stiff Clay	0.010H	0.020H
Soft Clay	0.020H	0.040H
H=Wall Height		

From Table 2, more movement is required to reach the passive condition compared to active. This can best be explained in terms of the MC Failure envelope, in that changes in the stress state of a soil will proceed toward or away from exceeding the failure envelope. Less movement of the wall away from the wall is required to reach the active condition because, as the horizontal stress decreases, the soil approaches failure sooner than for a soil with an equal amount of stress increase. This relationship is illustrated in Figure 1.2-1, where K_a is the coefficient of active earth pressure and K_p is the coefficient of passive earth pressure. As shown in Figure1.2-1, for a constant vertical stress, as the horizontal stress decreases, the active condition, Mohr's circle increases in size to the left, approaching the failure envelope. However, if the horizontal stress increases, the passive condition, Mohr's circle increases in size to the right, and a much larger increase in stress is required to reach the failure envelope compared to the active condition.

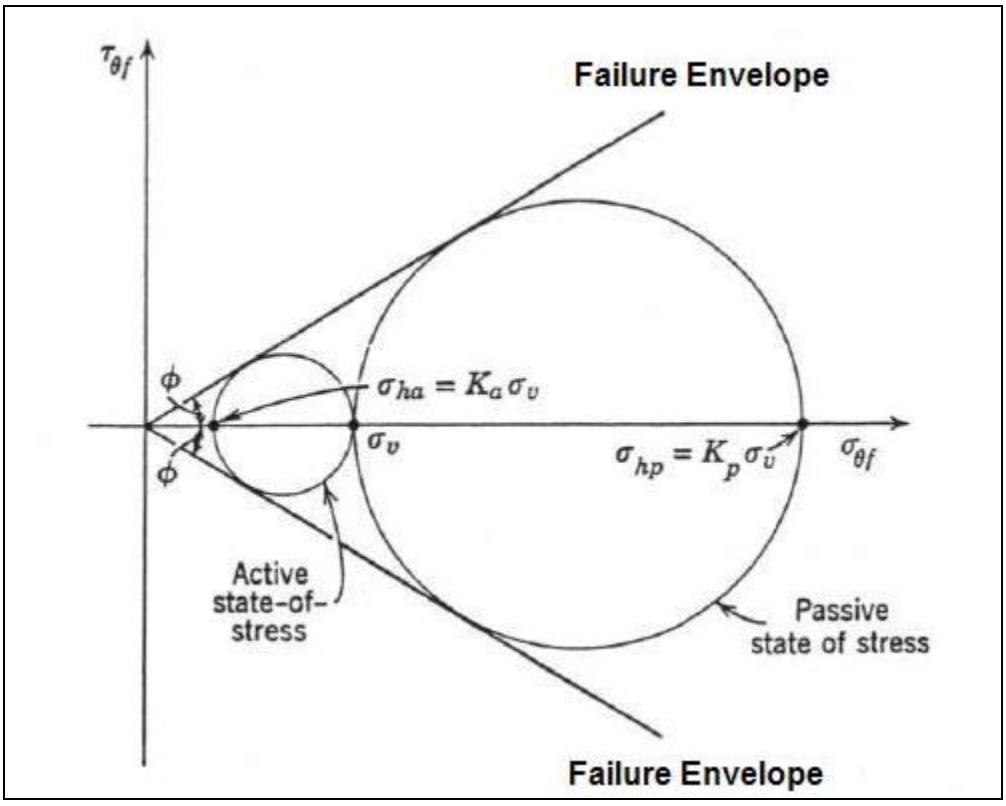

Figure 1.2-1 States of Stress (Lambe and Whitman, 1969)

As stated before, the pile framed retaining wall designed by TDOT is a novel design that is unlike conventional retaining walls. As a result there are no previous studies of such a wall system. For conventional walls the earth pressure formulations of Rankine and Coulomb are still in wide use today. Unfortunately, these formulations assume a certain amount of lateral movement to reach the active or passive conditions. So the question arises, for which condition should a pile-framed wall is designed? There has been extensive research on the earth pressures behind cantilever retaining walls (Paik and Salgado, 2003, and Goh, 1993). However, in these studies, the wall is free at the top to translate, and the researchers discuss the active pressures that develop. Other researchers

have discussed formulations for passive earth pressures (Soubra, and Macuh, 2002 and Zhu et al. 2002). Nonetheless, there is no previous research that provides a rational approach or justification of assumption of active or at-rest for the design of a pile framed retaining wall. The main objectives of this paper are to provide numerical results of the earth pressures that may develop behind such a wall.

1.2.2 Driven Piles

The pile framed wall consists of a battered pile inclined towards the soil, connected to a vertically driven pile, and a whaler that spans the frames. Both the battered and vertical piles are driven to refusal in rock. There is extensive research on the behavior and capacity of driven piles (Alawneh, 2005, Amde et al., 1997, Hegedus, 1984, and Rajashree et al., 2001,). Previous studies have examined individual piles under lateral loads, combined loads and also tensile or uplift loads, but not piles framed together. In addition, studies of driven piles are for deep foundation applications, not retaining walls where the piles will extend to heights above final grade. Thus, it is questionable to simply extend conclusions obtained from studies of driven piles to the behavior of driven piles for retaining wall applications.

Some researchers have even looked at the effects of the pile driving process on the surrounding soils and their properties (Hunt et al., 2002, and Skirrow et al., 1991). However these studies did not extend the research into the surrounding soil behavior if

soil is excavated on one side of the pile. Therefore, this research examines the behavior of driven piles that are framed together for use as earth retention systems.

1.2.3 Previous Research in Geotechnical Finite Element Modeling

The application of the Finite Element Method to Geotechnical engineering is by no means a developing trend. Researchers have been creating and refining finite element programs since the 1960s, and as a result numerous commercial programs and open-source codes are available for engineers. In addition, many textbooks have been written on the subject of finite elements in Geotechnical Engineering as well as the finite element method in general (Potts and Zdravkovic, 2001, Bathe, 2001). The important aspects and techniques found in the literature that proved useful in this numerical analysis are briefly discussed below.

Before any finite element model is developed to solve a problem, an estimate of the solution through simple methods or accepted theories, i.e. mechanics of materials, should be determined to validate the accuracy of the model. In the case of retaining walls, accurately predicting earth pressures with a finite element model is a sign of a good model. Calculated earth pressures were compared with solutions proposed by Rankine along the depth of a retaining wall at distances behind the wall to show stress distributions (Goh, 1993 and Benter and Abuzz, 2006). Displaying the results along with theoretical estimates confirms the quality of the model to some degree, but more so it reveals which soil condition (active, passive, at-rest) the wall should be designed for.

Issues of boundary influence and meshing are very important in finite element modeling. If the boundaries of a model are not of sufficient spacing from the zones of interest, the boundary conditions will affect the results of the analysis. Franzius and Potts 2005 created plots of vertical settlement vs. boundary distance in the direction of a tunnel alignment to prove that the boundary distances were not affecting their results. Meshing is how finite elements are distributed or arranged in a model. Mesh density is simply the number of elements in a mesh, where the terms coarse and fine are used to describe areas of a mesh. It is most advantageous to localize a high number of elements in regions of the model that are of most interest. The finest mesh is required near the loaded area to capture the step stress and gradient in these areas (Saad et al., 2005).

Classical methods for the design of retaining walls typically consider the wall instantly in place and cannot factor how the wall was built or how the soil properties may be affected during construction procedures. The capabilities of finite element programs make it possible for time dependent construction activities to be examined. Borja et al. 1989 simulated excavation of soils by removing elements of a mesh in different stages and comparing the effects of different sequencing. Results indicated the uniqueness of the solutions with respect to the final calculated deformations which were independent of the number of stages. Other researchers went beyond excavation modeling to also include the imposed loads during construction of a concrete culvert (Simmonds and Playdon, 1988). In their study they used a technique to add elements to a mesh without causing yielding of other elements. To do so they used "preloading" by which they would

gradually apply a load representing the new elements, in this case the pouring of concrete, before the elements were added. After the new elements were added, the "preload" was removed and the steps were repeated for subsequent elements. This produced good results and eliminated the unrealistic stresses that would develop if the preloading was not employed.

1.3 Overview of Thesis

In Chapter 2, a brief introduction of the finite element modeling is provided along with much of the terminology that will be used throughout this study. The development of the basic model of the pile-framed wall system is discussed with focus on the basic modeling decisions.

The most important modeling aspects are addressed in Chapter 3. The optimal model geometry and mesh are determined by an evaluation of options. The choice of material model for the soil is evaluated to best model the real behavior. The importance of modeling the construction sequence is explored to determine if the results are dependent on the sequence. Lastly, the results of the model employing the best decisions are verified against classical earth pressure methods.

In, Chapter 4 parametric studies are conducted with the most refined model to investigate effects of design parameters such as pile boundary conditions, tie-down

anchor loads, wall heights, and other input parameters. In addition, the ultimate capacity of the wall model is investigated by applying a surcharge to the backfill until failure is reached.

In Chapter 5, the input parameters, procedures, and results of this study are summarized and important conclusions are discussed. Lastly, design recommendations are proposed based on analysis results to reduce construction costs and time. Finally, suggestions for further research are provided.

CHAPTER II

ADINA MODEL AND BASIC ASSUMPTIONS

2.1 Introduction

The numerical analysis of a two-dimensional model of the pile framed retaining wall system was performed with the 900-node version of the Automatic Dynamic Incremental Non-linear Analysis (ADINA) 8.4 computer program (ADINA, 2006). The software has numerous analysis options and is typically used for displacement, stress, fluid and thermodynamic analysis. ADINA was used to create the models, run the analysis, and then process the results. The model was refined for an optimum mesh in terms of the model geometry, element types, and mesh density. In addition, the models were set-up so the analysis considered geometric, material, and contact nonlinearities.

2.2 Finite Element Modeling

The finite element method is a method to analyze structures or systems by dividing the components of a structure into finite elements. The elements are then connected by nodes. The finite element mesh refers to the elements and nodes. Loads or displacements are then applied to the mesh and differential equations are used to obtain

nodal displacements based on principles of mechanics. The nodal displacements are then used to output stresses, strains, and forces for each of the elements.

.

2.2.1 Solution Process

An explanation of the mathematical framework for the ADINA is beyond the scope of this thesis and a very detailed one is provided by K.J. Bathe, 1996. This section provides the basic choices made for analysis. The Full Newton Iteration Scheme with a sparse equation solver was the default setting in ADINA, thus was used during analysis for equilibrium iterations. The maximum number of iterations was set to 200 to take advantage of the computing power and reduce problems with convergence. The automatic time-stepping (ATS) feature was also used for the non-linear analysis to obtain convergence by using a smaller time (or load) step during equilibrium iterations than the defined time (or load) steps that were too large. The only change to the default setting was changing the maximum number of subdivisions allowed to 1000. The default convergence criterion was set to Energy, and the chosen energy tolerance was 0.001 or 0.1%. Definitions of the iterations schemes and convergence criteria are given in ADINA, 2006.

2.2.2 Definition of Stress and Strains

The small stress and strain formulation was the basis for analysis. This formulation uses engineering stress and strain relationships for element and material inputs, and the

outputs are Cauchy stresses and engineering strains. ADINA illustrates the stress and strains terms with the case of a rod subjected to uniaxial tension Figure 2-2.1. For small strains, the initial undeformed area is unchanged and the strains are less than 2%.

The stress and strain terms are defined by the following equations:

Engineering strain: $e_o = \frac{\ell - \ell_o}{\ell_o}$

Engineering stress: $\sigma = \frac{F}{A_o}$

Cauchy stress: $\tau = \frac{F}{A} = \frac{\sigma A_o}{A}$

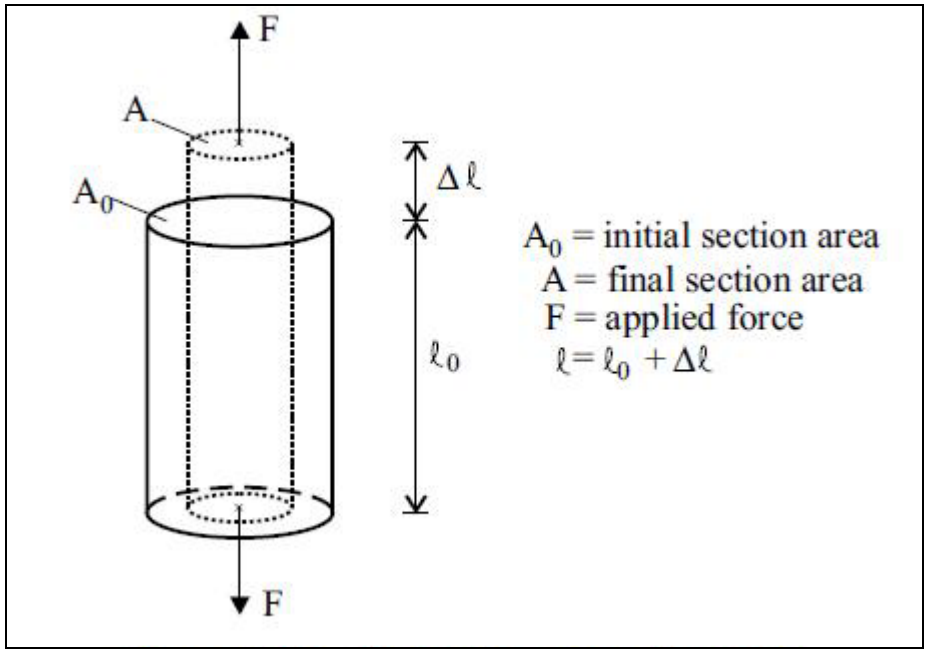

Figure 2.2-1 Rod under uniaxial tension (ADINA, 2006)

2.2.3 Plane Strain Approximation

Plane strain is an analysis approximation that simplifies the model of a system to two dimensions. It is best suited for problems where there is no variation in the properties or geometry of a structure in the longitudinal direction, such as dams and retaining walls. Since properties in one dimension are relatively constant, deformations in that direction are assumed zero and only behavior of one plane is analyzed assuming all cross sections of the structure will behave similarly. A representative cross section of unit length can be chosen for the structure that includes the structure geometry and material properties, the section properties per unit length, and in the case of a retaining wall, the geometry and properties of the soil.

There are several limitations to the plane strain approximation that can't be overlooked. In the case of the pile framed retaining wall, there will be variation in wall geometry and construction quality and even more variation in soil properties. The selection of the representative section for analysis was based upon the loading diagram presented by TDOT, in Figure 2.2-2. Shown in the diagram is the total height of the West Hills (WH) wall, 9.44 m (31 ft), measured from finished roadway grade to top of wall. This cross section was used for analysis and parametric studies of wall geometry were included to better understand the behavior of different wall cross sections.

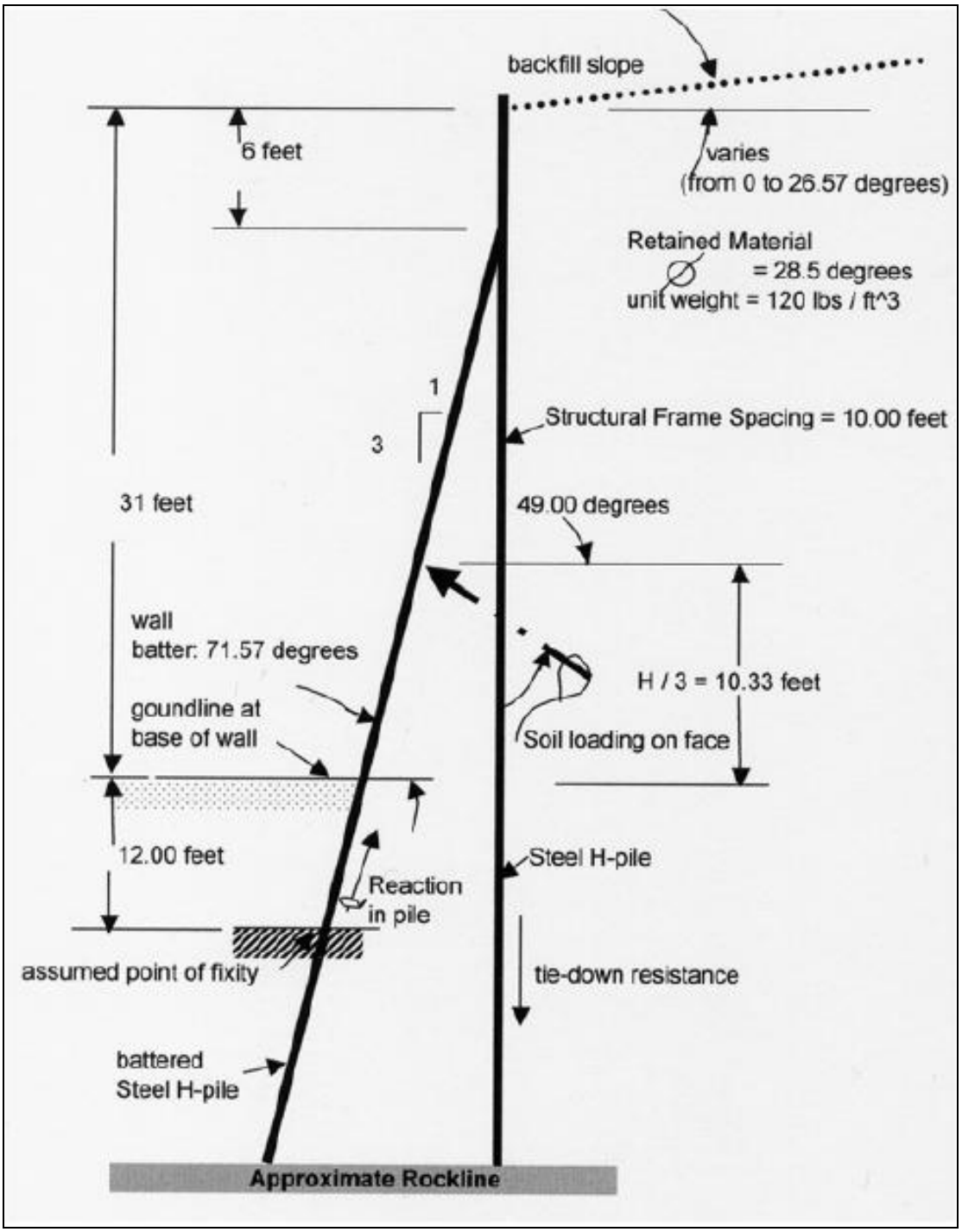

Figure 2.2-2 Representative Section of West Hills Wall (Pate and Haddad, 2007)

The pile frames of the wall are spaced every 3.04 m (10 ft) with tie-down anchors spaced 0.762 m (2.5 ft) from the centerline of the pile frames. Figure 2.2-3, taken from the construction contract drawings shows an elevation of two frames connected by a whaler and the location of the anchor.

For every frame there was a 3.04 m tributary width of concrete facing and two tie-down anchors. To approximate the wall for plane-strain conditions, a section was assumed to be the system of the steel piles, two contributing tie down anchors, and a 3.04 m width of concrete, since this system repeats every 3.04 m. Thus the wall was approximated for a 1 m unit width. The anchors were grouped together and modeled as one anchor with the properties of two anchors per unit width. The steel piles were modeled per unit width by dividing the dimensions in the longitudinal direction by the unit width, namely the web and flange thickness. The concrete facing and battered piles were modeled as a composite beam with the properties per unit width. The steel whaler was neglected in analysis of the cross section because it does not add much rigidity for bending in plane and serves primarily to transfer the tie-down forces to the pile frames. Lastly, plane strain elements in ADINA must be defined in the YZ plane, thus all analysis was defined in this plane.

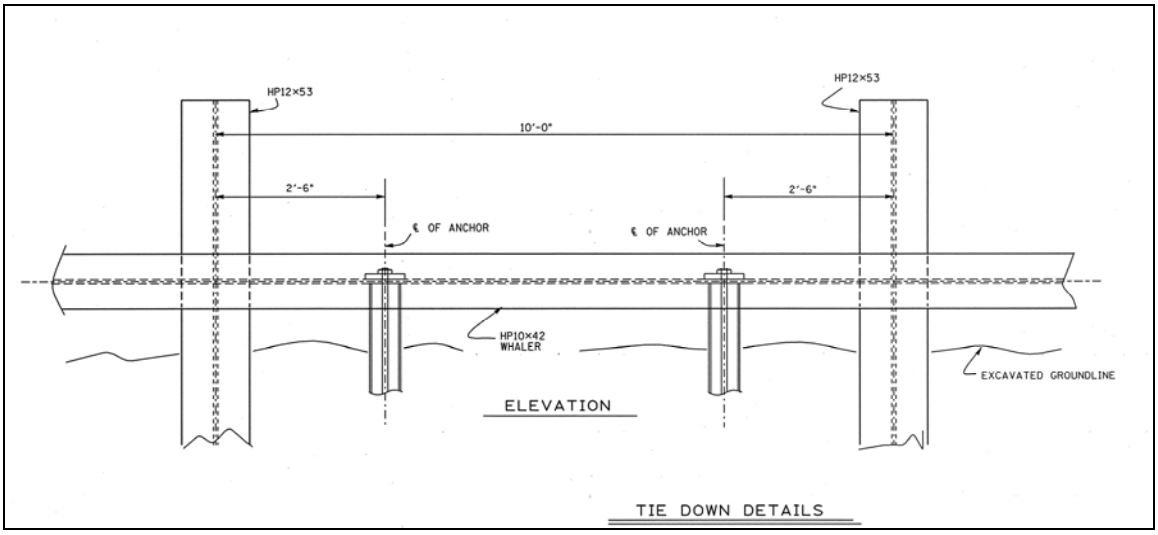

Figure 2.2-3 Pile Frame and Tie Down Elevation Detail

2.3 Modeling Assumptions

2.3.1 Initial Material Properties

The pile framed wall is built with steel piles, reinforced concrete, wood lagging, and steel tie-down anchors. To create the initial model, only two materials are defined, the soil and the steel. Later sections will explain the modeling representations of the other components of the wall. For the preliminary linear elastic models the necessary inputs to define the materials are the modulus of elasticity, Poisson's ratio, and the density or unit weight. Tables 3 and 4 provide typical values for these parameters.

Table 3 Typical Values of Elastic Modulus

Material	**Modulus of Elasticity, kPA (psf)**	**Source**
Very Soft Clay	2,000-15,000 (41,800 - 313,000)	Bowles 1995
Medium Clay	15,000-50,000 (313,000 - 1,044,000)	Bowles 1995
Hard Clay	50,000-100,000 (1,044,000 - 2,089,000)	Bowles 1995
Sandy Clay	25,000-100,000 (522,000 - 2,089,000)	Bowles 1995
Dense Glacial Till	150,000-720,000 (3,133,000 - 15,000,000)	Bowles 1995
Loess	15,000-65,000 (313,000 - 1,358,000)	Bowles 1995
Loose Sand	10,000-25,000 (208,900 - 522,000	Bowles 1995
Dense Sand	50,000-81,000 (1,044,000 - 1,692,000)	Bowles 1995
Silt	2,000-20,000 (41,800 - 418,000)	Bowles 1995
Screened Ottawa Sand	179,000-301,000 (3,739,000 - 6,286,000)	Lambe & Whitman 1968
Well Graded Sand	103,000-193,000 (2,150,000 - 4,031,000)	Lambe & Whitman 1968
Steel	200,000 (4,177,000,000)	AISC 2006

For the purpose of analysis, the parameters selected for the steel modulus, Poisson's ratio, and density were, 200 MPa, 0.29, and 77 kN/m^3 respectively. For the soil, the selected parameters were 71.82 MPa, 0.32, and 17.3 kPa. For normal weight concrete, with a density approximately 23.6 kN/m^3 (150 lb/ft^3), the modulus, E_c, is approximated as:

$$E_c = 4{,}700\sqrt{f'_C} \qquad \text{for} \qquad (20.7 \leq f'_c \leq 34.5 \text{ MPa})$$

$$E_c = 57{,}000\sqrt{f'_C} \qquad (3{,}000 \leq f'_c \leq 5{,}000 \text{ psi})$$

For analysis, f'_c was chosen as 20.7 MPa (3000 psi) since this was the specified compressive strength for the concrete facing on the West Hills wall, and would result in a slightly more conservative analysis.

Table 4 Typical Values of Poisson's Ratio and Unit Weight

Property	**Value**	**Source**
Poisson's Ratio, ν		
Clay Soils	0.4 - 0.5	Bowles 1995
Cohesionless Soils	0.2 - 0.4	Bowles 1995
Steel	0.28 - 0.29	Lambe and Whitman 1968
Unit Weight, γ, kN/m^3 (lb/ft^3)		
Clays	12.5 - 17.5 (80 - 110)	Coduto 2001
Sands	85 - 135 (13.5 - 21)	Coduto 2001
Gravels	16 - 22 (100 - 140)	Coduto 2001
Steel	77 - 80 (490 - 500)	AISC 2006

2.3.2 Linear Elastic Material Model

In numerical analysis programs the material models are the mathematical relationships between stresses and strains. A detailed review of the material models available in ADINA and the theoretical basis for available material models can be found in the supporting literature (ADINA, 2006 and Bathe, 1996). The following summarizes the important points of the material model used for preliminary analysis.

The linear elastic-isotropic material model is based on Hooke's law, which states that strains are directly proportional to stresses. An isotropic material is one that has identical properties and characteristics in all directions. The elastic model is a widely accepted choice for steel materials and was used throughout the entire analysis for steel piles. For service loads, the concrete sections remain uncracked so the linear elastic model was a used for the composite sections as well. For preliminary analysis, the soil was initially modeled as linear elastic. In reality, the properties and behavior of soil are highly

variable; however, in some cases a linear elastic model can approximate soil behavior fairly well. Therefore the results with linear elastic soil were compared with a more advanced model, which is described later, to evaluate the choice of soil material model.

2.3.3 Boundary Conditions

The master degrees of freedom for the plane strain problem were rotation about the longitudinal axis of the wall, and lateral translation in plane. Since the plane strain model must be defined in the YZ plane in ADINA, the X-axis is the longitudinal axis of the wall. The basic finite element mesh is shown in Figure 2.3-1, along with selected boundary conditions. For the soil mass, the vertical side boundaries are fixed against lateral translation, but allow vertical translation and rotation. The horizontal bottom boundary is a pinned boundary, restricting translation in each direction but not rotation. Since the underlying bedrock is significantly stiffer than the soil, the deformations are small relative to the soil, so the base is pinned, and rock was not meshed.

The steel H-piles are driven to refusal onto rock, creating boundary conditions that are not truly fixed (all degrees of freedom restrained), or truly pinned. It was assumed that piles driven to refusal are closer to a fixed condition so the piles were initially modeled as fixed. The other ends of the piles are welded together at the flanges. To model this rigid connection, the ADINA option to model the beams with rigid ends of infinite stiffness was selected. The length of the rigid ends was chosen as the width of the flange of the batter HP 10x42 sections.

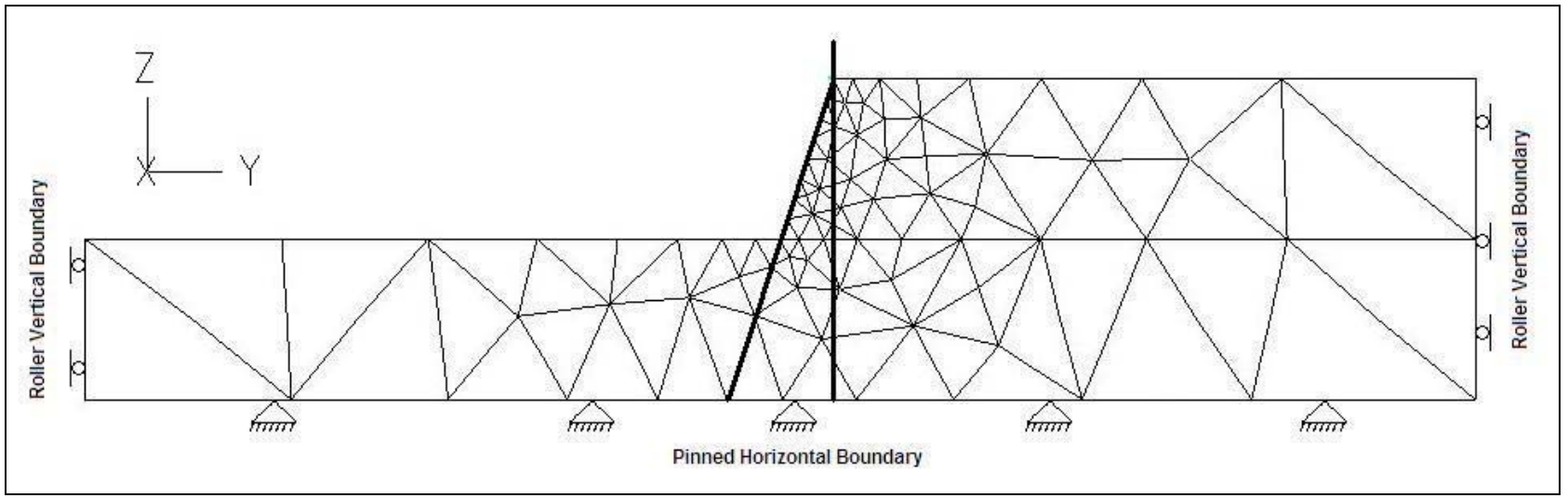

Figure 2.3-1 Typical Mesh Showing Boundary Conditions

2.3.4 Meshing

2.3.4.1 Soil Elements

The soil was modeled with 2-D solid elements. ADINA allows for the use of three-noded triangular, up to nine-noded quadrilateral elements. Since the wall face is inclined, causing irregular geometry and a large number of model geometries were analyzed, the seven-noded triangular elements was selected with Delaunay free forming meshing. Delaunay meshing is the ADINA default mesher for 3D geometries because it is fast and works well for complex geometries. The free-form meshing creates triangular elements automatically after the geometry lines of the model are subdivided. Thus, there is some uniformity in the method of the mesh generation for all the different geometries, while eliminating the need to manually define the element meshing. The seven-noded elements were chosen over three-noded elements because they are less stiff in bending. In addition, a default of seven integration points per element is used compared to a default of only one point for the three-noded element (ADINA, 2006). Figure 2.3-2 illustrates the three and seven-node solid elements used by ADINA.

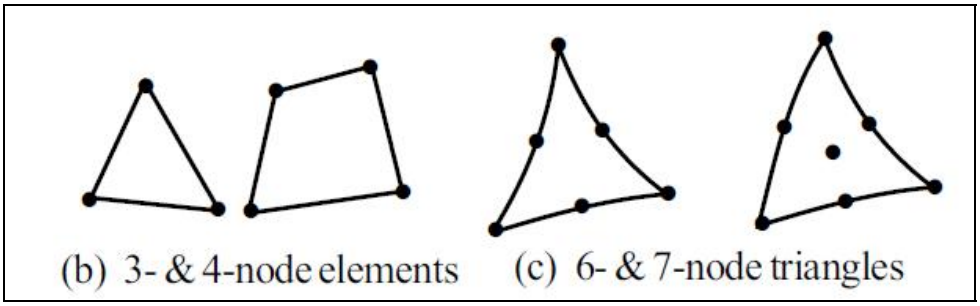

Figure 2.3-2 ADINA 2D Elements (ADINA, 2006)

2.3.4.2 Steel Beam Elements

The H pile members were modeled using two-noded Hermitian beam elements in ADINA, which have six degrees of freedom at each node. The conventions used for the degrees of freedom of the beam element are shown in Figure 2.3-3. The local directions of a beam element (r, s, t) are defined by a plane that is defined by the beam local nodes 1, 2 and an auxiliary point. The local s direction lies within this plane and local r is perpendicular to the s direction. The t direction is out of the plane defined by the local nodes and the auxiliary node. The auxiliary node must be defined correctly relative to the orientation of the beam so the section properties match the degrees of freedom of the beam elements.

2.3.4.3 Contact Elements

The behavior of a retaining wall is a problem of soil-structure interaction because the soil deformations induce stresses in the structural members and vice versa. To model this interaction contact elements were employed to represent contact between the soil and the concrete facing of the wall. The analysis in ADINA becomes nonlinear when contact elements are used even if no nonlinear material models are used since, in ADINA, there are three possible situations for contact; no contact, sliding, and sticking. Although, frictionless or contact with Coulomb friction can be modeled, frictionless contact was used for analysis because it is difficult to accurately quantify frictional coefficients, the use of contact requires more computation effort, and a solution without contact should be obtained first before conducting analysis with contact (ADINA, 2006).

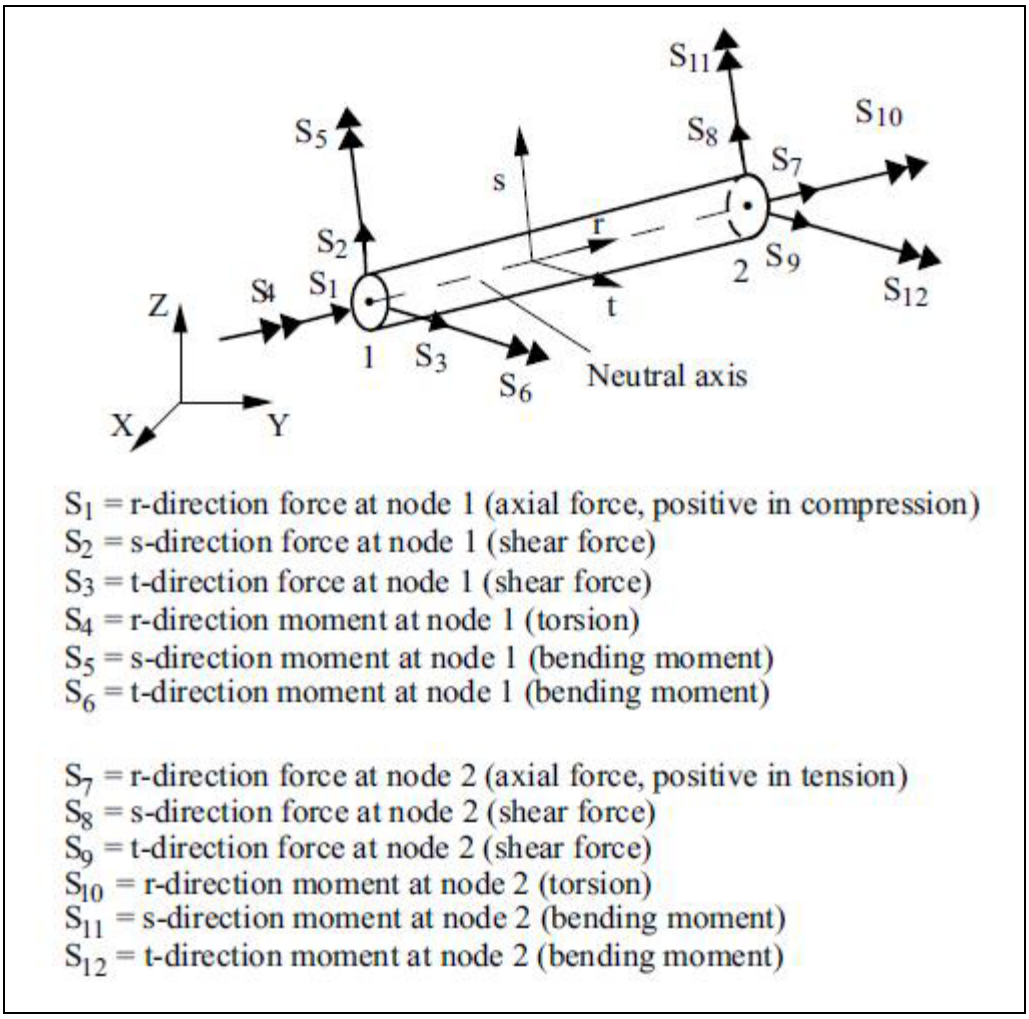

Figure 2.3-3 ADINA Conventions for 2-node Beam Elements (ADINA, 2006)

The default algorithm for solution with contact is the Constraint Function method. This method is used to prevent penetration of contacting bodies, follows frictional parameters, and is more effective in most frictionless contact problems (ADINA, 2006).

To define contact interfaces, a contact element group is first defined, and then surfaces within that group are defined to represent lines or edges of bodies. Next, contact pairs of two surfaces that may come in contact are defined for a contact group. In each pair one

surface is selected as the target surface and one surface is the contactor surface. The orientation of the surfaces must be defined correctly because the orientation defines the inside of the contact body. The choice of target or contactor is also important, in general, the more rigid surface should be the target surface, unless the rigid surface has a finer mesh, in this case the surface with the coarser mesh, elements spaced farther apart, should be the target surface (ADINA, 2006). Figure 2.3-4 illustrates the result of improper contactor-target selection for fine and coarse meshing; notice how the contactor surface does not have capability of deforming around the target surface due to a lack of nodes.

Lastly, if two surfaces are to be in contact but they are coincident meaning they are defined by the same coordinates, then they must be meshed so there are separate nodes for each individual surface. The contact surfaces are defined by the nodes of the meshed line or bodies, thus there needs to be separate nodes for two separate contacting bodies. Figure 2.3-5 illustrates how the contact surfaces were setup up for the analysis on a typical model showing orientation and choice of target-contactor bodies.

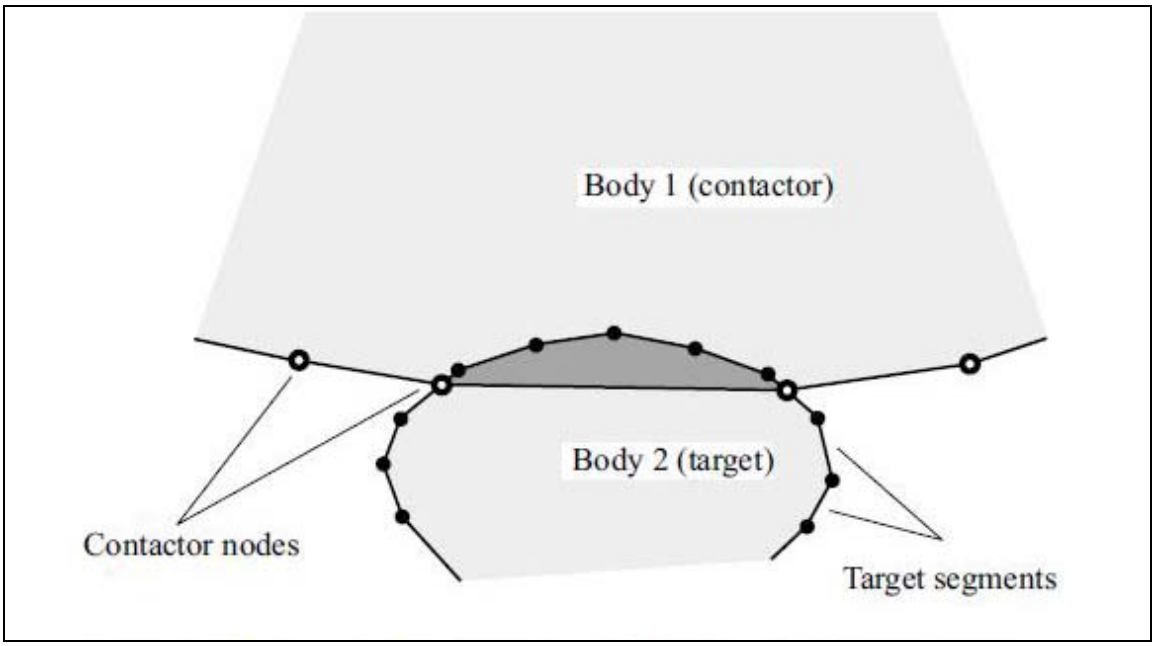

Figure 2.3-4 Improper Selection of Contact Surfaces (ADINA, 2006)

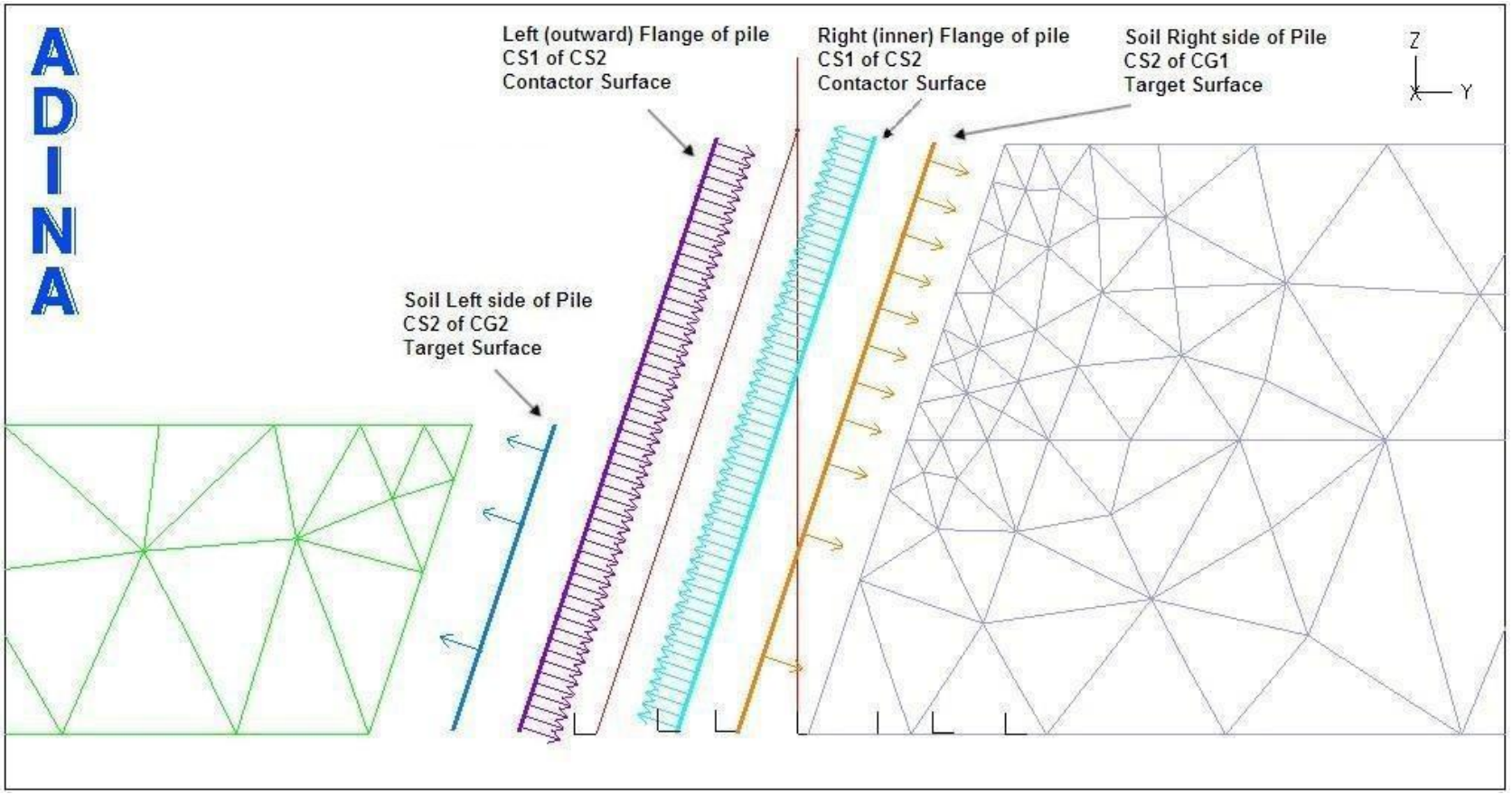

Figure 2.3-5 Contact Surface Orientation

2.3.5 Structural Element Idealizations

2.3.5.1 Steel H-Piles

Two different pile sections are used to construct the pile frame. There cross sections are defined in ADINA using the general cross section inputs, requiring the Moment of Inertia with respect to strong-axis bending (beam t-axis), the cross sectional area, and the effective shear area. The section properties and dimensions were taken from the AISC Steel Construction Manual, and properties per unit width were calculated, and provided in Table 5 along with properties for the composite sections. The steel beams elements were meshed or subdivided into 0.304 m (1 ft) increments. This was chosen since most structural loads or properties are discussed on a per foot basis. ADINA output results for the beam bending moments and shears at the element end points, so the subdivisions were selected so that the output would be in terms or dimensions common to most engineers. In addition, a per foot mesh density of the piles was assumed fine enough so that results would not change if the mesh density was increased.

2.3.5.2 Steel-Concrete Composite Section

For analysis purposes the steel pile composite properties were utilized for the batter pile above the grade making the section much stiffer than the HP section acting independently. To determine the composite properties, it is assumed that the concrete and steel are bonded sufficiently so they strain equally. This is accomplished by the use of mechanical shear connectors welded to the pile and embedded in the concrete.

Table 5 Pile Section Properties

Cross Section*	Property	Metric Units		English Units	
	Moment of Inertia, I_g	m^4	per unit width, m^4/m	in^4	per unit width, in^4/ft
1		1.635E-04	5.366E-05	393	39.3
2		1.433E-03	4.701E-04	3443	344.3
3		8.739E-05	2.867E-05	210	21.0
4		2.966E-03	9.731E-04	7127	712.7
	Gross Area, A_g	m^2	per unit width, m^2/m	in^2	per unit width, in^2/ft
1		9.999E-03	3.281E-03	15.5	1.55
2		1.111E-01	3.645E-02	172.2	17.22
3		7.999E-03	2.624E-03	12.4	1.24
4		1.548E-01	5.080E-02	240.0	24.00
	Shear Area, A_v	m^2	per unit width, m^2/m	in^2	per unit width, in^2/ft
1		3.311E-03	1.086E-03	5.133	0.5133
2		2.610E-03	8.564E-04	4.046	0.4046
3		2.597E-03	8.520E-04	4.046	0.4046
4		3.311E-03	1.086E-03	5.133	0.5133
*Note: 1-Vertical HP 12x53, 2-Batter Composite Pile, 3-Batter HP 10x42, 4-Vertical Encased Top					

With this assumption, the stress in each material will be dependent on its respective modulus, and the modulus of steel will be *n* times that of the concrete. Therefore, the concrete can be transformed into an equivalent in steel so that the composite section can be thought of as entirely steel. Values for the modulus of steel and concrete are provided in section 2.3.1. Procedures to calculate transformed section properties are found in numerous textbooks on steel design, the procedure used for this analysis can be found in McCormac 2003.

There are two composite sections in the pile framed wall, the first is the batter pile and concrete facing, and the second is the top of vertical pile and the concrete cap. Figure 2.3-6 is a typical cross section of the wall showing the composite sections and reinforcing steel layout taken from the contract drawings. The reinforcing steel was ignored for the computation of the composite section properties and in ADINA models. The properties for the batter were calculated by idealizing the composite section as the HP section with a wide concrete flange. The properties of the top section of the wall were calculated by idealizing the section as and encased section. For both sections, the concrete was assumed to not crack, thus no reductions in the rigidity of the sections.

From the composite properties, the bending moment and shear capacities were determined by following standard procedures. These capacities served as metrics for the preliminary and final results from the numerical analysis. For bending in which the concrete is in compression and the steel is in tension, the capacity was based on the plastic moment of the section. For bending that creates tension in the concrete, the bending moment capacity is based on the steel section alone since the tensile strength of concrete is very low and can be ignored. The shear capacity of the steel was determined in accordance with the AISC steel manual and the shear capacity of concrete was ignored for conservatism. Since the encased section at the top of the wall is more massive than the composite section along the batter pile, the bending capacity was assumed much greater, so the bending capacity of the batter section was chosen as the maximum bending capacity.

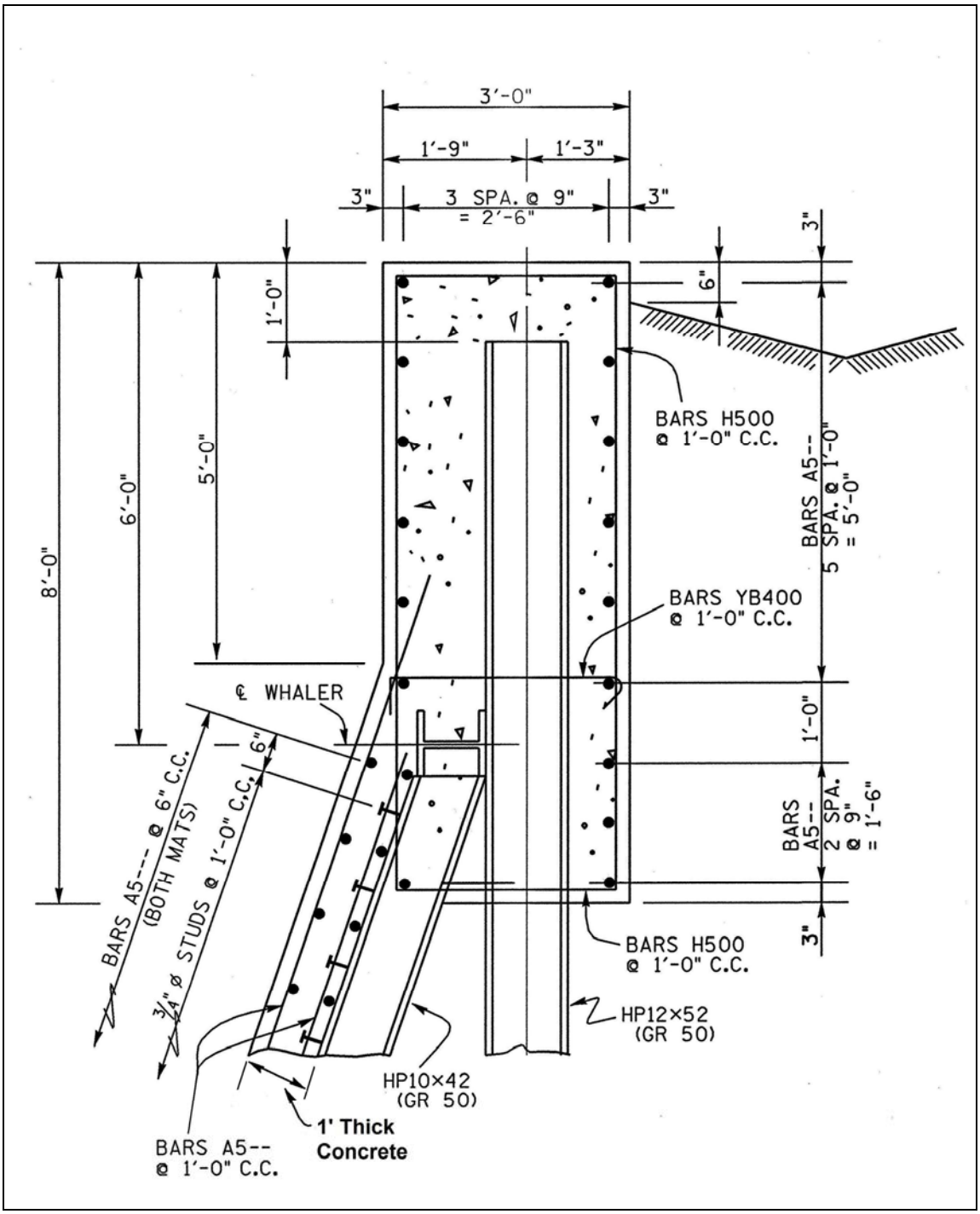

Figure 2.3-6 Typical Section of Wall Showing Composite Sections

According to the contract notes, the concrete facing extended to a depth of 0.46 m (1.5 ft) below the final roadway grade, while the HP 10x42 pile was driven to rock. Thus composite section properties were only assigned to beam elements starting one foot below the geometry line representing the roadway grade, up to the pile connection point. The composite section properties for the encased section were assigned to all beam elements of the vertical pile above the pile connection point. The concrete encasement at the top of the wall extended below the pile connection point, but this construction detail was assumed to contribute very little to the rigidity of the pile frame and was ignored. The bending and shear capacities for the two sections are shown in Table 6.

Table 6 Bending and Shear Capacity of Cross Sections

	Pile Section			
Capacity	HP 10x42	HP 10x42 Composite	HP 12x53	HP 12x53 Encased
(+) Bending Moment	80.8 (18,100)	290 (65,100)	124 (27,700)	290 (65,100)
(-) Bending Moment	80.8 (18,100)	80.8 (18,100)	124 (27,700)	124 (27,700)
Shear Force	178 (12,100)	178 (12,100)	225 (15,400)	225 (15,400)
Note: Bending Moment units: kN-m/m (ft-lb/ft) Shear units: kN/m (lb/ft)				

Since the composite sections are significantly stiffer than the individual pile sections, once framed to together, the composite sections will attract the internal forces such as moment and shear. Therefore, the internal forces in the vertical pile below the connection point are not considered in this thesis because the internal reactions are assumed to be insignificant compared to the batter piles. The capacity of the composite vertical pile above the connection point is much greater than the batter pile, so this section was not considered either.

2.3.5.3 Tie-Down Anchor

The vertical tie-down anchor is attached to the frame through the horizontal whalers that span between frames. The anchor is placed through a hole in the web of the whalers and the reaction plates are jacked against the whalers. The centerline of the anchors was aligned with the center of the HP 10x42 whalers. The centerline of the anchor is at a distance of half the depth of the vertical pile plus half the depth of the whaler from the centerline of the vertical pile, which is10.825 inches or 0.275 m. Figure 2.3-7 shows the centerline of the anchor relative to the two piles. To model the anchor, two options were considered. The first was to model the anchor as a truss element with an initial strain, connected to the centerline of the vertical pile and apply a moment at top of the anchor equal to the force times the eccentricity. The second option was to take advantage of the rigid link option in ADINA to model the offset of the anchor from the vertical pile. The rigid link is typically used to model off center beam elements. For simplicity, the rigid link option was chosen.

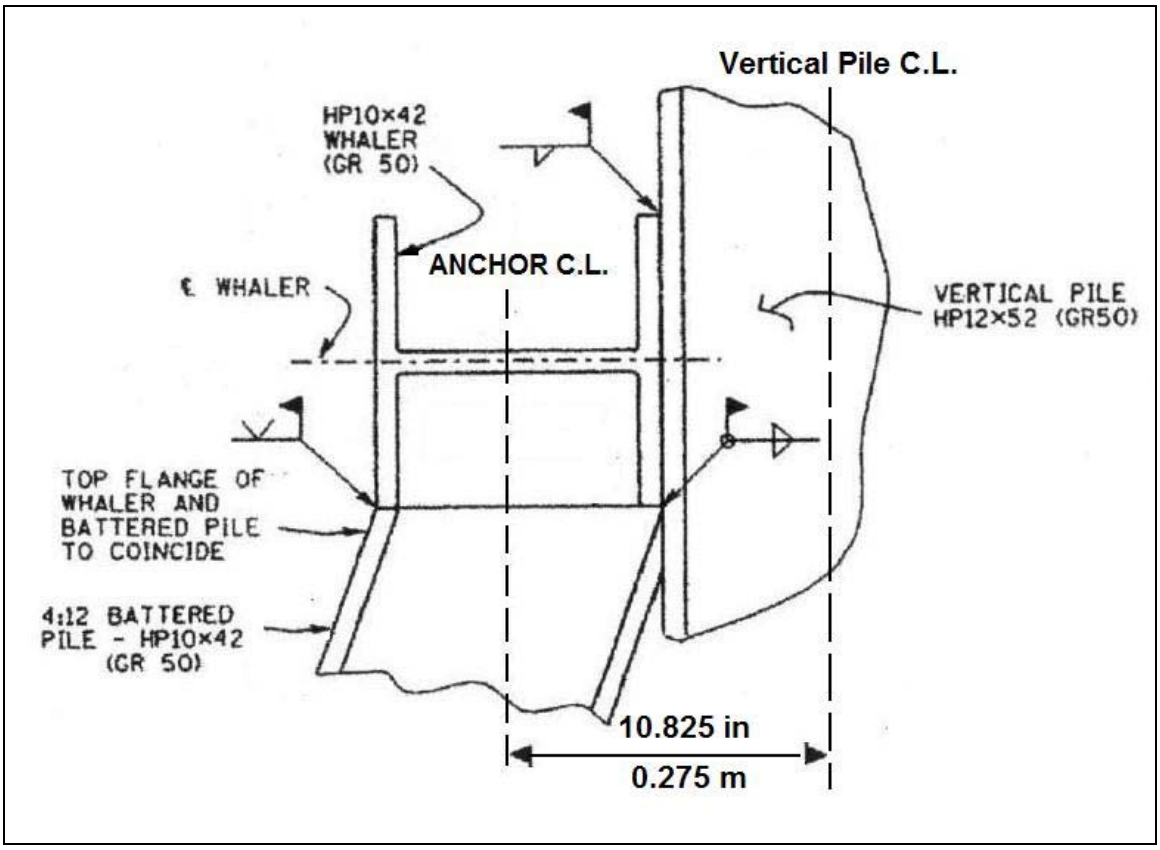

Figure 2.3-7 Tie-Down Anchor Location Relative to Piles

2.3.6 Contact Surface Idealizations

Soil pressures are transferred to the pile frame through contact with the concrete facing. Therefore, contact surfaces were meshed between the lines that represent the composite batter pile and the soil elements. In reality, the piles are driven into soil so there is contact on each side of the pile. For the batter pile, two separate contact interfaces were meshed on either side of the batter pile beam. The earth pressures behind the wall make the wall bend out toward the roadway, but the soil on the roadway side of the wall resists outward bending. The geometry lines defining the soil elements were coincident with

lines defining the piles to simulate direct contact between the soil and pile after the pile is driven. As a result the surfaces defining the soil elements were meshed with independent nodes for each line of soil elements as well as the beam elements. In other words, at coordinates along the batter pile, there were three coincident but separate nodes, to model conditions with soil on both sides of the pile. There is one node for the pile and one for each line of elements on either side of the pile. For conditions with one sided contact there were only two coincident but separate nodes.

For the vertical pile, contact was neglected altogether. The rigidity of the vertical pile compared to the composite section is so small that it is assumed to contribute little to the lateral resistance of the wall. There is retained soil below the pile connection point and between the wall facing and the vertical pile so it was assumed that the earth pressures act on the wall facing and not the vertical pile. When the vertical pile is driven it creates a small void around the pile, the size of which depends on the type of soil and the details of the driven pile (Skirrow, 1991). It is assumed that some amount of arching around these voids will occur. Arching is that phenomenon in a soil which permits it to transfer load to points of rigidity (Macnab, 2002). The rigid points are considered the undisturbed soil on either side of the vertical pile below the connection point. Thus the forces that act on the relatively thin pile were ignored by not modeling contact elements along the vertical pile below the connection point.

Since the concrete cap exists above the cap retaining the soil that is backfilled after the wall is constructed, the soil-structure interaction can't be ignored. However, instead of meshing soil and contact elements for the backfill above the connection point, equivalent pressure loads were applied to the vertical pile. This reduced the amount of nodes required and was assumed reasonable since the likelihood of yielding in the top layer of backfill is small since the stresses are so small. The equivalent pressure was determined by using the coefficient of lateral earth pressure and a linearly increasing vertical stress distribution.

2.3.7 Loading

2.3.7.1 Definition of Loads in ADINA

The application of loading in ADINA is done in two parts. First the type, location, magnitude and direction of the load are defined. Then the variation of the loads with time is defined. There are various types of loading options in ADINA, those employed in this analysis included concentrated forces, distributed loads, pressures, and mass proportional loading. Concentrated forces were used to apply loads at nodal points, distributed loads are applied to beam lines, pressures were applied to edges of 2D solids (i.e. soil elements), and mass proportional loading was used to apply body forces, i.e. gravity to the model. When the loads were applied and removed was defined by specifying different time functions for the different loads. Values are defined for time points in each time function and these constants are basically multipliers for the defined loads at the specified points in time.

2.3.7.2 Assumed Loading Conditions

Working loads were selected for this analysis to evaluate the general behavior for service conditions. This represents the loads that the wall will experience during normal daily conditions. To simplify the analysis, the effects of pore pressures from groundwater were not included in the model. This was accomplished by assigning the soil parameters in terms of effective stress conditions to simulate long-term drained loading conditions. Although, the inclusion of pore pressures can be handled with ADINA, the finite element modeling will be more complex, and total stress analysis can be considered for a more specific analysis of the wall behavior.

2.3.7.3 Loads Applied to Model

The force due to gravity was defined with the mass proportional load, which acted in the negative Z direction with a magnitude of unity since this load is multiplied by the unit weight of the soil elements. Gravity was applied gradually over 10 time steps. The forces from the two tie-down anchors per frame were lumped together and applied as concentrated loads at the end of the rigid link connected to the pile frame. The magnitude was the applied force during construction per unit width of the wall. This load was applied in one step since the loading of the anchor is relatively instantaneous compared to the whole construction process.

Self weight of the steel pile was applied as a distributed line load in the Global Z direction, where the pile was meshed with 0.304 m long elements. The magnitude of the distributed load was based on the per foot weight of the beam per unit width of the wall.

For example, the HP 10x42 pile is 0.613 kN/m (42 lb/ft) and the distributed load per unit width is 0.0615 kN/m/m (4.2 lb/ft/ft). Since the pile was divided every foot, the units of the distributed load were found in both English and SI units as 0.0186 kN/m/ft. The magnitude of the distributed line load acts in the beam local S direction, but the weight acts in the Global Z direction. So the calculated weight per foot of the batter pile had to be resolved into the load perpendicular to the beam for input in ADINA. Since the batter pile local S direction is at an angle from the Y and Z directions, the Z component of the magnitude was applied to the line. The local S direction of the vertical pile is in the Global Y direction, so the magnitude of the self weight was applied as traction in the beam r direction, or in this case the global Z direction.

The magnitudes of the loads for the concrete sections were calculated based on the unit weight and the area per unit width of the wall. Along the batter pile, the concrete was 0.304 m (1ft) thick but along the top of the vertical pile it was 0.914m (3 ft) thick. The concrete load along the top of the vertical pile was applied as Z traction. The concrete load along the batter pile was handled differently. The line defining the batter pile extended from the bedrock to the connection point, but the concrete facing extended from the connection point to 1 ft below the grade. This meant the concrete load couldn't be defined by a distributed line load along the entire batter pile. Instead, the weight of the concrete was applied as nodal loads in the Global Z direction on nodes of the composite section. The portion of the vertical pile above the connection point was defined as a

separate line from the portion below the connection. The weight of the concrete was applied to that line as Z traction

Section 2.4.6 discussed the representation soil pressures at the top of the wall with pressure loading. The magnitude of the vertical pressure is the unit weight of the soil multiplied by the depth, which was 1.83 m (6 ft). The at-rest earth pressure coefficient, K_o was used to calculate the distribution of lateral earth pressures applied to the top of the wall. To define the variation of the lateral earth pressure with depth, a spatial function was assigned, so the magnitude of the load is a function of the distance along the line. The magnitude of the pressure was the unit weight of the soil times the 1.83 m depth of the backfilled layer. At the top of the vertical pile the value of the function was zero, at the bottom the function value was K_o. Table 7 summarizes the loads used for basic modeling.

Table 7 Summary of Loading for Basic Model

Load	ADINA Load Type*	Magnitude	Direction/Component
Gravity	1	1	Global -Z
Tie Down Anchor Force	2	-160 kN/m (11,000 lb/ft)	Global Z
HP 10x42 Steel Self Weight	3	0.0588 kN/m (13.26 lb/ft)	Beam Local S
HP 12x53 Steel Self Weight	3	0.07416 kN/m (16.76 lb/ft)	Global Z
Batter Pile Concrete Self Weight	3	-6.667 kN/m (1500 lb/ft)	Global Z
Vertical Pile Concrete Self Weight	3	-20 kN/m (4500 lb/ft)	Global Z
Equivalent Vertical Earth Pressure	4	-γ*Z	Global Z
Lateral Earth pressure	4	Ko*-γ*Z	Global Y
*Note 1=Mass Proportional, 2=Concentrated Nodal Load, 3-Distributed Line Load, 4, Pressure; Ko= At-rest earth pressure coefficient, z=depth, γ=unit weight of soil			

CHAPTER III

MAJOR MODELING DECISIONS

3.1 Introduction

To arrive upon an accurate model that best represents the behavior of the wall, many important decisions were made in terms of the model geometry, meshing, soil material model, and sequencing of the construction process. Comparisons of the relative effects of changes in model geometry were made to develop a model with sufficient boundary distances. In general, soil behavior is very complex so comparisons have been made between a Mohr-Coulomb elasto-plastic soil model and a simplified model linear elastic model. The construction sequence of the wall was modeled to evaluate its importance to the results of the solution and its necessity to accurately model the behavior of the wall. The mesh was refined to optimize the 900 node limit and ensure the results are independent of the meshing chosen. Finally, model results are compared to classical solutions for lateral earth pressures to verify the accuracy of the predicted results.

3.2 Model Geometry

3.2.1 Model Geometry Terminology

The purpose of this section is to determine the model geometry that will produce reliable results and optimizes the limited number of nodes. A uniform notation/terminology has been adopted to organize and describe the geometry of the model. Definitions were chosen arbitrarily, but with the goal to be as simple and straightforward as possible. The total distance from the ground line at the base of the wall to the topmost part of the wall will be referred to as the total wall height (TWH). As shown previously in Figure 2.2-2 a typical height for the top of the wall is 9.45 m (31 ft). The wall is to be constructed from the top down with an initial excavation behind the wall of 2.44 m (8 ft) as shown in Figure 3.2-1. This 2.44 m was excavated to give the contractor room to drive the batter and vertical piles and connect them. The bottom of this initial excavation is 0.61 m (2ft) below the batter and vertical pile connection.

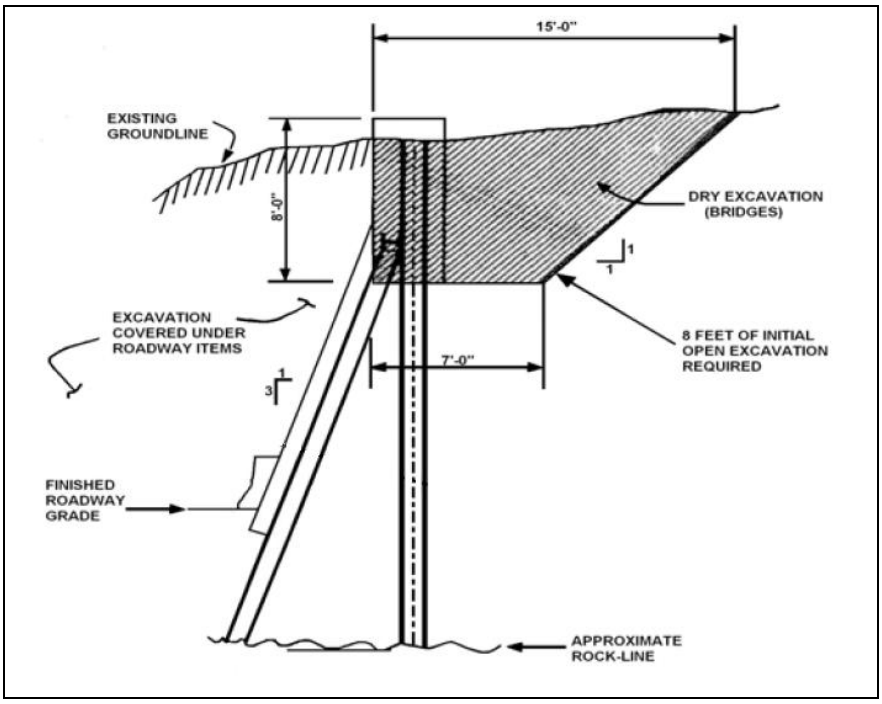

Figure 3.2-1 TDOT Specified Limits of Excavation (Pate and Haddad, 2007)

During construction, the soil on the roadway will be removed in lifts and temporary lagging installed. Thus, during construction the wall will have to support a depth of soil behind the wall from the ground line at base of wall to the bottom of the initial excavation 0.61 m (2 ft) below the pile connection point. For simplicity, the initial two feet will be neglected, so that the supported height of soil is from the ground line at base of wall to the pile connection point, which is 7.62 m (25ft) above the ground line for the typical section. This height will be referred to as the effective wall height (EWH), because it is the height of soil the wall must support during construction. The terminology as it pertains to the wall is shown in Figure 3.2-2

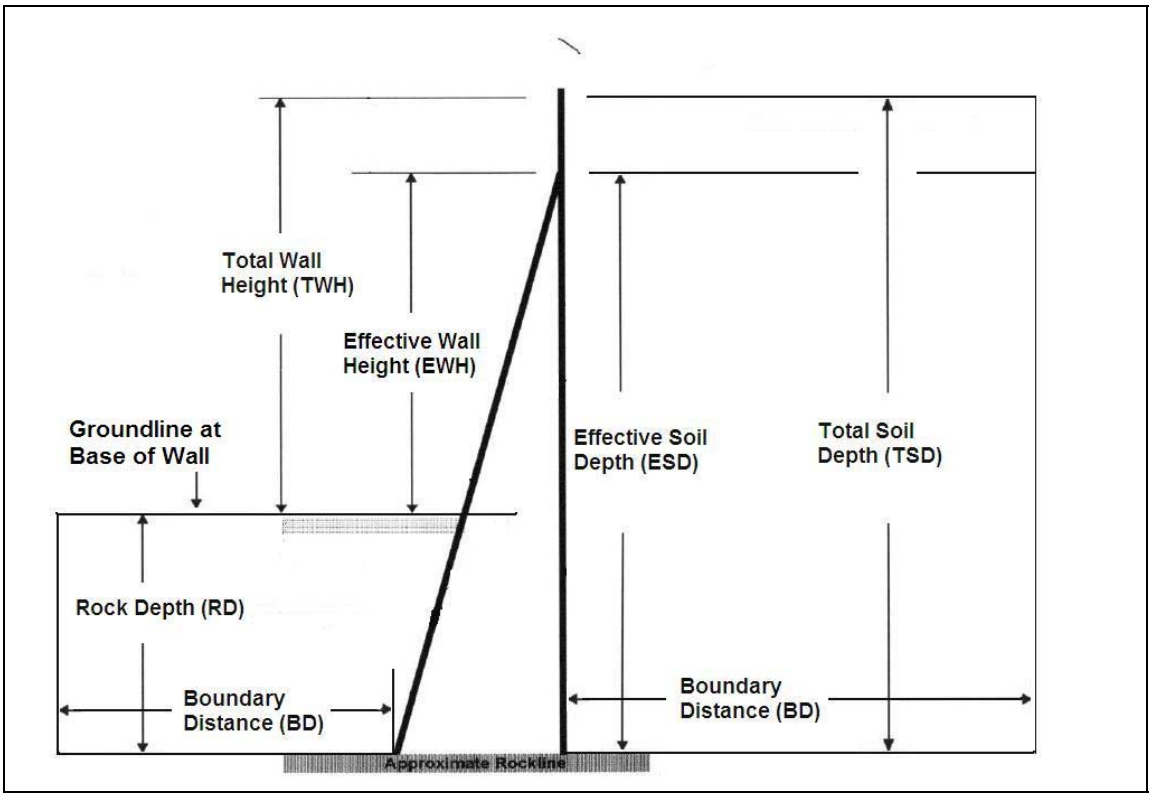

Figure 3.2-2 Explanation of Geometry Terminology

The remaining terms shown in the figure refer to the depth to rock below the ground line, the soil depth behind the wall, and the distance to the boundaries used in the numerical analysis. The rock depth (RD) below the ground line is the depth to rock that the piles will bear on. The depth of soil behind the wall that includes the EWH and RD will be referred to as the effective soil depth (ESD), and the depth that includes the TWH and RD will be the total soil depth (TSD).

3.2.1.1 Distance to Vertical Boundaries

In finite element analysis (FE), the horizontal boundaries must be sufficiently removed from the structure being analyzed so that the boundaries do not impact the results. The solution must be unique, regardless of the position of the boundaries. To evaluate horizontal boundary distances, the ESD was chosen as a reference for various boundary distances (BD), in terms of BD/ESD ratios of 1, 1.5, 2.0, 2.5, and 3. In doing so, all geometric features are related to the EWH by some coefficient. A RD of 7.62 m (25 ft) was chosen since it is much greater than the assumed 3.65 m (12ft) depth to fixity used by TDOT in their design procedure. This results in a starting ESD of 15.62 m (50ft). A model with the decisions outlined in Chapter 2 was used to evaluate the relative effects of the distance to the vertical boundaries as well as the horizontal boundaries.

3.2.1.2 Distance to Horizontal Boundary, Bedrock

Due to the fluctuations in site conditions, especially in East Tennessee, the rock depth (RD) below the finished grade is highly variable and will be varied in the FE analysis to study its effects on wall behavior. RD as a function of EWH was chosen to determine a logical range. The following RD/EWH ratios were used to study its effect and decide upon a suitable depth for further parametric studies: 0.1, .5, 1.0, and 1.5. When the RD is added to the EWH, the result is the effective soil depth (ESD), which is the depth of soil retained by the wall and the depth of soil below grade. Relating the RD to the ESD, the ratios of RD/ESD studied are 0.091, 0.333, 0.5, and 0.6.

3.2.2 Results of Geometry Study

3.2.2.1 Distance to Vertical Boundaries

The relative effects of the vertical boundary distance were considered for the lateral displacement of the wall (Δy), and vertical settlement at the boundary (Δz). The settlement a distance away from the wall was evaluated because excavations in urban environments are often monitored to limit the disturbance of adjacent structures. The results for the effect of the different model geometries are provided in Figure 3.2-3 and 3.2-4. The following conclusions were drawn:

- Based on the effects of model geometry, there is little justification to extend the mesh boundaries past a BD/ESD ratio of 2.
- BD/ESD ratios greater than two did not have much effect on Δy at the top of the wall. There was a 9.6% increase in Δy between BD/ESD=2 and BD/ESD=3 and only a 13.2% decrease between BD/ESD=2 and BD/ESD=3
- The Δz at the top right boundary was insensitive to model geometry. Δz only decreased 4.94% between BD/ESD=1 and BD/ESD=3

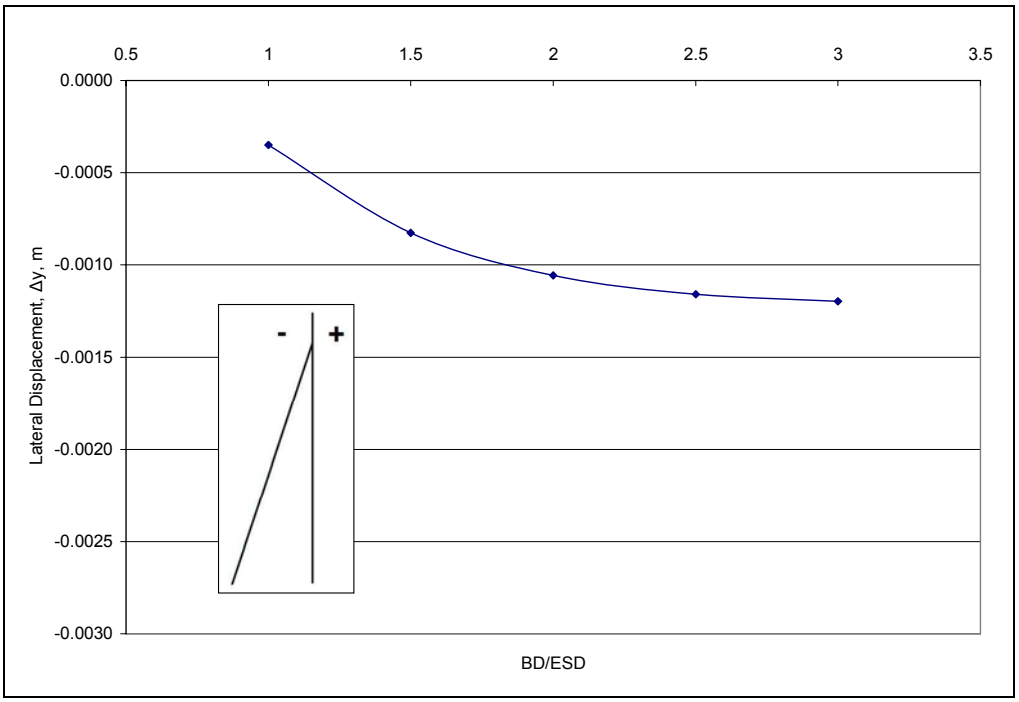

Figure 3.2-3 Vertical Boundary Distance Effect on Wall Displacement

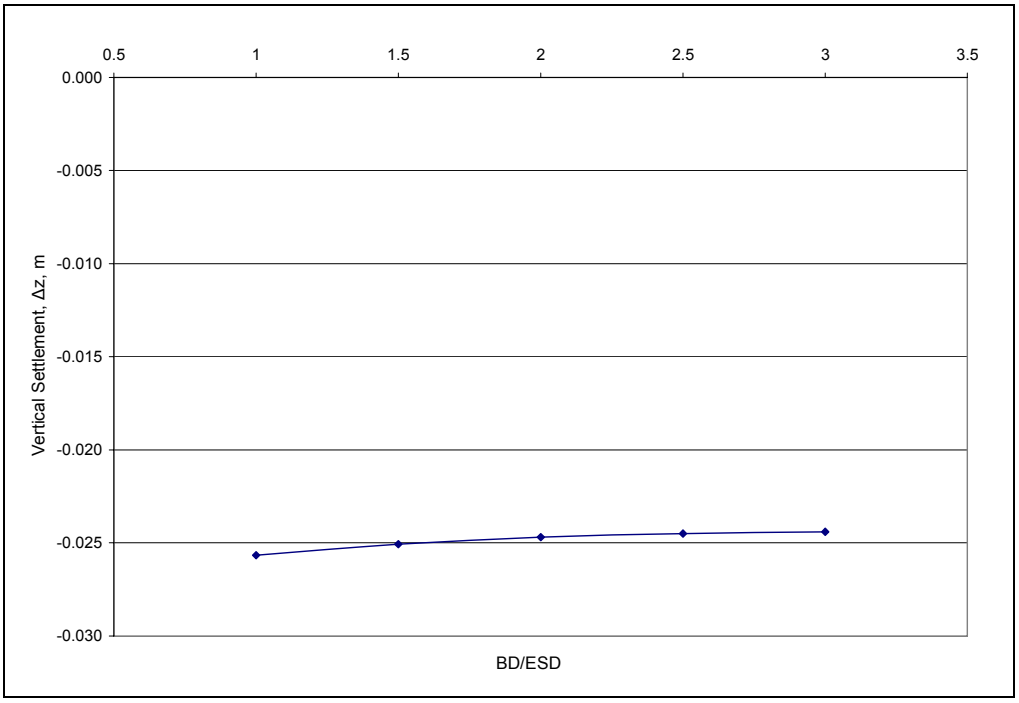

Figure 3.2-4 Vertical Boundary Distance Effect on Settlement

3.2.2.2 Distance to Horizontal Boundary, Bedrock

Since the ESD is the sum of the EWH and the RD, as the depth to rock increases, the ESD increases as well, so direct comparisons of settlement and wall movement can't be made. As the depth of the soil layer increases, the settlement will increase because there is more compressible material, resulting in misleading plots comparing Δz between different ESDs. The effective height of the pile frame is the ESD, so the frame height will increase with changes to RD. Δy of the wall under certain loading will be dependent on the unbraced height of the frame, which increases with RD. Instead, the effects of the horizontal boundary distance were only considered for the earth pressures behind the wall, since these results are most important to the behavior of the wall. The BD/ESD ratio of the models was held constant at 2. The effect of the different model geometries are provided in Figure 3.2-5. The following conclusions were drawn:

- The earth pressure distribution was relatively consistent over the lower 1/2 of the wall and below grade line for all RD/ESD ratios.
- The differences in pressures near the top are due to increased settlement with rock depth which creates large gaps between the soil and the wall. This reduces the pressures between the soil and wall.
- A RD/ESD ratio of 1 would limit the amount of contact lost behind the top of the wall, while allowing the TDOT assumption of 3.65 m (12 ft) depth to fixity to be evaluated for any EWH greater than 3.65 m.

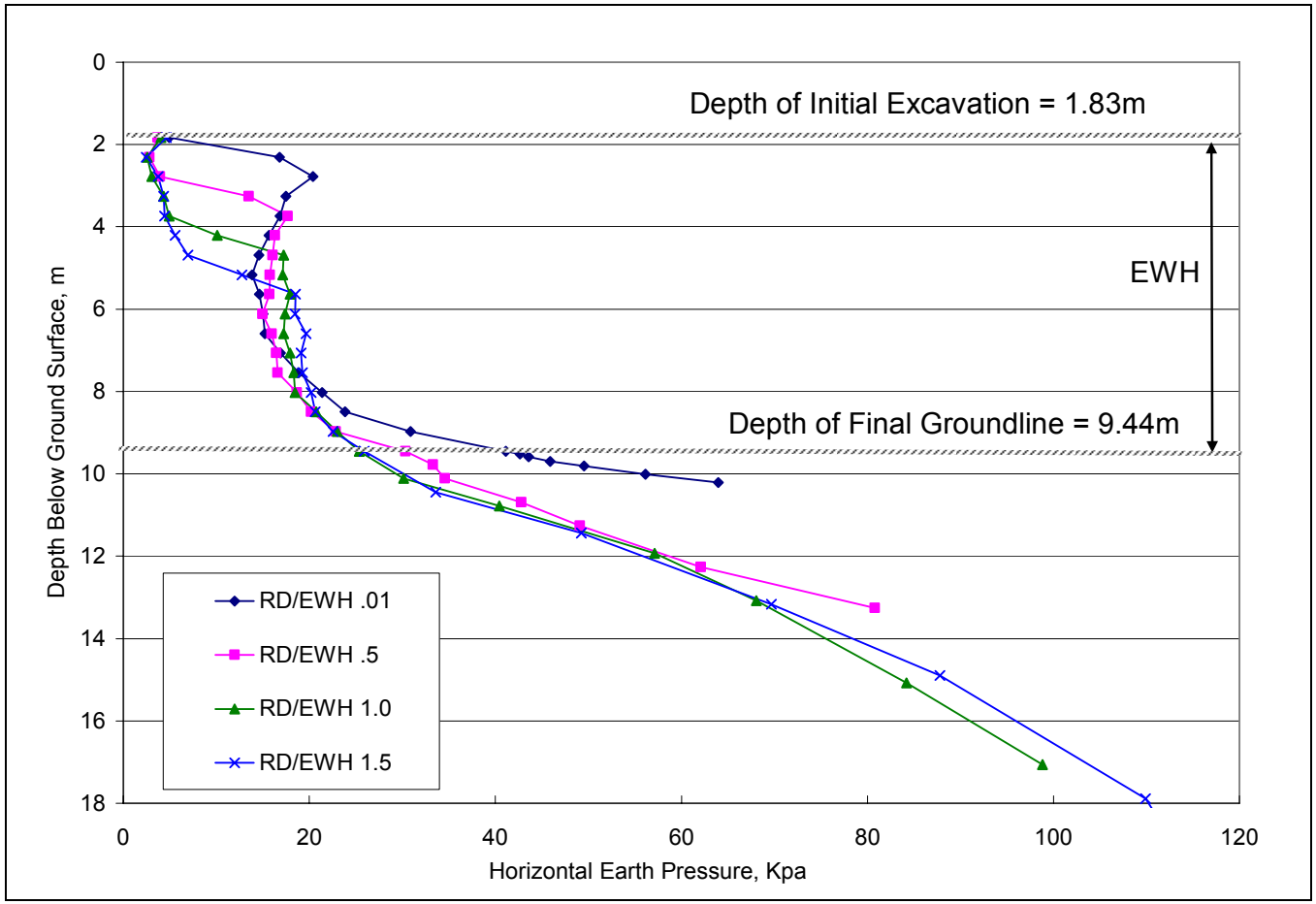

Figure 3.2-5 Effect of Model Geometry on Lateral Earth Pressures

3.2.3 Selected Model Geometry

From the results of the previous section the selected BD/ESD and RD/ESD ratios were 2 and 1 respectively. For any wall height modeled, setting the boundary distances according to these ratios will provide reliable results. Based on a typical wall section, the EWH was 7.62 m (25 ft), resulting in vertical boundaries 30.5m (100 ft) to the right of the vertical pile and left of the base of the battered pile. This also results in a RD of 7.62 m, and an ESD of 15.4 m (50.5 ft). Figure 3.2-6 shows a meshed model with the selected geometric relationships. The general behavior of the initial model is illustrated by 3 plots, the deformed shape, a plot of the lateral earth pressures, and internal force diagrams of the pile frame. These are provided in Figures 3.2-7 – 3.2-9, respectively.

Figure 3.2-7 shows that the soil behind the top of the concrete facing settles down and away, explaining the low earth pressures in that area. The deformed shape of the pile, magnified 280 times, suggests that the majority of the lateral yielding occurs just above final grade. The band plot of horizontal stresses shown in Figure 3.2-8 agrees with Figure 3.2-5 in that the maximum pressure behind the concrete facing is approximately 20 kPa. The shear and bending moment diagrams of Figure 3.2-9 support the assumption that the reactions in the vertical pile below the connection point are insignificant compared to the forces developed in the stiffer composite sections. The shear force in the vertical pile above the connection point is substantial, but since it has a greater capacity then the batter concrete facing, the assumption to neglect forces there is reasonable.

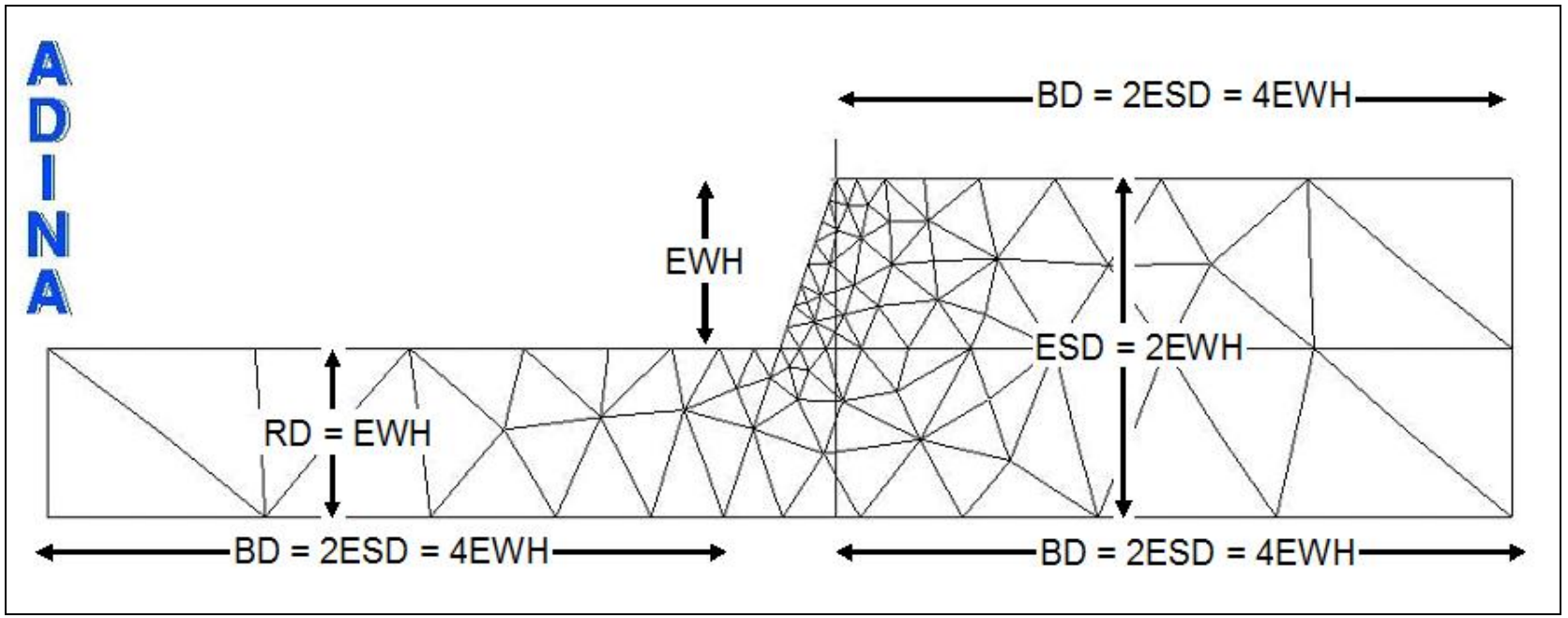

Figure 3.2-6 Typical Mesh with Selected Geometry

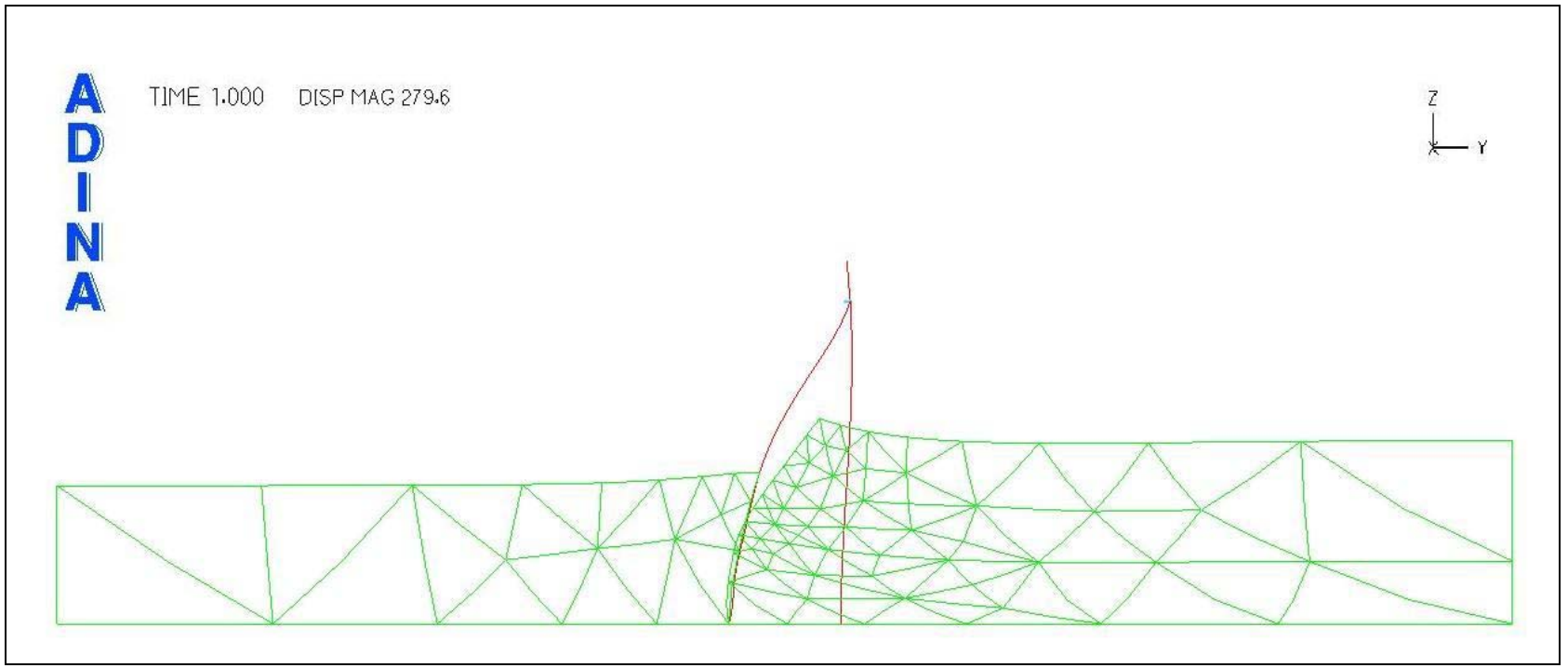

Figure 3.2-7 Deformed Shape for Selected Geometry with Linear Elastic Soil

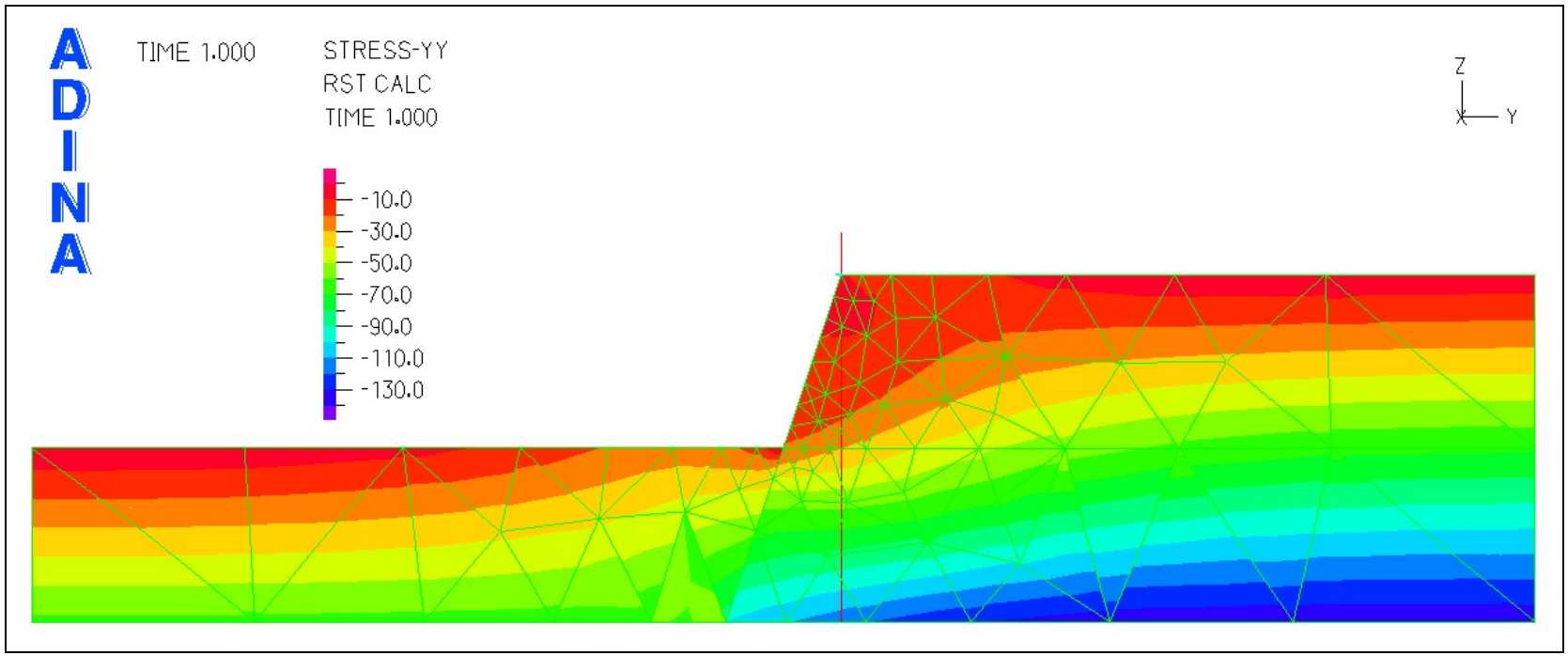

Figure 3.2-8 Lateral Earth Pressure Behind Concrete Facing for Selected Geometry

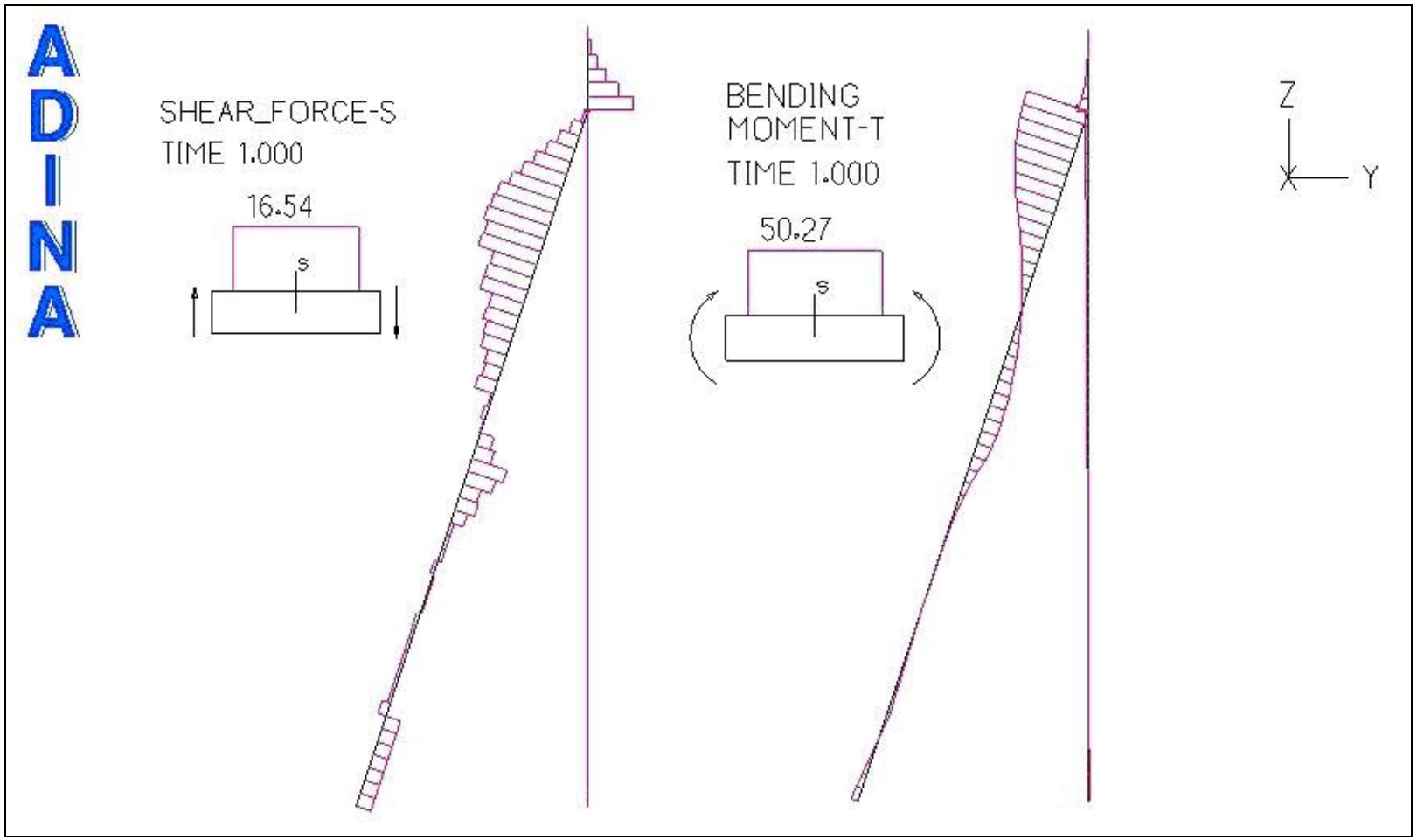

Figure 3.2-9 Shear and Moment Diagrams in Pile Frame with Selected Geometry

3.3 Mohr-Coulomb Soil Model

All results thus far have been for a model with linear elastic soil elements. To evaluate this choice of models, soil elements were switched to the Mohr-Coulomb (MC) model provided in ADINA. The MC model introduces the theory of plasticity to the soil material. Plastic strains increase under a constant stress and are irreversible. In the MC model plasticity begins beyond initial yielding. The yield criterion is defined by a failure envelope of the shear strength, τ, discussed previously:

$$\tau = c + \sigma \tan \phi$$

The MC strength criteria are highly dependent of the stress history of the soil. If the soil is initially unstressed, it may reach failure due to a small increase in shear stress. Where as if soil is initially high normal stress, a large change is shear stress is required to reach failure. Therefore it is not enough to use the MC to represent soil without accounting for the geostatic stress due to gravity, because failure will be reached in the model, when in reality the soil wouldn't fail. The linear elastic model is sufficient in loading the soil from zero because the elastic model doesn't have strength criteria like the MC model and the end result is independent of the stress history or time variation. The strength criteria in the MC model make the stress variation with time very important. To model the wall at its final stage, the stress variation with time must be accounted for, meaning the model must progress from the soil under only geostatic stress through all changes during construction.

The first two walls were built at sites with different soil conditions. To include a range of possible soil conditions that may be encountered the soil conditions at the first two sites were modified to create a more inclusive range of soil properties. The soil conditions were used to create two different models, whose results would represent wall behavior for a wide range of soil conditions. The first soil case is a clay type soil with a high cohesion and low internal friction angle, based on the soil conditions at the West Hills project, Site 1. The second soil case is a silty-sand type soil with low cohesion and a high friction angle, typical of the SmartFix project, Site 2. The silty-sand type material attempts to represent cohesionless materials, because modeling a true cohesionless material was impractical. The MC material model has difficulty converging when very low values of cohesion are input. In order to reduce problems of convergence, a relatively low cohesion value was adopted to represent cohesionless materials.

The Poisson's ratio of the soil, ν, controls the lateral deformations of the soil material in ADINA, whereas it is typically represented by the coefficient of lateral earth pressure, K_o, in soil mechanics. In the MC model in ADINA, K_o, is not defined explicitly. In order to do so, the Poisson's ratio was back-calculated from K_o using the following equation:

$$K_o = \nu / 1 - \nu$$

The coefficient of lateral earth pressure for the soil was determined by the friction angle, ϕ, with the Jaky equation as follows:

$$K_o = 1 - \sin\phi$$

The WH soil was assigned a value of ϕ =20°, and the SF soil was given a higher value of ϕ = 32°, corresponding to K_o values of 0.470 and 0.658 respectively. From these friction angles the calculated Poisson's ratios for the WH and SF soils were, 0.397 and 0.320 respectively, falling within the range of typical values from the literature. The SF soil was used to compare the linear elastic and MC models and, comparisons of wall behavior for both soil types are carried out in Chapter 4. Material parameters for the two soils are provided in Table 8

Table 8 Mohr-Coulomb Model Parameters for Two Representative Soils

Property	**Symbol**	**Value**
SmartFix (SF) Soils		
Elastic Modulus, kPa (psf)	E_{sl}	71,820 (1,500,000)
Poisson's Ratio	ν	0.32
Total Unit Weight, kN/m^3 (pcf)	γ	17.29 (110)
Internal Friction Angle	ϕ	32
Cohesion, kPa(psf)	C	4.78 (100)
Tension Cut-off, kPa (psf)	T	2.39 (50)
Dilatation Angle, degrees	Ψ	1
West Hills (WH) Soils		
Elastic Modulus, kPa (psf)	E_{sl}	71,820 (1,500,000)
Poisson's Ratio	ν	0.397
Total Unit Weight, kN/m^3 (pcf)	γ	17.29 (110)
Internal Friction Angle	ϕ	20
Cohesion, kPa(psf)	C	23.94 (500)
Tension Cut-off, kPa (psf)	T	11.97 (250)
Dilatation Angle, degrees	Ψ	1

Two additional properties are involved in the definition of the MC model, dilation angle, Ψ, and Tension Cut-off, T. When using the MC model, the volume dilatancy due to shearing is only governed by the dilation angle (ADINA 2006). Dilatation in soil is the change in volume due to shear deformations caused by stress changes. One example is a dense sand that when compressed in one direction, will increase in volume (Lambe and Whitman, 1968). According to ADINA, a dilatation angle smaller than the friction angle is specified to reduce large material dilatation. For the purpose of analysis, the dilation angle was set to 1°, to eliminate the effects of material dilation. The tension cut-off accounts for the low tensile resistance of soils. Stress states in excess of the specified tension cut-off are not possible and the material will have reached tension failure. The tension cut-off value T is three times as large as the tensile strength of the material (ADINA, 2006). Defining the tensile strength of soils is difficult, so for analysis purposes, the T value was set to half of C. In some models, tension yielding created convergence problems so the T value was set to C.

3.4 Excavation Simulation

3.4.1 Construction Sequence

TDOT specified two sequencing options for the construction of the concrete facing. Option 1 consists of two general steps. First, place reinforcement and pour the concrete for the top eight feet of the wall. Secondly, excavate soil in 2.13m (7 ft) lifts, placing

reinforcement and shear studs on batter pile, apply shot crete in 1.52 m (5 ft) lifts to the bottom of wall stopping 0.46 m (1.5 ft) below bottom of wall. The first steps in Option 2 are to excavate soil in 1.52 m lifts placing wood lagging between batter piles, then apply shear studs to batter piles. Secondly, place reinforcement for top 2.43 m of the wall then pour concrete. The first wall built at the West Hills site was built with the second option, and the same contractor constructed the second wall and employed this same option. For the purpose of analysis, the second option sequence was simulated in this study. Figure 3.4-1 is a photo of the wood lagging during construction.

3.4.2 Modeling Construction Stages

3.4.2.1 Application of Gravity

The same geometry of the linear elastic model was used as a starting point. However, to get the soil state of stress equal to the geostatic stress, for the elements in front of the wall, soil elements were meshed to create a level surface across the entire model at the level of the initial excavation as discussed in Section 2.2. The stress in the soil before construction is actually based on the TSD so a uniform pressure was applied along the top of model to represent the pressure from the initially excavated soil. Gravity and the pressure load were applied over 10 steps to induce the geostatic stress in the soil. The piles elements were present in the model from time zero. In order for the piles to deform with the soil due to gravity, the steel was given a small modulus. This would create direct contact between the soil and pile, as if the piles were driven into the soil.

Figure 3.4-1 Construction Photo of Wood Lagging (Courtesy of Saieb Haddad)

The stress distribution in a soil mass by itself due to gravity would increase uniformly with depth and the soil would deform straight down. If a pile frame with zero modulus is present in the soil mass, the piles frame would be expected to deform straight down with the soil. Since the piles could not be assigned a zero modulus, the results at the end of gravity application were not quite perfect; however, the slight imperfections were small enough to be neglected. Figure 3.4-2 shows typical results of vertical stress distribution in the soil. The vertical stress distribution increased almost uniformly with depth, with the exception of a few zones of irregularity near the base of the batter pile which was fixed. This was attributed to the piles having a small value of stiffness that affected the deformation and stress in the soil.

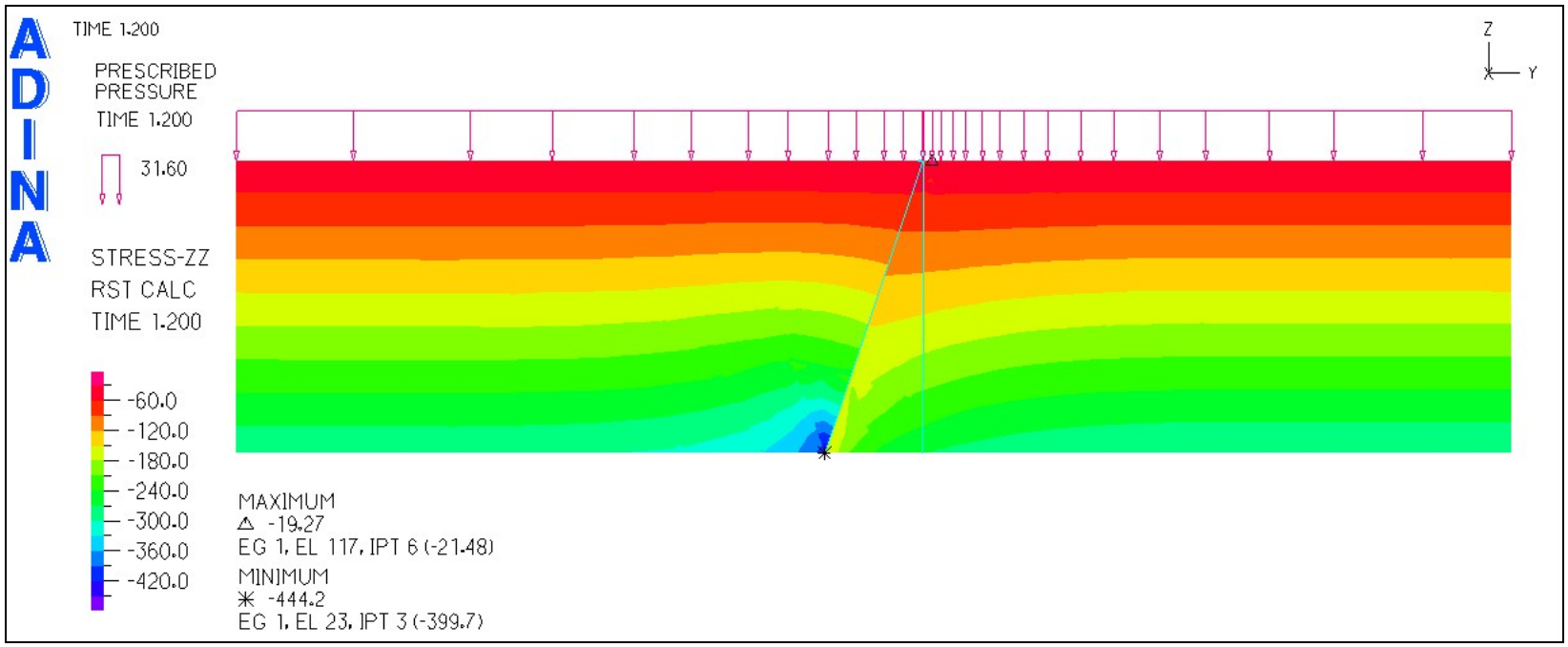

Figure 3.4-2 Vertical Distribution of Stress after Gravity Application

The deformed shape of the pile frame magnified by a factor of 156 is shown in Figure 3.4-3. The pile frame displaced to the left suggesting that the weight of the soil above the battered pile forced the frame to the left. Ideally the pile frame would be undeformed and the vertical pile would be plumb, however, the irregularity of pile driving will make it impossible to construct a perfectly vertical frame. The displacement at the pile connection point was only 0.011m (0.436 in), which is primarily due to the modeling approximation. This deformation due to gravity was neglected, since all deformations due to construction were taken relative to the stage after the anchor load is applied.

3.4.2.2 Restart Analysis for Construction Sequence

With the geostatic stress in the soil, the restart analysis option was used so that model inputs could be updated and a new analysis performed. The restart option is used to continue an analysis beyond its previous end point, or change the analysis type, loads, or boundary conditions or tolerances (ADINA, 2006). In addition, model geometry cannot be changed but time function and time increments can be changed. The results from the gravity application file are appended to the new file using restart.

In the second analysis, time functions are updated to start at the time of the end of the first analysis and include the excavation sequencing and load increments. Next, the modulus of the steel is changed back to the correct value for steel. Then the cross sections were updated to include the portions of the wall that have composite properties. Although the composite section does not reach full rigidity until the concrete hardens,

this construction detail was neglected, and the composite properties were present before excavation commenced. In reality the soil is excavated and wood lagging is placed between the frames to serve as temporary support. So the rigidity of the wall during excavation is between the rigidity of the temporary support and the rigidity of the steel composite section. This assumption is relevant considering the fact that construction details can never be exactly simulated due to the variability in construction practices and the amount of time the soil is unsupported relative to the time it takes for maximum pressures to develop

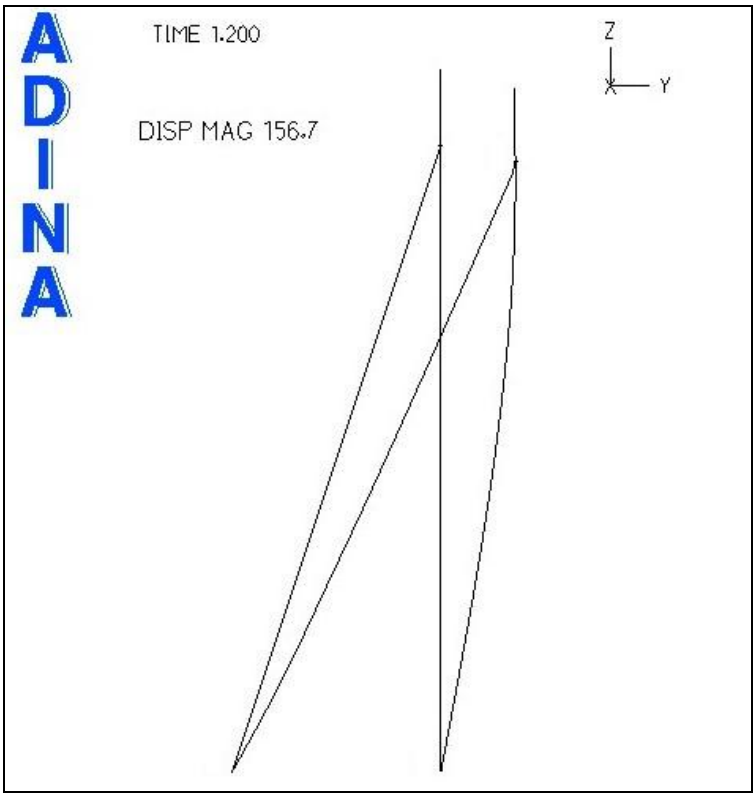

Figure 3.4-3 Deformed Shape of Pile Frame due to Gravity Application

The first step of the analysis was the removal of the pressure load along the top of the model to simulate initial excavation. The analysis is restarted with no pressure along the top so that the restart analysis begins at the point where the top of the soil is excavated and the piles are already driven. The removal along the entire top is another deviation from TDOT's specified construction sequence, which calls for a minimal amount of soil excavated for pile installation. To simplify analysis this excavation detail was neglected, considering the fact that the contribution of stresses from the top 2.43 m (8 ft) of soil aren't as significant as all the soil below ground. Since the restart analysis begins at the stage when the piles are driven and connected, the self weight of the steel members was fully applied when the restart analysis began. The forces from the two tie-down anchors per frame are applied in the first time step. In reality, the anchor forces are applied to the anchors on either side of the frame one at a time, which creates some bending in the direction of the longitudinal axis of the wall. The plane strain approximation doesn't consider deformation along the longitudinal axis, so the forces were applied at the same time. At this stage, the frame is connected and the anchor force is applied, thus was chosen as the reference point to relate all displacements due to construction.

After the anchor was applied, excavation of soil in lifts from the top down was performed by removing elements from the model with the death option in ADINA. Elements can be removed at the specified time of death, individually or by entire element groups. The excavation of the 7.6 m (25ft) typical wall was carried out in four lifts of 1.9 m (6.25 ft), to match the 7 ft lift height specified by TDOT. The four lifts were meshed as four

separate geometry surfaces and four element groups with the same properties. By doing so the element groups were given different death times to remove all the elements of the lift at the same time. The different lifts are illustrated in the rendered mesh of Figure 3.4-4. The different colors represent the different element groups, the green group outlined in bold represents the soil not excavated and the four different colors represent the four lifts over four time steps.

After the lifts were removed, the load from the wet concrete poured into the forms was applied to the piles. The loads along the batter were applied in one step simulating pouring of the concrete the full height of the wall, and then the loads for the cap at the top of the vertical pile were applied. The last stage in the construction sequence was the simulation of the backfill of the top layer of soil. The pressure load was reapplied to the top of the soil, along with the lateral component applied to the top of the vertical pile that increased with depth. The construction sequence is summarized in Table 9.

Table 9 Construction Sequence Summary

Step	Load	Construction Process
1	Self Weight of Steel Piles	Top Soil Removed
2	Anchor Force Applied	-
3-6	-	Soil Removed in 4 Lifts
7	-	Prepare for Concrete Pour
8	Weight of Concrete Facing Above grade	-
9	Concrete Weight on Top of Vertical Pile	-
10-11	Weight of Backfill	Backfill in 2 Lifts

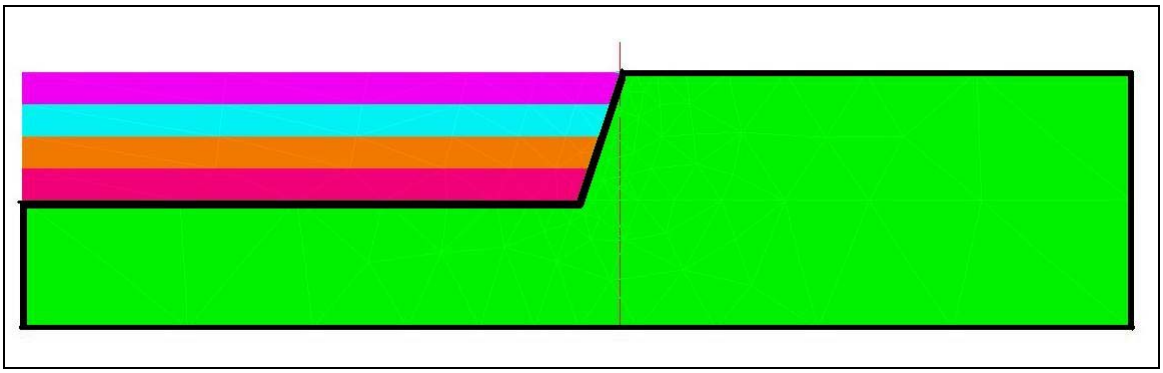

Figure 3.4-4 Soil Element Groups Removed in Excavation Sequence

3.5 Discussion of Results with Model Improvements

The behavior of the wall model with Mohr-Coulomb (MC) and the construction sequence can be illustrated by examining the same three plots used to evaluate the linear elastic soil model, along with a plot of the MC yield zones. The results from the advanced model were significantly different than the model with linear elastic soil and no construction sequencing. The deformed mesh of Figure 3.5-1 reveals double curvature in the batter pile with lateral movement into the soil just above toe of the concrete facing. The lateral movement explains the large horizontal stresses above the toe as seen in Figure 3.5-2. Figure 3.5-3 shows the double curvature of the pile increases the shear and moments above the toe, as well as showing that the forces in the vertical pile are not important. These differences in frame behavior make the inclusion of the construction sequence necessary. As seen in Figure 3.5-4, the presence of soil yielding near the top of the wall, proves the necessity of the MC soil model to accurately evaluate the soil-wall behavior.

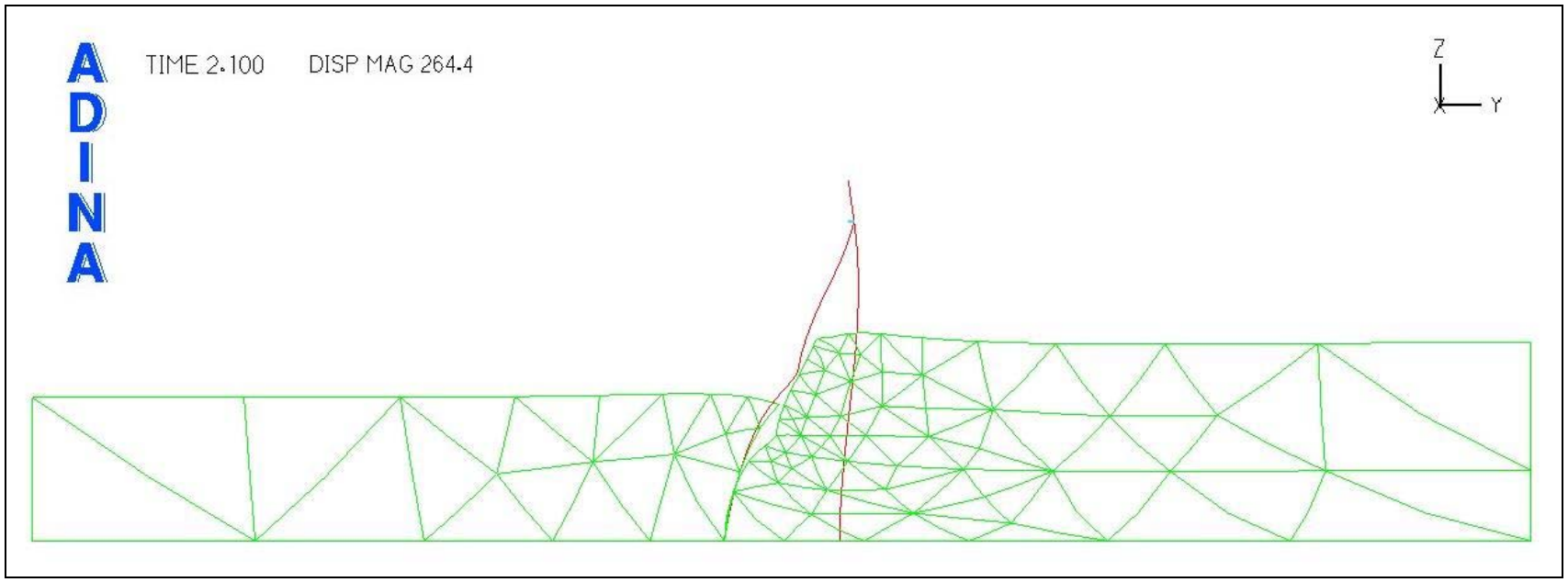

Figure 3.5-1 Deformed Shape of Mohr-Coulomb Soil Model due to Construction Sequence

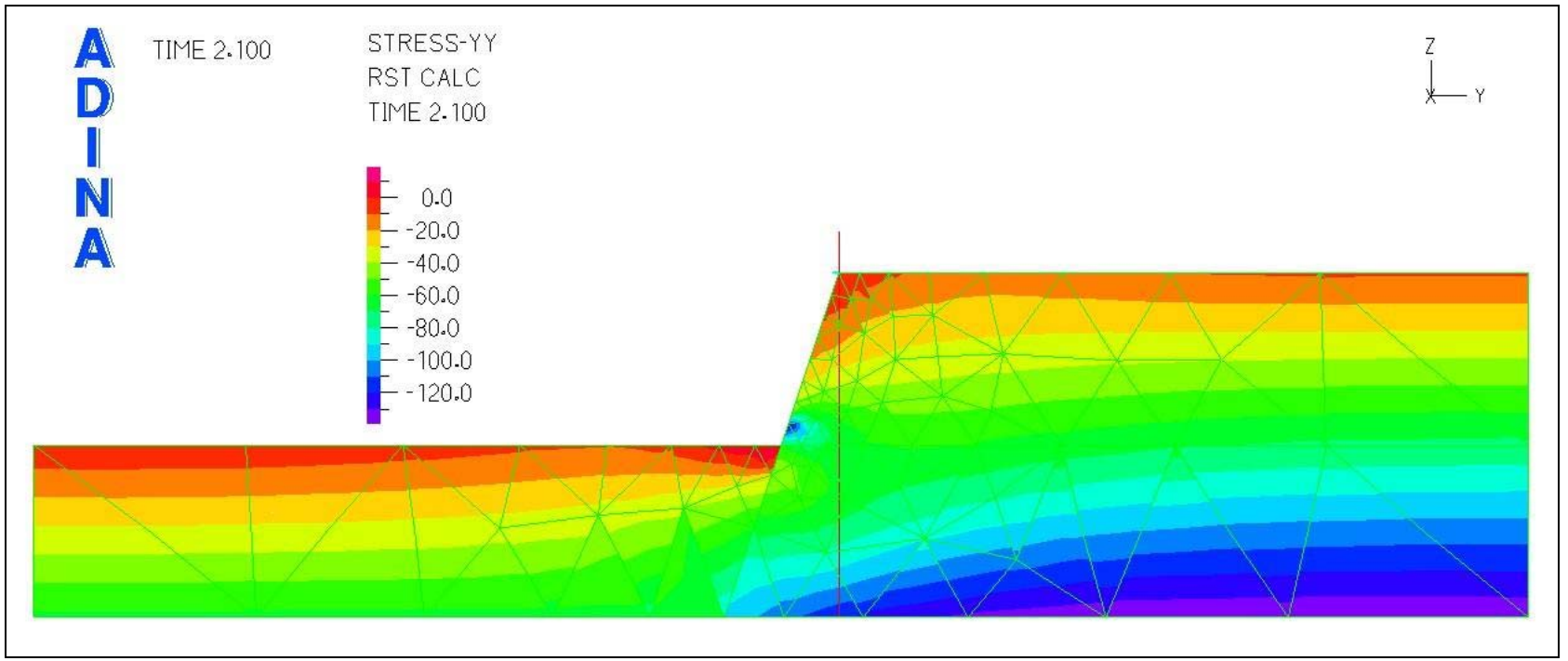

Figure 3.5-2 Lateral Earth Pressure Behind Concrete Facing for Advanced Model

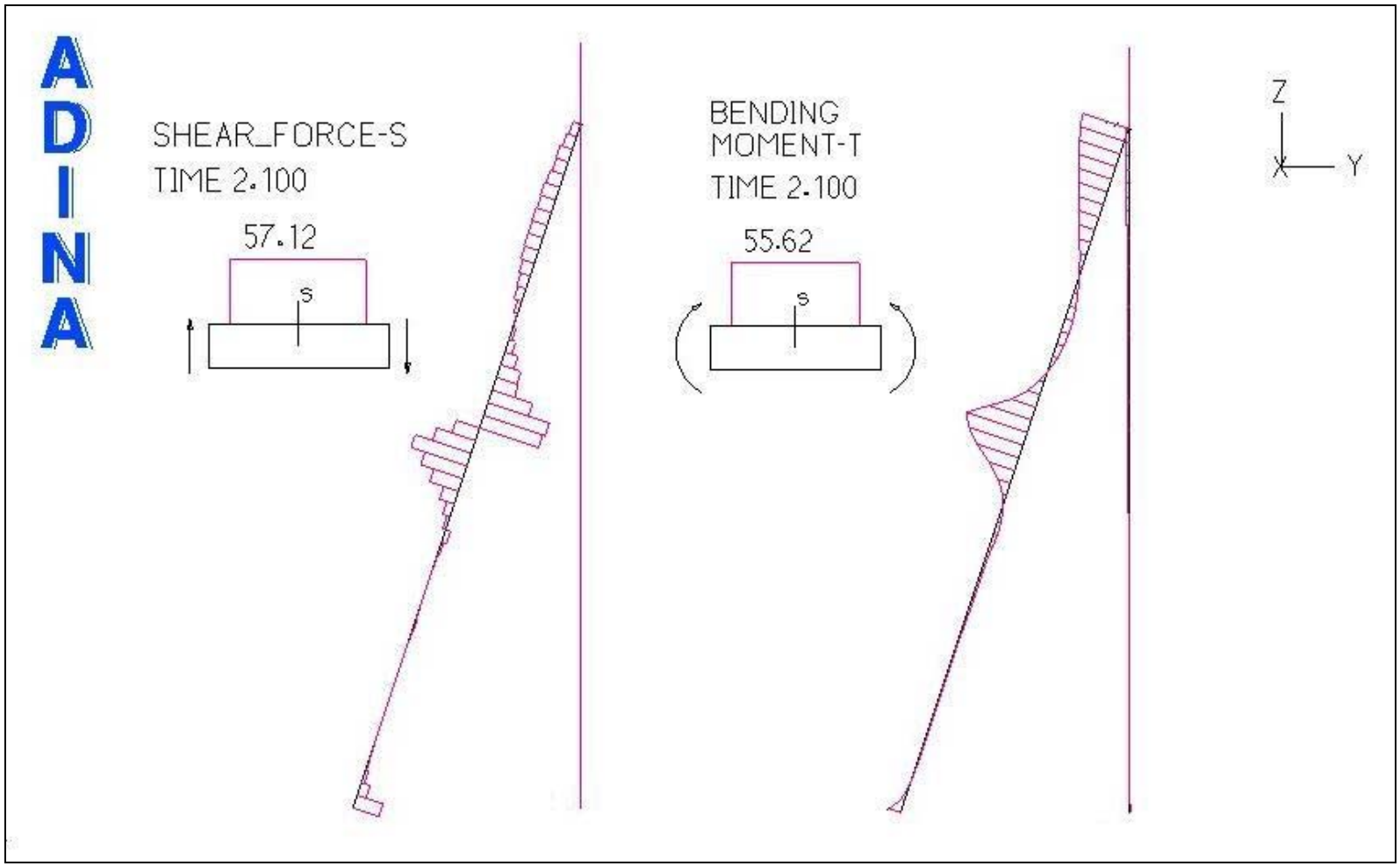

Figure 3.5-3 Shear and Moment Diagrams for Advanced Model

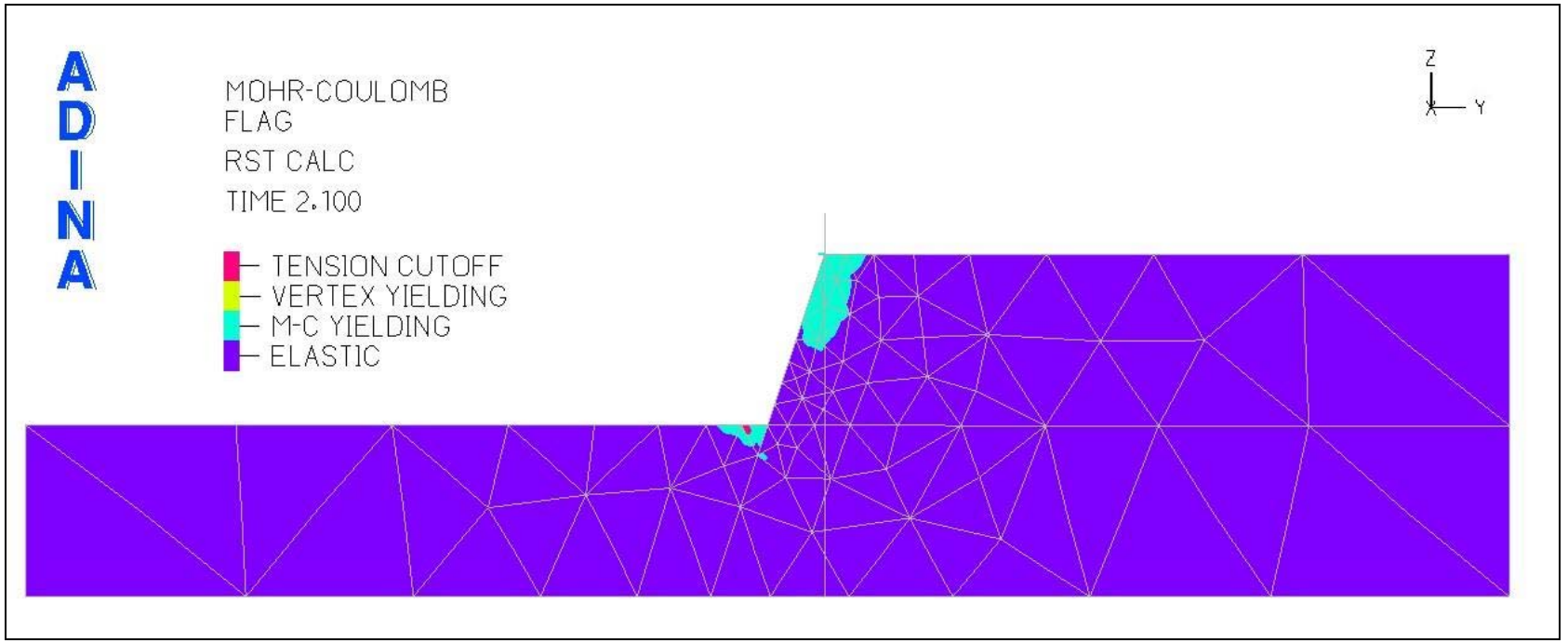

Figure 3.5-4 Mohr-Coulomb Yield Zones

3.5.1 Simplified Analysis of Pile-Frame

The high localized pressure above the toe was not what is predicted from conventional earth pressure theory. Therefore, a simplified analysis of only the pile frame elements was conducted. The main objective of the simple analysis is to reproduce the general behavior of the full model to prove its validity in terms of the distribution of earth pressures, not to exactly reproduce the results. The general behavior of the wall is a result of the construction sequence. Prior to excavation there is soil on either side of the batter pile which has equal horizontal and vertical stress. The anchor load is applied to the frame causing internal forces in the frame. Next excavation of soil in front of the pile removes support from soil on that side of the pile causing the wall to deflect in the direction of soil removal. The excavation is conducted in lifts so the unexcavated soil still provides lateral support, thus the pile is relatively fixed with respect to the unsupported length of the pile. This abrupt change in boundary condition creates high shear forces in the pile at the level of the top of the unexcavated soil. This large shear force causes the pile to deform into the retained soil and creates local bending in the direction of the retained soil. The bending produces the double curvature in the pile which was found in the deformed shape. The high lateral deformation of the pile into the soil produces the high lateral stress in the soil zone just above the toe.

The simplified model was created to match the full model closely, but not exactly. The same boundary conditions for the full model at the base of the frame were used in the simple analysis. Since the SmartFix soils used for the advanced model have a low value

of cohesion, the soil pressures acting behind the wall were applied with an increasing distributed line load equivalent to Coulomb's active earth pressures for cohesionless soil. The soil pressures were applied over three time steps to simulate the gradual increase in gravity like the full model. Spring elements were used to represent the soil supports along the front side of the pile. Spring elements have stiffness in one degree of freedom, in this case, perpendicular to the beam. The anchor load was applied after earth pressure application. After the anchor loading, excavation of soil occurred in one step by removing the soil springs along the height of the wall, while leaving the soil springs for the soil below grade in front of the wall. Undeformed and deformed shapes of the model with loading and spring elements are provided in Figure 3.5-5. Figure 3.5-6 shows the shear and moment diagrams for the pile frame.

The deformed shapes show that the pile deflects outwards above grade where support was removed. More importantly, the shape of the shear and moment diagrams agree well with the diagrams of the full model, supporting the result that the removal of soil supports creates large shears and moments at the new location of support. The differences in magnitude between the simple model and full model are a result of the simplifications adopted and the differences in modeling.

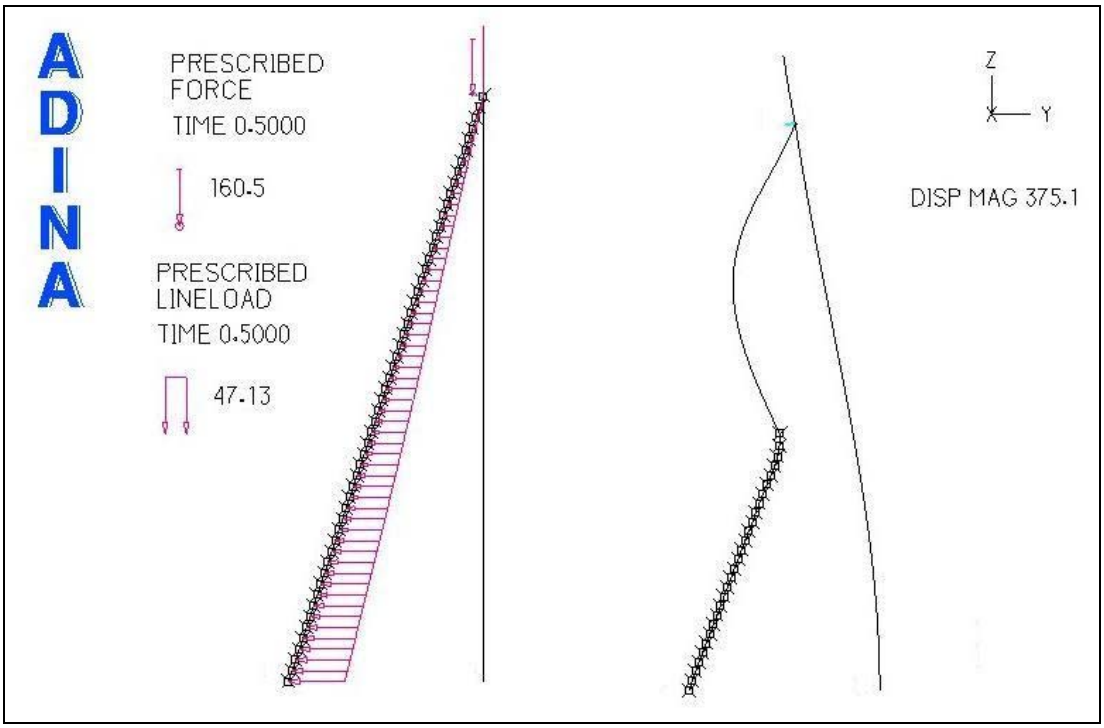

Figure 3.5-5 Simple Frame Analysis Undeformed and Deformed Shapes

The limitations of the simplified analysis include the approximation of the lateral earth pressures, the imperfect use of spring elements, and the simplification of the construction sequence. The simplified distribution of load applied to the pile increased linearly with depth according to classical earth pressure theory, but this was not exactly as predicted by the full model. The pressures on the wall affect the shear in pile, so differences in pressure will result in different shear diagrams. In reality, the stiffness of the soil increases with depth, but it would be too complex to model the spring elements accordingly. Therefore, one value of spring stiffness was assigned the entire length along the batter pile. The excavation was modified since only one removal of support was necessary to illustrate the effects of support removal on the behavior of the pile.

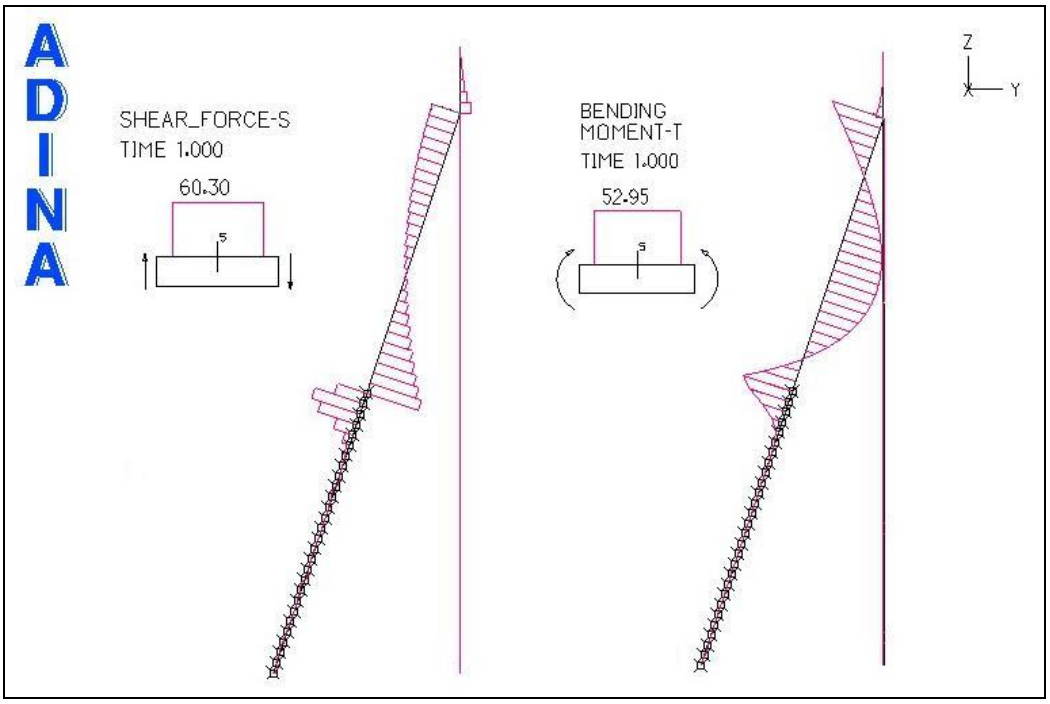

Figure 3.5-6 Simple Frame Analysis Shear and Bending Moment Diagrams

3.6 Comparison of Linear Elastic and Mohr-Coulomb Model

As previously shown, results from the linear elastic model are very different from the advanced model with excavation. Table 10 compares several results from the two models. The top deflection for the linear elastic model was taken as the deflection at the final solution time, whereas the deflection for the MC was taken relative to the stage after gravity and the anchor force was applied. A negative value of the displacement means movement away from the soil. The maximum positive moment represents bending that causing compression on the side of the wall facing outwards.

Table 10 Comparison of Linear Elastic and Mohr-Coulomb Model Results

Result	Linear Elastic	Mohr-Coulomb
Δy at Top of Wall, m	-1.06E-03	-1.36E-02
Δz at vertical boundary, m	-2.47E-02	-2.45E-02
Maximum Moment , kN-m/m	50.27	60.4
Maximum Shear, kN/m	16.54	56.7

In the MC model the maximum moment occurred in the middle of the wall near the grade. The maximum moment in the linear elastic model occurred at the top of the batter pile at the frame connection, where the anchor is applied. The large moment is due to the anchor force applied with some eccentricity. The magnitude of the maximum shear is much larger for the advanced model. These differences prove quantitatively, that the simple linear elastic model is not adequate in modeling the behavior of the wall.

To further investigate the accuracy of the predicted localized stress just above the grade, the construction sequence was simulated with a linear elastic soil. For a linear elastic model changes due to loading and unloading are recoverable and thus superposition is valid. Using a LE model with construction resulted in almost identical results as with the MC soil model. Thus, the localized behavior near the toe is not dependent on the soil model. Figure 3.6-1 shows the distribution of earth pressures along the entire batter pile for the three models discussed, revealing that the LE model without excavation fails to predict the large stress increase at grade. Since the MC model predicted soil yielding near the top of the wall, the MC model will be used with excavation for all subsequent analysis to most accurately evaluate the behavior of the pile-framed wall.

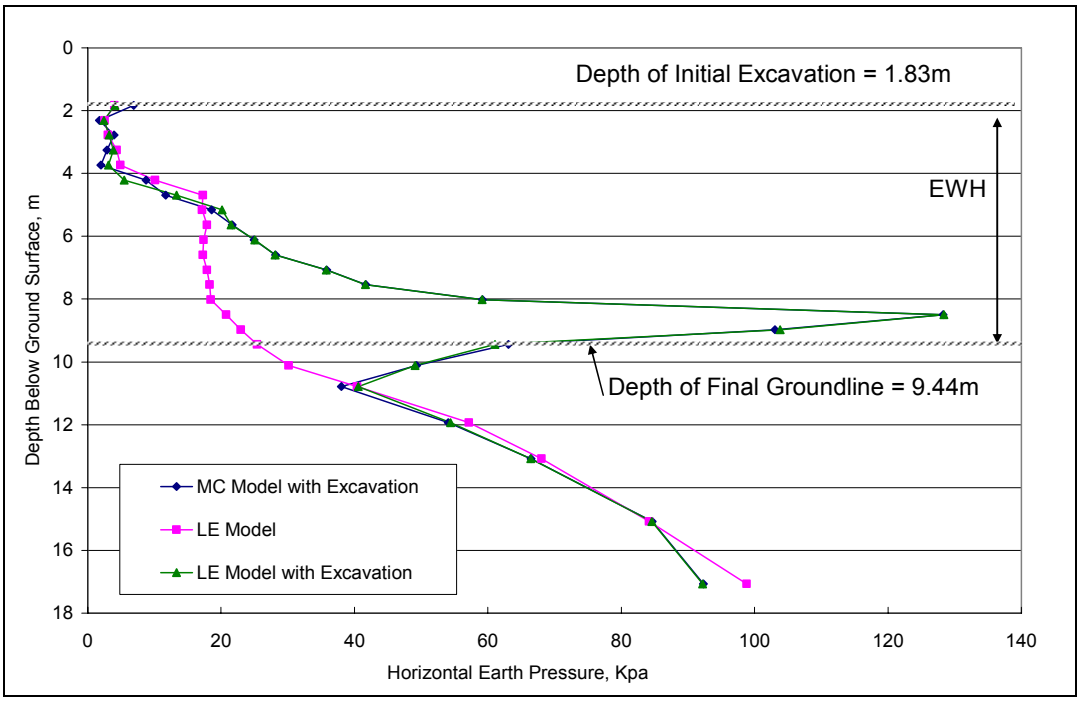

Figure 3.6-1 Effect of Model Type on Earth Pressure Distribution

3.7 Mesh Refinement of Mohr-Coulomb Model

The wall model used 723 nodes and 292 elements. To verify that the meshing was sufficient and not dependent on the number of nodes used, one stage of mesh refinement was carried out. The refined mesh used 855 nodes of the 900 available nodes with an increase of nodes near the wall. The results from the refined mesh were not significantly different; Figure 3.7-1 shows negligible differences to the earth pressure distributions. As a result, the mesh with 731 nodes was used for subsequent analysis since it will slightly reduce computation time and file sizes without compromising results.

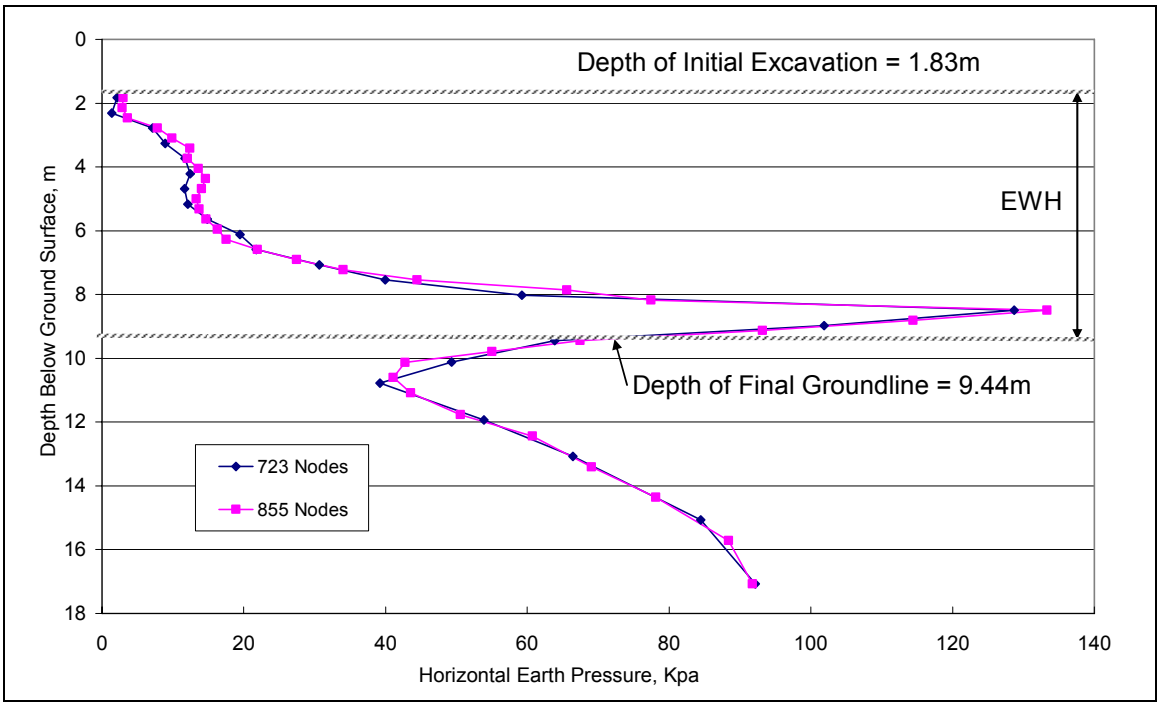

Figure 3.7-1 Effect of Mesh Refinement on Earth Pressures

3.8 Verification of Results

3.8.1 Classical Earth Pressures Estimations

The three common conditions for lateral earth pressure are at-rest condition, active, and passive. These conditions are based on the assumptions that the soil is homogenous and isotropic, the wall is very long, the soil extends back a long distance, and the soil is drained so no pore pressures are present. These methods are widely accepted for predicting earth pressures applied to retaining structures. Results from ADINA are compared to classical estimations to validate the accuracy of the model.

3.8.1.1 Rankine Pressures

Rankine developed the following equations for the coefficient of active, K_a and passive, K_p, earth pressure for cohesionless soils for a level ground surface:

$$K_a = \tan^2 (45 - \phi/2)$$

$$K_p = \tan^2 (45 + \phi/2)$$

For soils with cohesion there exists a maximum height that a vertical cut in the soil will support itself due to the inherent bonding forces. This height is referred to as the Critical Height, H_c, which is determined with the expression:

$$H_c = \frac{2c}{\gamma\sqrt{K_a}}$$

For a wall of height H, if $H < H_c$, the wall is unnecessary because the soil can stand alone. If $H > H_c$, there will be a zone at the top of the wall with no lateral pressure because the soil in that zone supports itself and the theoretical lateral pressure distribution would look like Figure 3.8-1

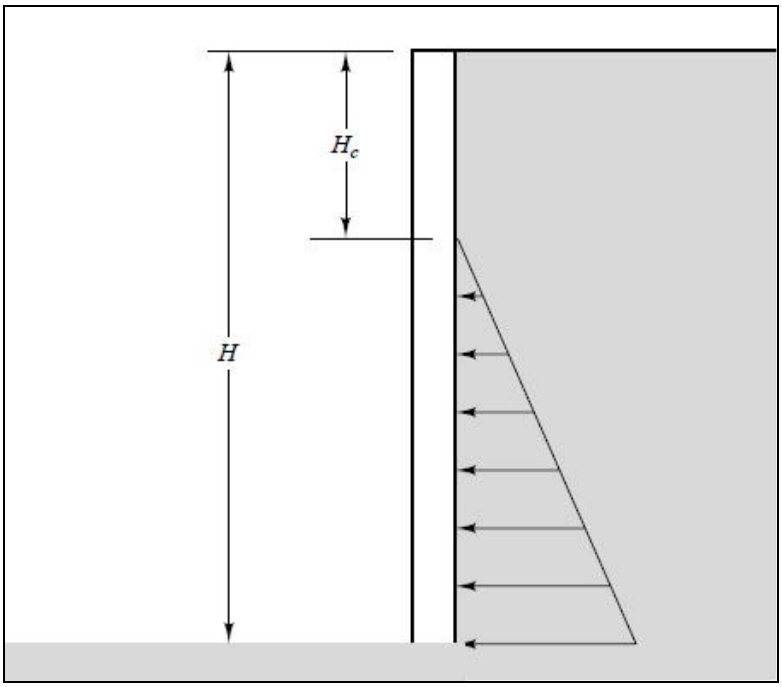

Figure 3.8-1 Theoretical Active Pressure Distribution for Cohesive Soils (Coduto, 2001)

3.8.1.2 Coulomb Pressures

Coulomb developed a formula to determine the coefficient of active earth pressure that considered the inclination of the wall, where α is the inclination of the wall from the vertical, positive counter-clockwise. The formula also considers the wall-soil interface friction angle, ϕ_w, which is typically taken as two thirds of the soil internal friction angle.

$$K_a = \frac{\cos^2(\phi - \alpha)}{\cos^2\alpha\cos(\phi_w + \alpha)\left[1 + \sqrt{\frac{\sin(\phi + \phi_w)\sin(\phi - \beta)}{\cos(\phi_w + \alpha)\cos(\alpha - \beta)}}\right]^2}$$

3.8.2 ADINA Predicted Earth Pressures

Since the concrete facing transfers the soil pressures to the structural frame, Figure 3.8-2 shows the distribution of earth pressures behind the concrete facing along with classical predictions that vary linearly with depth. The predicted and classical pressures are based on service loads after the 1.83m of backfill is placed to return the ground to its pre-construction elevation. The lateral displacement of the wall away from the soil reduced the horizontal pressures acting on the wall. For the upper two-thirds of the wall, the predicted lateral pressures along the wall correspond well with the Rankine active pressures for cohesionless soils. The lateral pressures increase significantly in the lower third of the wall beyond at-rest pressures, possibly because of the lateral yielding of the wall into the retained soil. Predicted results agreed fairly well with Coulomb's active pressure, however, compared to Rankine, Coulomb's method underestimated the pressure behind the wall more.

The resultants of the predicted and classical pressures were computed using depth at grade as the datum. The ADINA predicted distribution was divided into segments averaging the earth pressures over the segment width. The sum of the products of the area of the segment multiplied by the distance to the centroid of segment from grade was divided by the total area of the segments to obtain the resultant. A similar process was used for the classical pressures however one area was required because of the linear increase with depth.

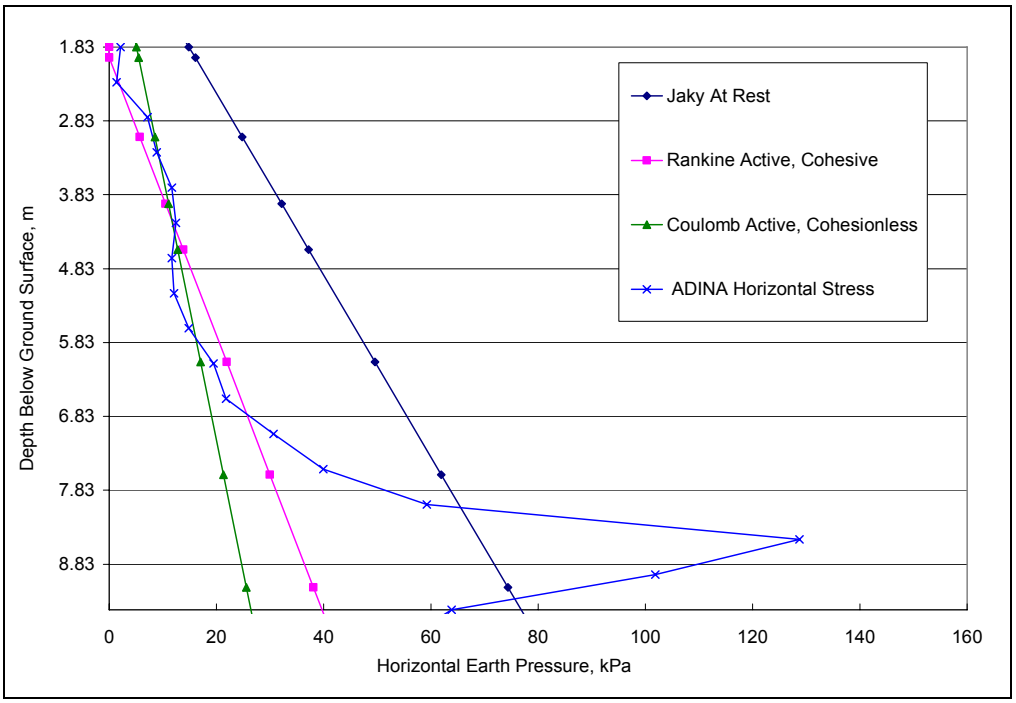

Figure 3.8-2 ADINA Predicted Lateral Earth Pressure vs. Classical Methods for SF Soil

Table 11 compares the computed location and magnitude of the earth pressure resultant behind the concrete facing. The predicted earth pressure resultant magnitude agrees well with Rankine's active; however the localized stress increase near grade results in a lower prediction of the location of the earth pressure magnitude. In spite of these results the earth pressures predicted by ADINA are within range of accepted classical methods. Therefore, it was concluded ADINA model was sufficient to proceed to the parametric study.

Table 11 Earth Pressure Resultants behind the Concrete Facing for SF Soil

	ADINA	At-Rest	Rankine Active
Resultant, kN/m (lb/ft)	246 16,795	350 23,980	228 15,622
Distance Above Grade, m (ft)	1.85 6.07	2.54 8.33	

	ADINA	At-Rest	Rankine Active
Resultant, kN/m (lb/ft)	246 (16,795)	350 (23,980)	228 (15,622)
Distance Above Grade, m (ft)	1.85 (6.07)	2.54 (8.33)	

CHAPTER IV

PARAMETRIC STUDY AND ULTIMATE CAPACITY

4.1 Introduction

A parametric study has been conducted to evaluate the effects of input parameters and design assumptions on the pile framed wall behavior. These parameters include boundary conditions, wall heights, tie-down anchor forces, representative soil types, soil stiffness, wall rigidity, and soil-wall interface friction. The resulting forces and displacements are considered in the wall along with the earth pressures along the concrete facing. In addition, the model has been loaded to failure to evaluate the ultimate capacity and to understand the failure mode associated with the pile framed retaining wall.

4.2 Parametric Study

As stated previously, the parametric study was carried out for two representative soil types to include a wide range of soil types that may be encountered in future wall designs. All effects were evaluated for both of the soils, the SF soil with low cohesion and high friction angle, and the WH soil, with the high cohesion and low friction angle. The stiffness of the soil or modulus of elasticity was the same for both soils for all studies

except when the modulus was varied itself. The model validated in the previous section was used as the standard case in the parametric studies. The steel piles were modeled with fixed end for all studies except for the study of pile boundary condition. In most cases the material inputs and analysis settings were kept constant, but in some instances, there was difficulty converging on a solution, thus certain model details were adjusted to overcome such difficulties. Modifications are discussed as they were made during the analysis and will be addressed where necessary in the following sections. Table 12 provides a outline of the parametric study, including the parameters addressed, the levels or number of values compared, the values chosen for study, and the investigated effects.

4.2.1 Effect of Pile Fixity

Since the piles are driven into refusal on rock, the base boundary conditions may not be completely fixed or pinned. Both conditions, along with the TDOT design assumption that the batter pile reaches fixity 3.65m (12 ft) below the grade were evaluated. For further comparison, the pile was fixed at grade to evaluate the effect of the most extreme fixity location. To impose fixed boundary conditions at these locations, all the degrees of freedom of a node on the pile were fixed nearest the desired depth. Figures 4.2-1 and 4.2-2 show the effect of pile fixity on moment distribution along the pile for two soil conditions. For both soils, selecting a fixed or pinned base doesn't make any difference on moments in the pile. The TDOT design fixity location results in lower moment values. Fixing the pile at grade gives the maximum negative moments in the pile, but this isn't important since the moment is well below the negative moment capacity.

Table 12 Parametric Study Analysis Matrix

Parameter	Levels	Values	Evaluated Effects
Pile Boundary Condition	2	Fixed	V and M in Piles
		Pinned	Earth Pressures
Location of Pile Fixity	3	Base	V and M in Piles
		3.65m Below Grade	Batter Pile Deflection
		At Grade	Earth Pressures
Wall Height (EWH)	3	4.57m (15ft)	V and M in Piles
(Piles Fixed)		7.62m (25ft)	Δ at Top of Wall
		10.7m (35ft)	Earth Pressures
Anchor Load vs. EWH	3	0	V and M in Piles
(Piles Fixed)		2 @ 55kips (245 kN)	Batter Pile Deflection
		2 @ 100 kips(445 kN)	Δ at Top of Wall
			Earth Pressures
			Earth Pressure Resultants
Soil Modulus	3	25 MPa (5.2E+6 psf)	Earth Pressures
(Piles Fixed)		72 MPa (1.50E+6 psf)	V and M in Piles
		125 MPa (2.6E+6 psf)	Δ at Top of Wall
Rigidity of Wall Sections	4	I_g Design	Batter Pile Deflection
(I_g of Composite Sections)		10% of I_g Design	Earth Pressures
		I_g Design x 10	
		I_g Design x 100	
Soil Wall Friction Coefficient	3	Frictionless	Batter Pile Deflection
		μ = 0.25	Earth Pressures
		μ = 0.75	
Notation: V-Shear, M-Bending Moment, Δ-Deflection			

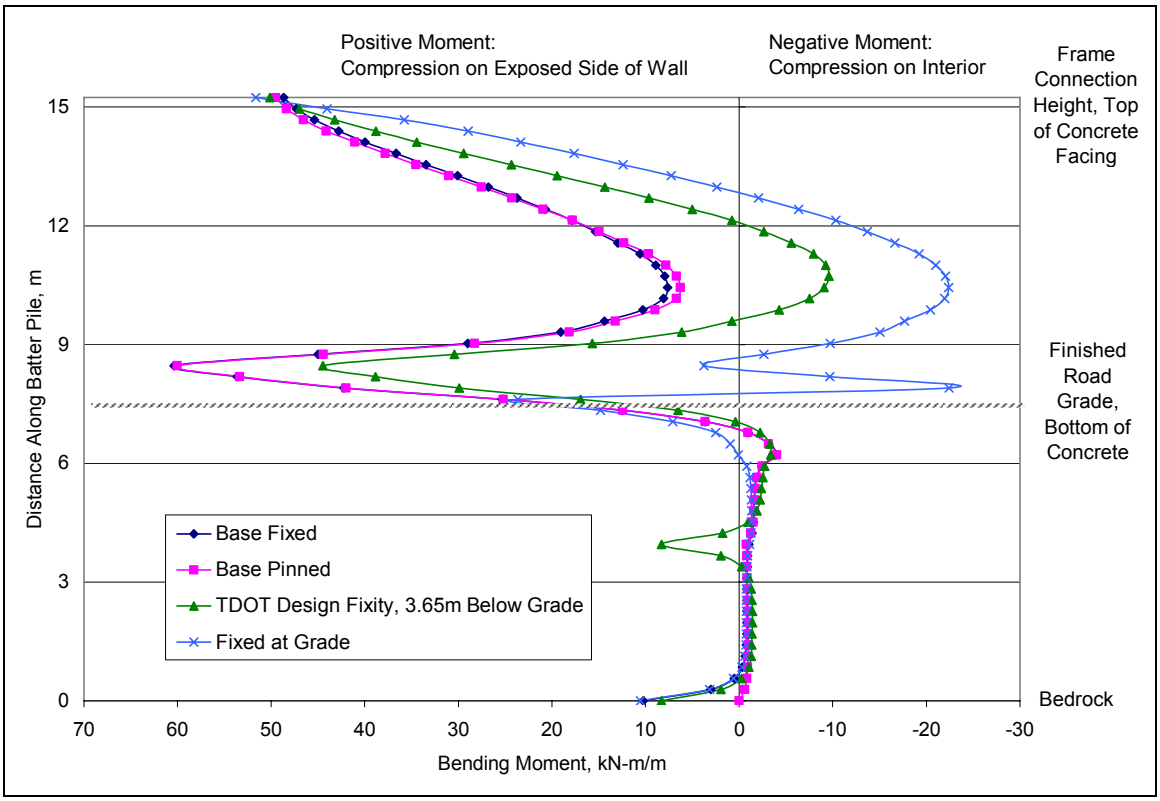

Figure 4.2-1 SF Soil - Pile Base Fixity Effect on Bending Moment in Batter Pile

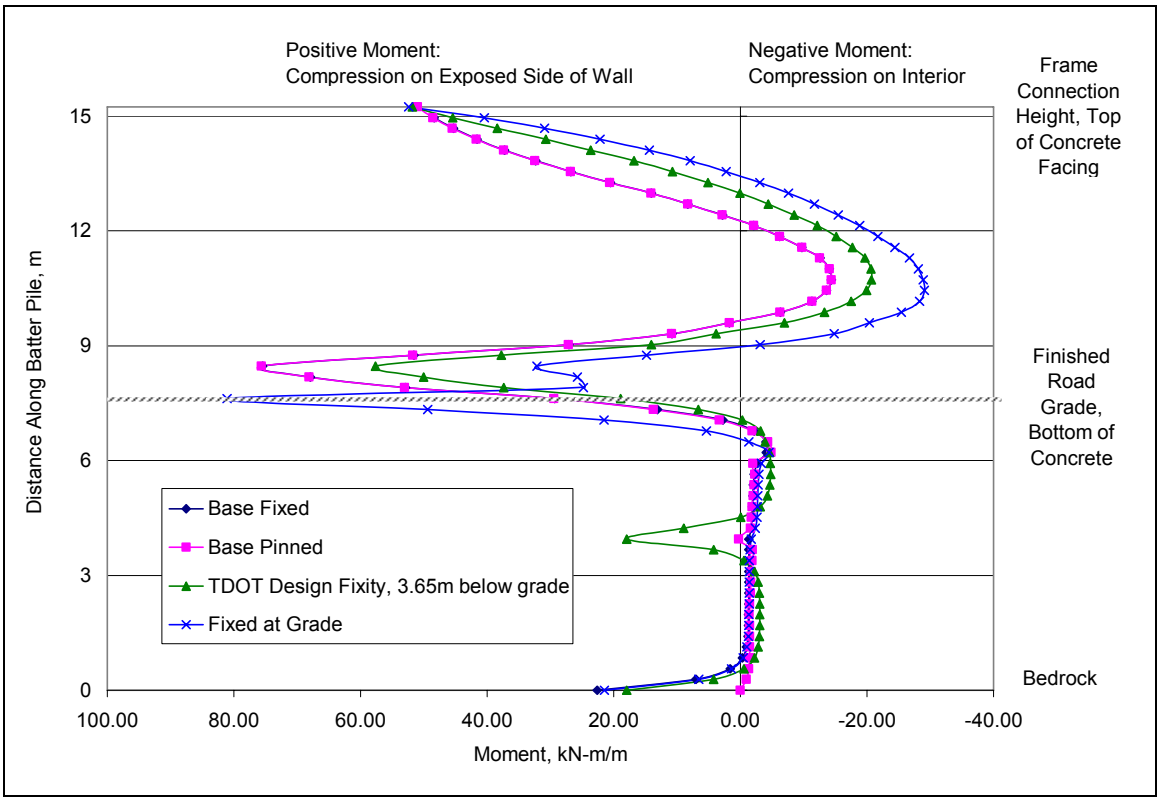

Figure 4.2-2 WH Soil – Pile Base Fixity Effect on Bending Moment in Batter Pile

Figure 4.2-3 shows the shear diagram of the batter pile for the SF soil, the WH soil is not shown since it produced the same distribution of moment as did the SF, with only higher values. Thus the effects of the pile fixity on shear for the WH soil can be scaled up from the results of the SF soil. The large shear values just above grade correspond with the large increase in earth pressures in that zone. Again the choice of boundary condition at the base made little difference on shear, and moving the fixity up along the pile results in a reduction of the maximum shears. The TDOT design fixity is a less conservative approach since assuming fixity at 3.65m below grade will under predict the maximum forces in the batter piles.

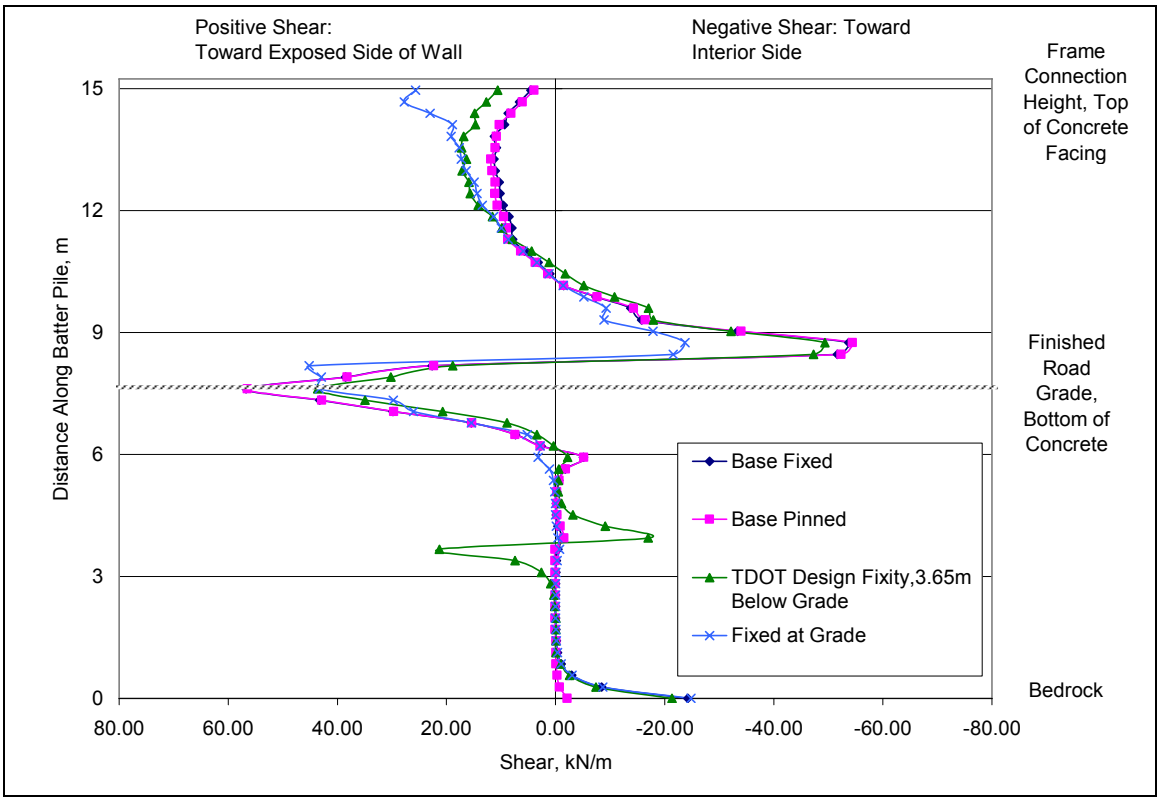

Figure 4.2-3 SF Soil – Pile Base Fixity Effect on Shear in the Batter Pile

Figure 4.2-4 shows the effect of fixity on the deflected shape the batter pile, negative deflections mean the pile deflects outwards. Again, the choice of base fixity makes little difference and displacements are reduced as pile fixity location rises along the batter pile. The deformed shape of the batter pile due to the WH soil was very similar to the SF with slight difference in values of displacements.

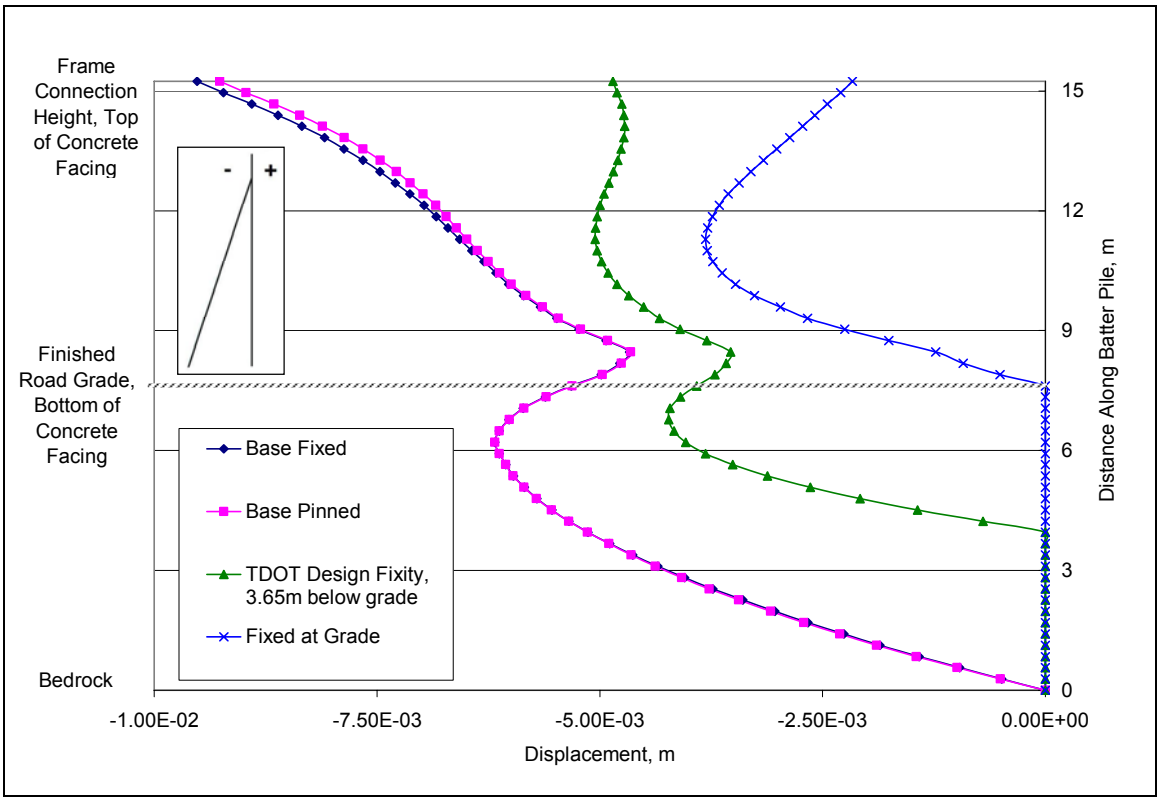

Figure 4.2-4 Fixity Effect on Deflection of Batter Pile

Lastly, Figure 4.2-5 shows the effect of fixity on the earth pressures behind the concrete facing. As shown in the figure the TDOT design fixity predicts only slightly different earth pressures near the grade but overall it is not significantly different from base fixity. Fixing the pile at grade increases pressure at the top of the wall possibly because less of the wall is unsupported so lateral yielding is less at the top of the wall compared to deeper fixity locations.

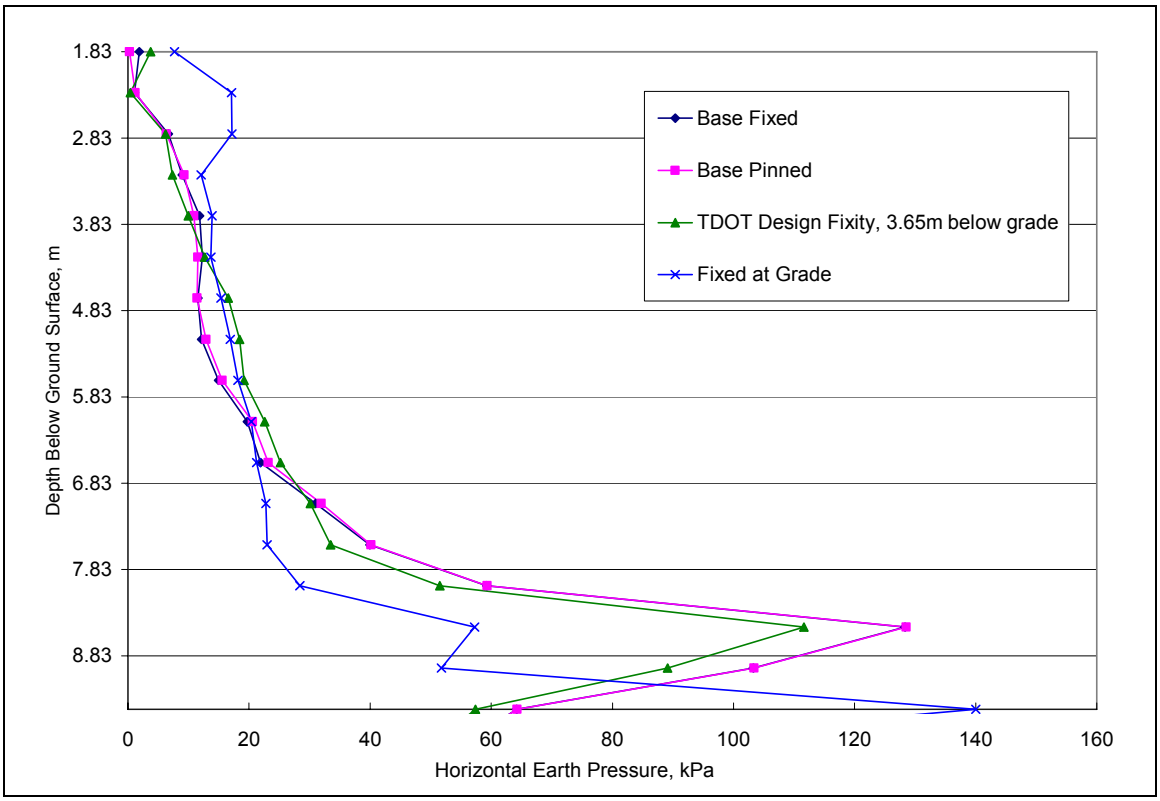

Figure 4.2-5 SF Soil - Effect of Fixity on Earth Pressures

4.2.2 Effect of Wall Height

The effective wall height varies along the longitudinal direction for a given wall, for initial analysis a typical height of 7.62 m (25 ft) was selected. Effective wall heights of 4.47 m (15ft) and 10.67 m (35ft) were analyzed to investigate to behavior of walls for a range of heights. For the 10.67 m model with SF soil, the model did not converge at all time steps, there was tension cut-off yielding in a few localized elements so the T value was set equal to the C value, a small increase from 2.39 to 4.78 kPa, that only affected a few elements, thus any possible differences as a result were neglected.

The deflected shape of the batter pile as a function of height as well as soil types is shown in Figure 4.2-6. The WH soil causes slightly greater lateral displacements except for the tallest wall. For heights up to 7.62 m the wall behaves rigidly, moving away from the soil with some displacement back toward the soil as a result of the tie-down anchor. The effect of the anchor, pulling the frame back and downwards, is more pronounced in the tallest wall. If the wall is compared to a cantilever column, in that the column is more likely bend as the unsupported length increases, then the deflected shape of the tallest wall exhibits flexible bending behavior due to the tie-down anchor load.

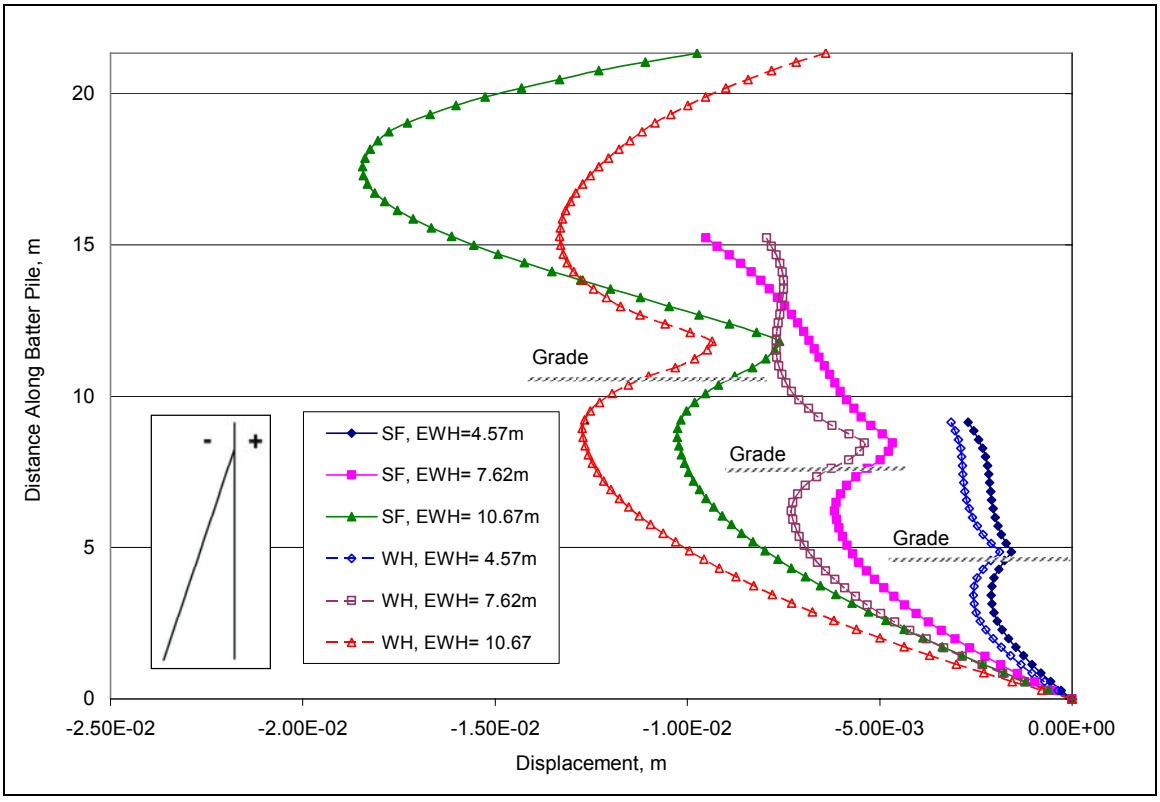

Figure 4.2-6 Deflected Shape of Batter Piles as a Function of EWH

The concrete parapet above the connection point is very rigid so no rotations occur in the top 1.83 m of the wall. Therefore, rotation of the top of the wall is the same as the rotation in the portion of the concrete facing below the connection point. Figure 4.2-6 shows that the top portion of the vertical pile for the 4.47 m and 7.62 m wall is tilted away from the soil, counter-clockwise rotation, whereas the 10.67 m wall is tilted into the soil, clockwise rotation. This agrees with rotations at the topmost node of the vertical pile for each height, Figure 4.2-7. With these rotations, the tallest wall will have its maximum deflection below the frame connection point, whereas the shorter wall will have maximum deflection at the top o the wall. This is illustrated in Figures 4.2-8.

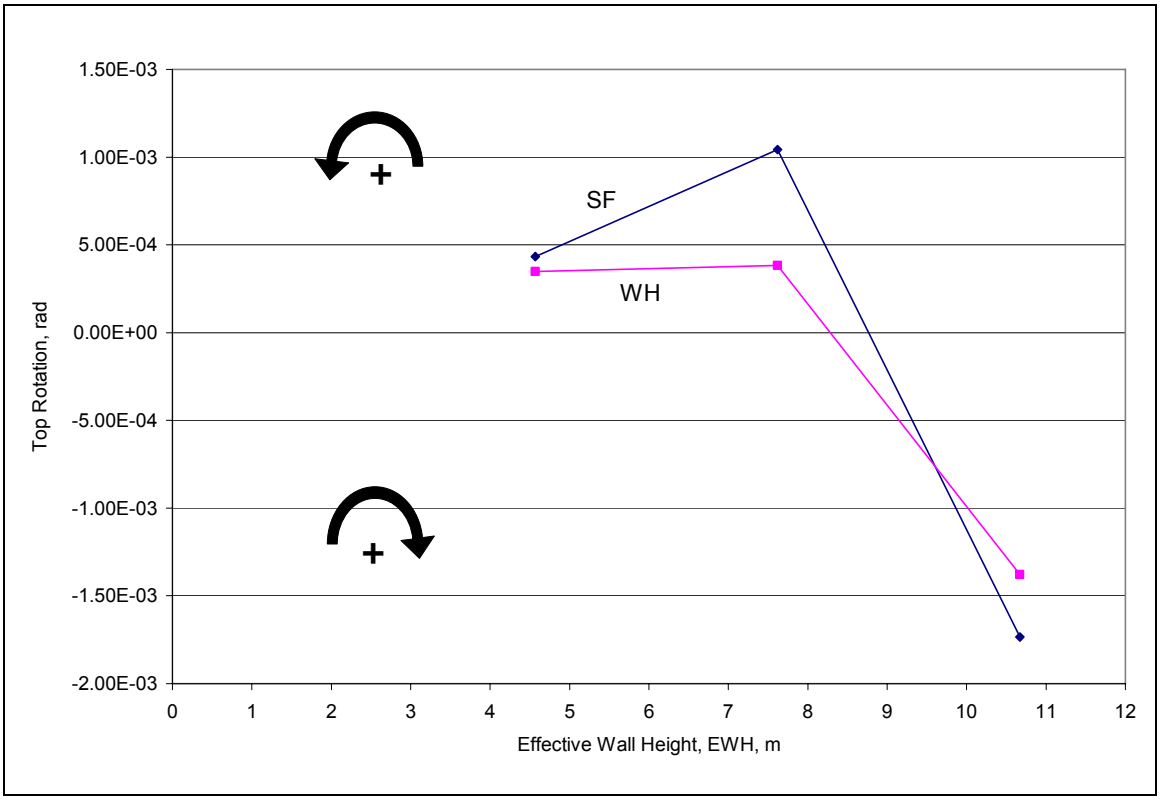

Figure 4.2-7 Effect of Height on Rotations at Top of Wall

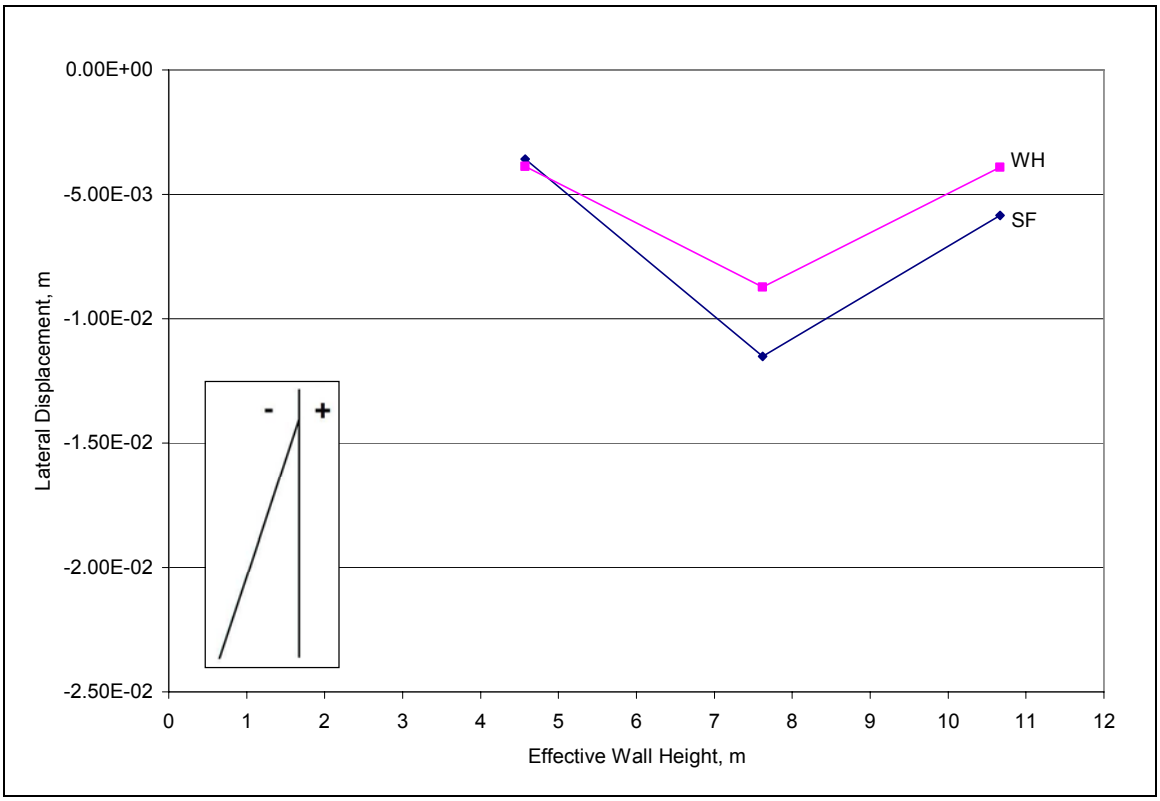

Figure 4.2-8 Effect of Wall Height on Deflection at Top of Wall

Typical moment distributions in the batter pile have been shown in previous sections, and are consistent for different wall heights. To illustrate the effect of wall height on internal forces in the pile, the maximum moment and shear in the batter pile for different wall heights is shown in Figure 4.2-9 and Figure 4.2-10 respectively. The maximum forces increase with wall height since the amount of earth pressure increases as the height of retained soil increases. The results for the SF soils are not linear because additional plastic deformations occurred in the SF soil model, but not for the WH soils with a large cohesion value. As the soil yields it cannot support itself, so the wall cannot separate from the soil similar to the at-rest condition, so pressures and deflections will be greater.

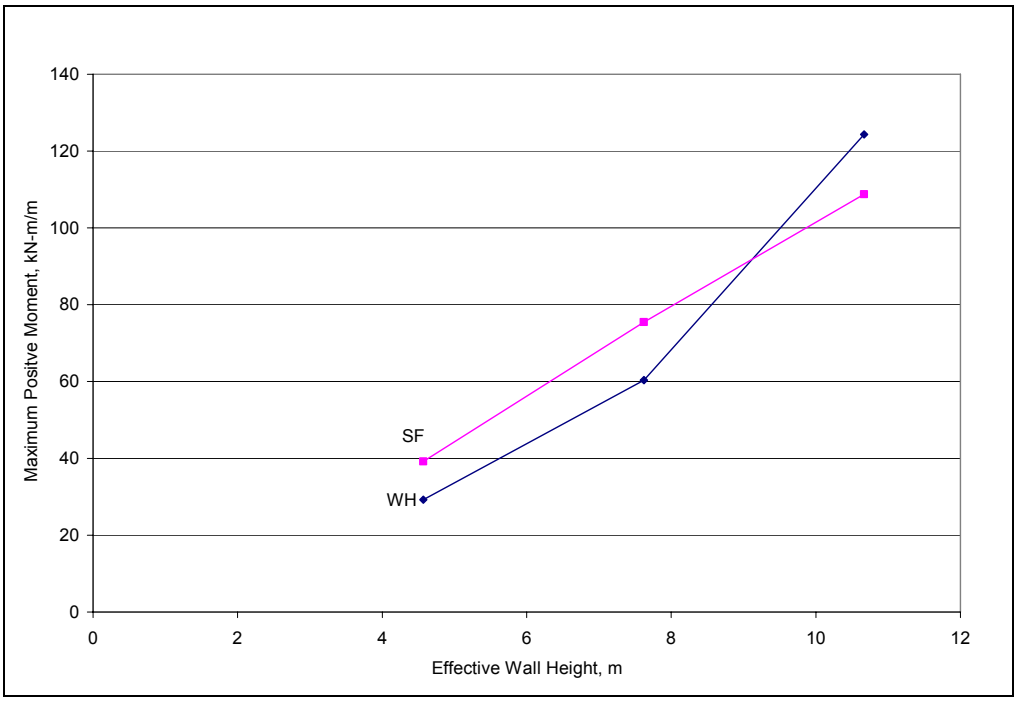

Figure 4.2-9 Maximum Moment in Batter Pile as Function of Wall Height

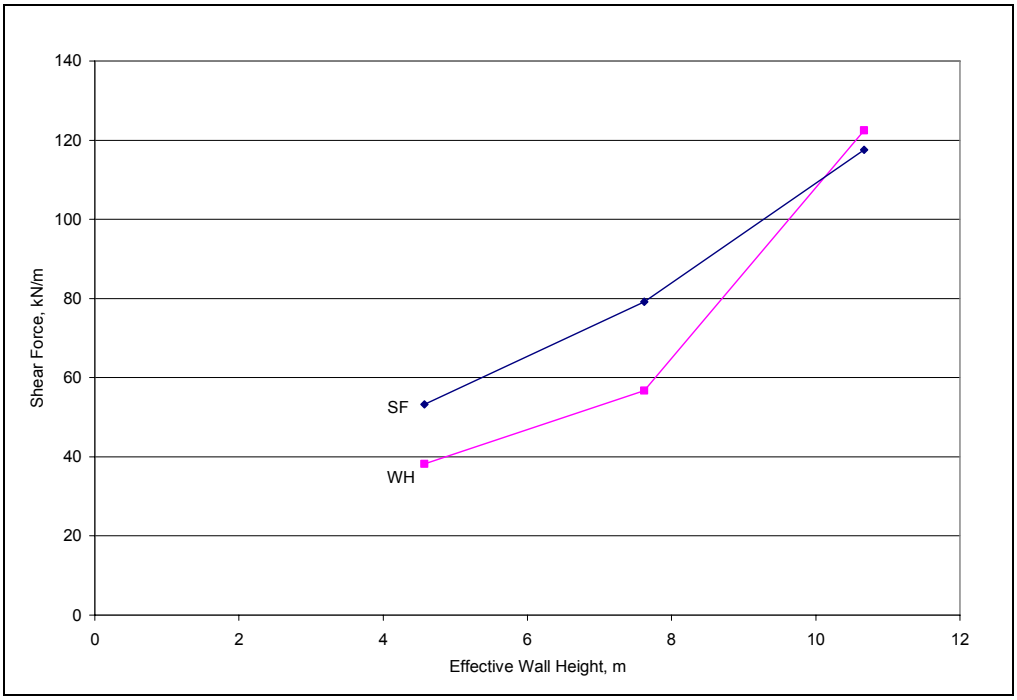

Figure 4.2-10 Maximum Shear in Batter Pile as Function of Wall Height

Lastly, the effect of wall height on earth pressures is evaluated in terms of the earth pressure resultant. In the model validation section, it was shown that ADINA predicts earth pressure resultants that agree well with Rankine's active predictions. Predicted earth pressure resultant calculations along with classical predictions are plotted for the three wall heights in Figure 4.2-11. It can be seen that for all wall heights, the earth pressure resultant is similar to that predicted by Rankine active earth pressure theory.

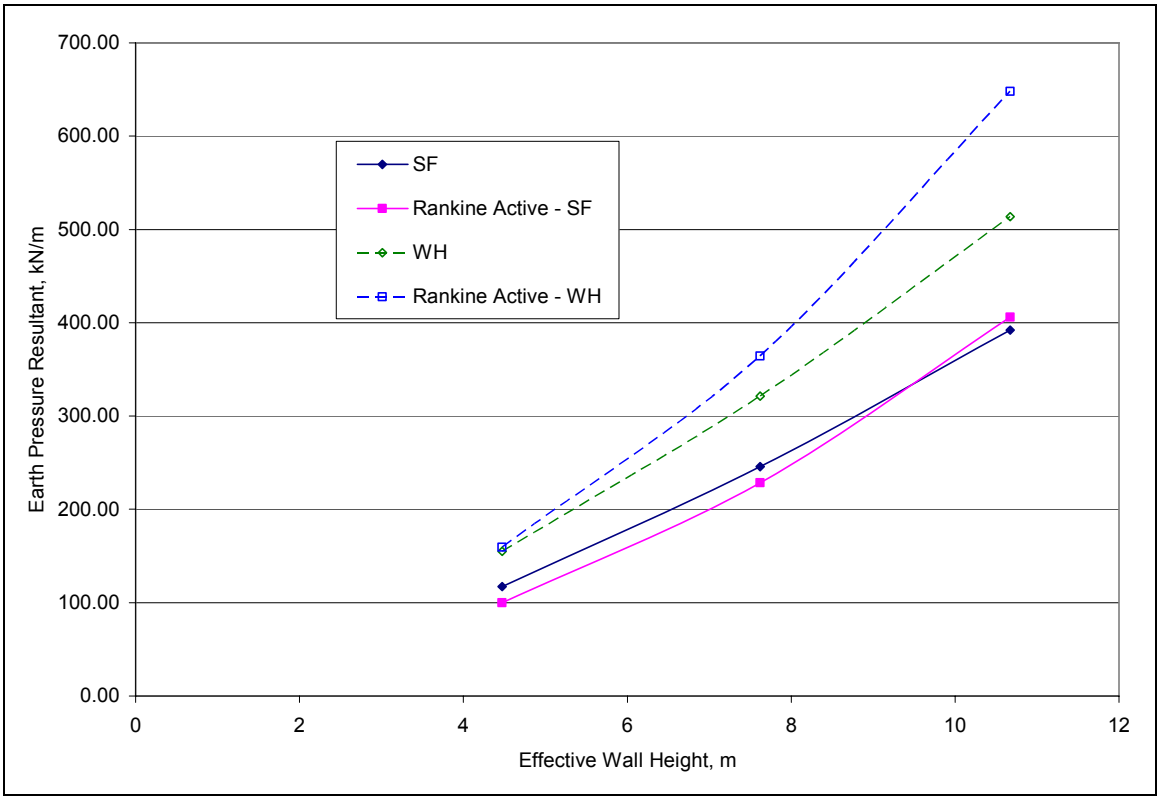

Figure 4.2-11 Effect of Wall Height on Earth Pressure Resultant

4.2.3 Effect of Anchor Load

TDOT's original design included a force per anchor of 245 kN (55 kips), which was based on engineering judgment. In the second wall built, designers increased the force to 445 kN (100 kips). The displacements of the batter pile with 3 levels of anchor load are shown in Figure 4.2-12 for the SF soils; the deflected shape was similar for the WH soils with slightly less magnitudes. Increasing the anchor load decreases the outward deflection of the frame, but even with no anchor the predicted deflection is less than 2.5 cm (1 inch). Although the effects of anchor forces on displacement become less significant beyond values of 245 kN, increasing anchor forces are very effective in limiting rotations in the wall.

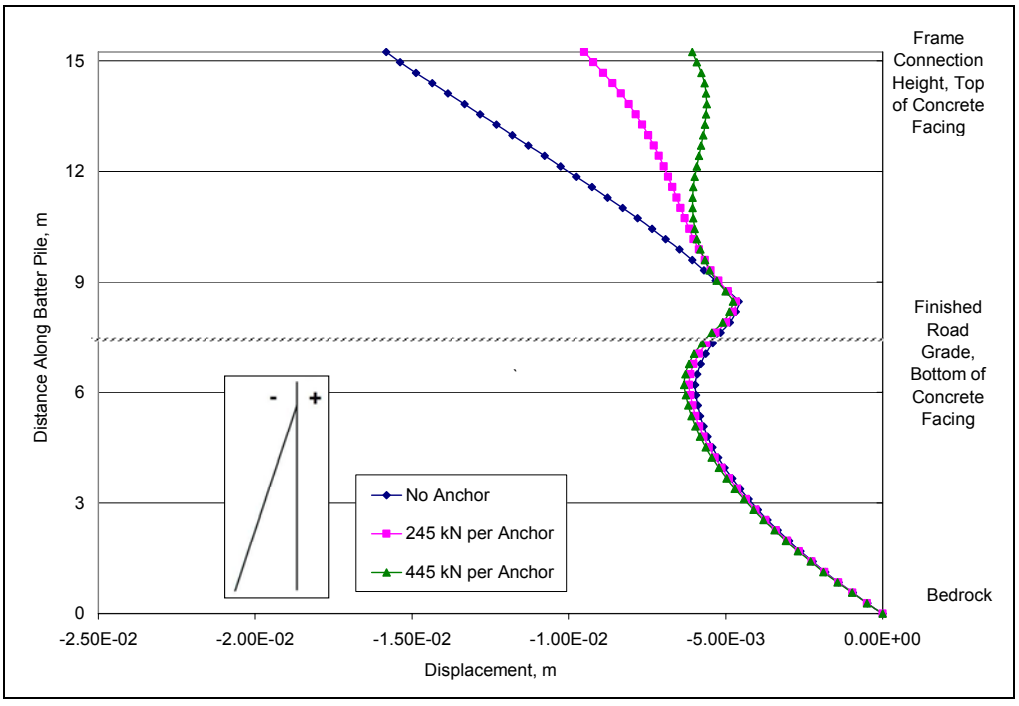

Figure 4.2-12 Effect of Tie-Down Anchor Force on Deflected Shape of Batter Pile

The deflection at the top of the wall as a function of anchor force and soil type is provided in Figure 4.2-13. The anchor is most important in limiting the deflections for the 7.62m height and for the SF soil. The anchor has little influence on deflections at the tallest height; this implies that the deformation for tall walls is controlled more by the soil pressures acting on it and less by the tie-down anchor as previously suspected.

The effect of anchor forces on the moment in the batter pile is illustrated in Figure 4.2-14 for the SF soils. As the anchor force increases the moment at the frame connection increases, but the maximum moment in the span doesn't change much. With no anchor there is a small amount of moment at the top, and a maximum moment near grade.

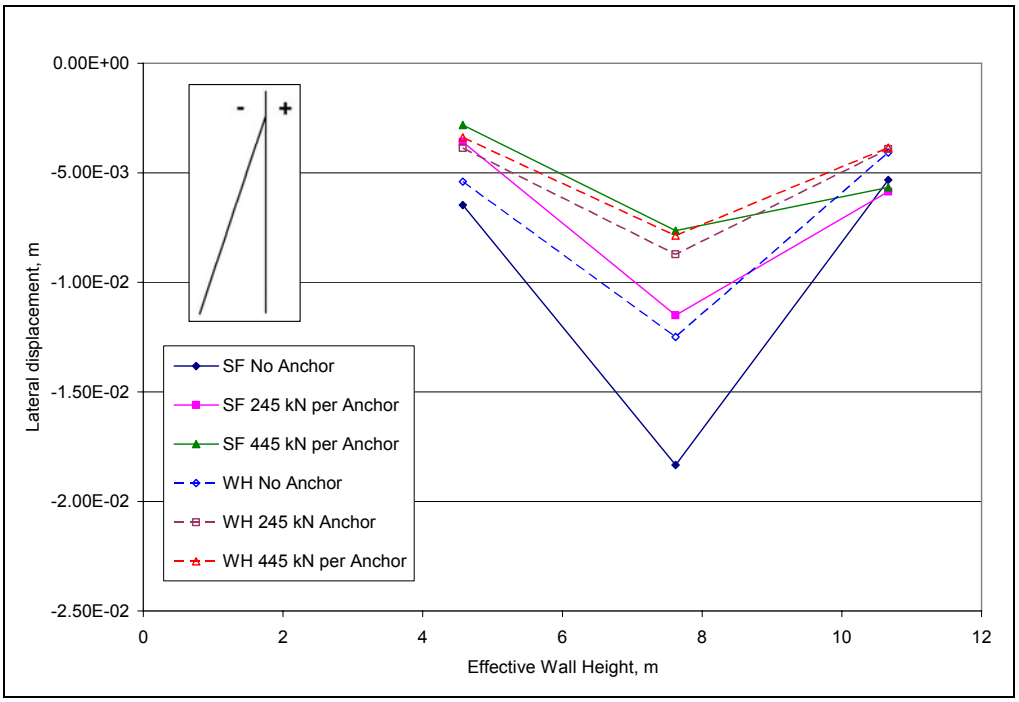

Figure 4.2-13 Effect of Anchor Force on Deflection at Top of Wall

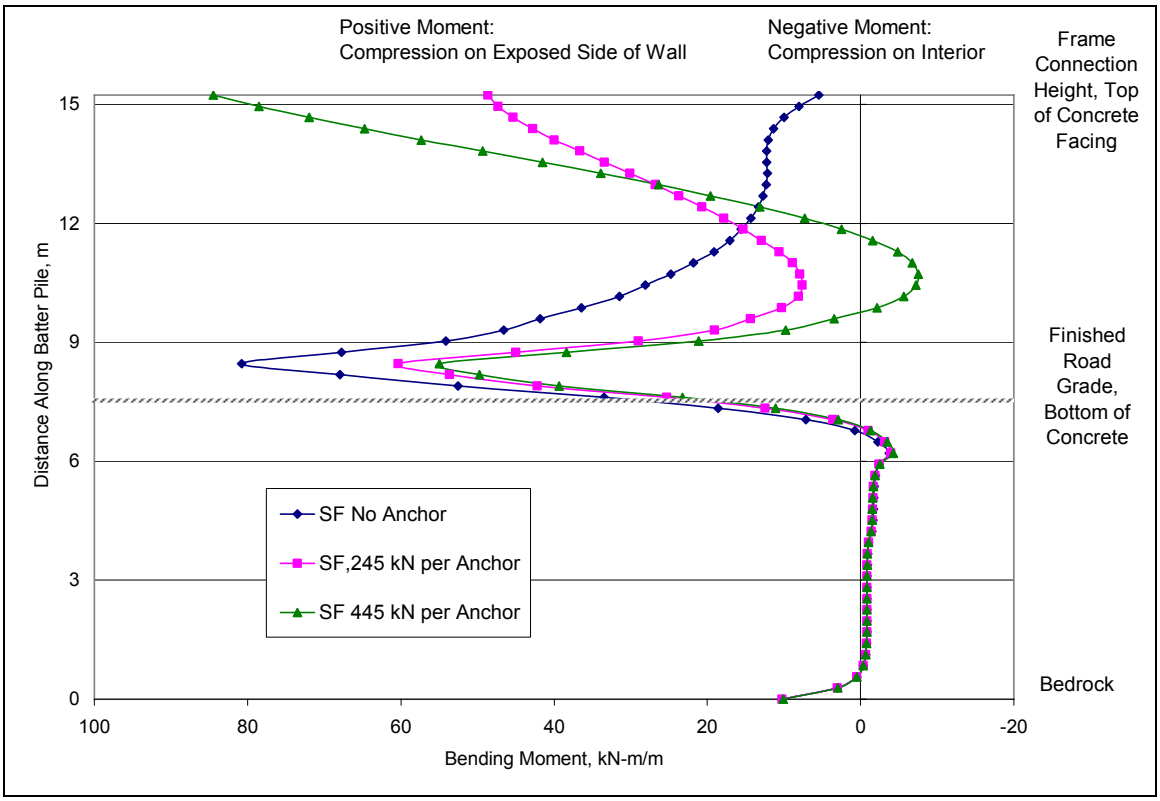

Figure 4.2-14 Effect of Anchor Force on Bending Moment in Batter Pile

The effects of anchor loads, wall height, and soil type on the internal forces in the batter pile are provided in the next three figures, 4.2-15, through 4.2-17. The maximum values shown in the figures were for the span of the batter pile excluding the top of the pile at the connection point. This was done because forces at that point are influenced by the applied anchor force and that area of the wall can be designed with additional reinforcement to resist large internal forces. In general, maximum moments and shears increase with wall height, the maximum moments increase with anchor load whereas the shears decrease with anchor load. Exception to this generalization occurs when plastic deformations are present.

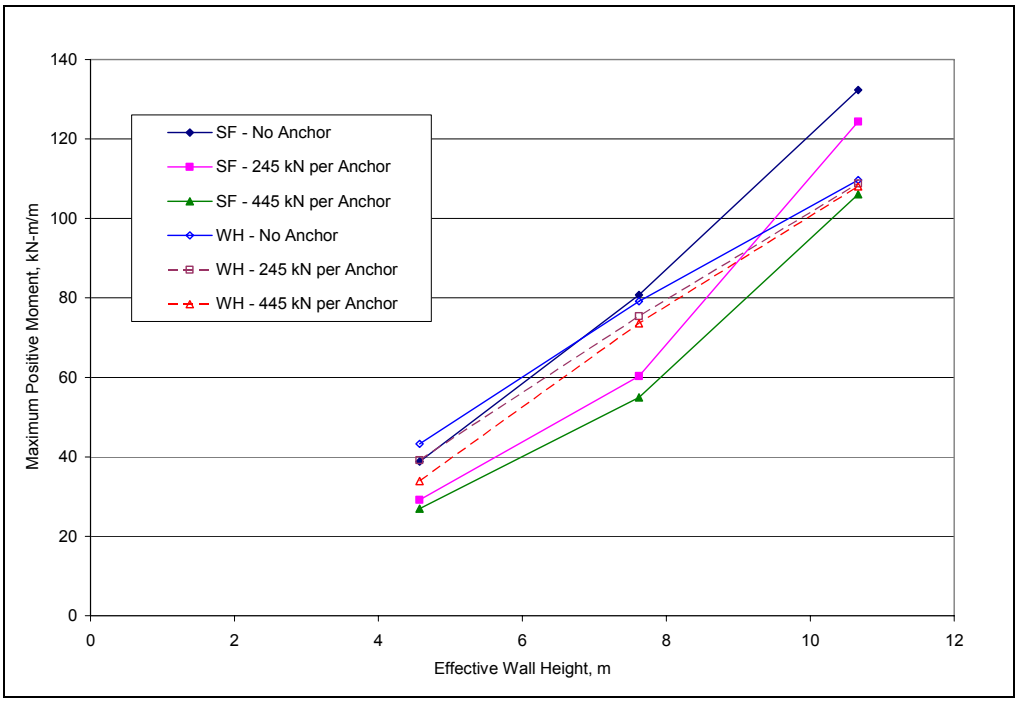

Figure 4.2-15 Effect of Wall Height and Anchor Force on Maximum Positive Moment

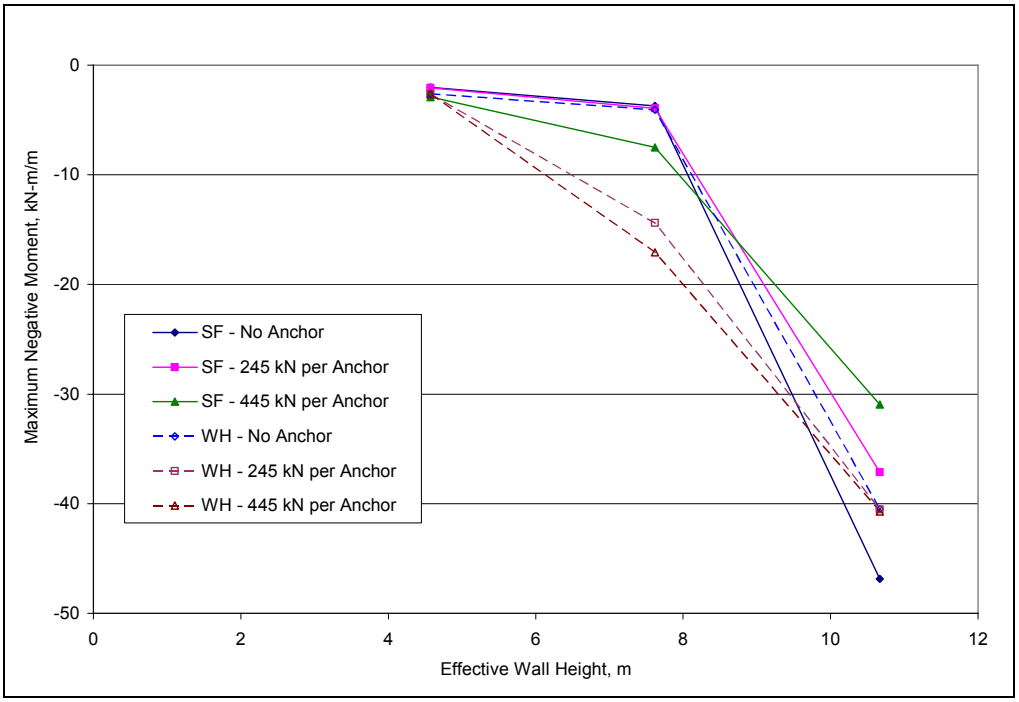

Figure 4.2-16 Effect of Wall Height and Anchor Force on Maximum Negative Moment

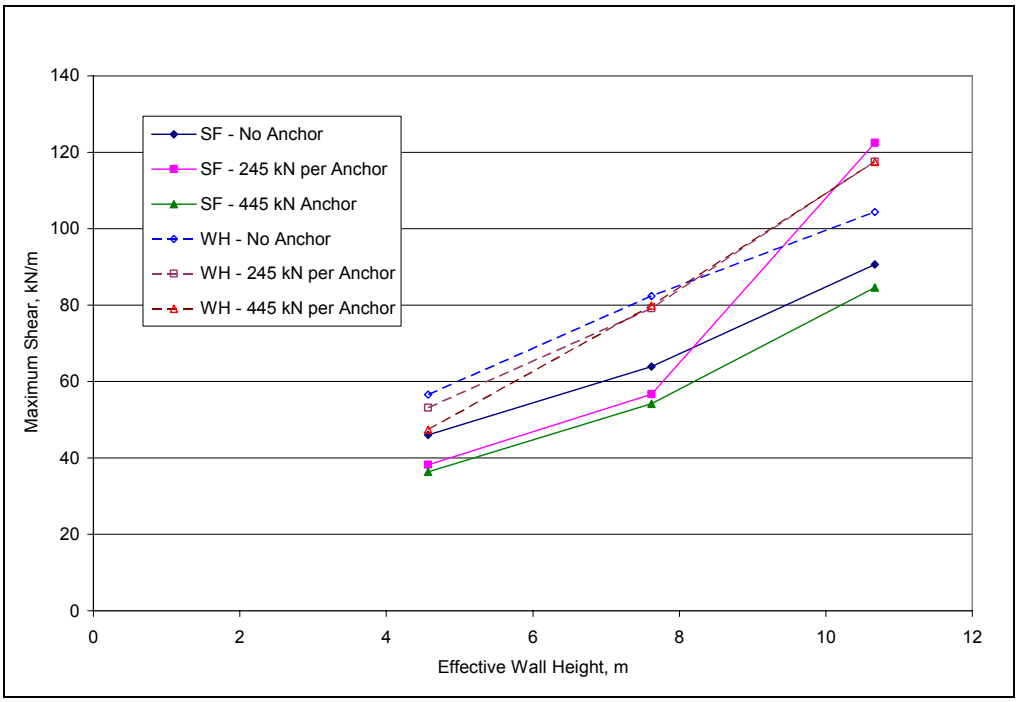

Figure 4.2-17 Effect of Wall Height and Anchor Force on Maximum Shear Force

As seen in Figure 4.2-17 the maximum shear does not increase linearly with all anchor force and soil type combinations. This is due to the fact that some cases did not produce negative moments above grade and thus the maximum shear was below grade, with a value less than cases where the negative moments are above grade, Figure 4.2-14.

The variation of earth pressures as a result of anchor loads, wall heights and soil types is summarized in Tables 13 and 14. Table 13 lists the calculated earth pressure resultants behind the concrete facing and Table 14 lists the location of the calculated resultants as a ratio of the wall height. Also listed are the earth pressure resultants for classical solutions, which act at a distance of one-third the height of the concrete facing.

Table 13 Summary of Earth Pressure Resultants

Soil Type		SF					WH				
		Force Per Anchor, kN			At-Rest	Rankine Active	Force Per Anchor, kN			At-Rest	Rankine Active
EWH		0	245	445			0.00	245	445		
4.47	Resultant, kN/m	96.8	117	136	153	100	134	155	179	214	160
7.62		229	246	266	349	228	301	321	341	489	364
10.67		384	392	395	621	406	503	514	525	870	648

Table 14 Summary of Earth Pressure Resultant Locations

Soil Type		SF					WH				
		Force Per Anchor, kN			At-Rest	Rankine Active	Force Per Anchor, kN			At-Rest	Rankine Active
EWH		0	245	445			0	245.0	445.0		
4.47	Resultant Location, Ratio of EWH	0.24	0.27	0.33	0.34		0.21	0.27	0.33	0.34	
7.62		0.24	0.24	0.27	0.33		0.19	0.23	0.26	0.33	
10.67		0.21	0.22	0.22	0.33		0.27	0.21	0.22	0.33	

In general, ADINA calculated resultants agreed very well with Rankine active resultants, most often predicting a resultant less than Rankine's. The exception is at low wall heights where the predicted resultant force was as much as 36% greater for a 445 kN anchor force and nearly 20% for the design force of 245 kN per anchor. ADINA predictions did not agree so well in terms of the location of the resultant forces above the base of the wall. ADINA predicted locations of the earth pressure resultant below one-third the height of concrete facing, generally about, one-fourth the height, because of the large increase in pressures just above grade.

4.2.4 Effect of Soil Stiffness

The initial value for the elastic modulus of the soil, E_{sl} was taken as 72 MPa (1,500,000 psf) from a wide range of values available in literature. To evaluate the effects of soil stiffness, two more values were selected from typical values, E_{sl}=25 MPa (522,000 psf) and E_{sl}=125 MPa (2,611,00 psf). The three values selected represent soils from loose sands to stiff clays. Since the soil stiffness controls deformation, the restart file and the input file in which gravity was applied had to be modeled with the same stiffness value to obtain accurate solutions. The model with SF soils and E_{sl} = 125 MPa failed to reach convergence during the solution. To overcome this, the maximum number of iterations was set to 500 and the Line Search option was selected using its default settings. The Line search option is useful for problems with plasticity and/or contact elements, and its function is to reduce incremental displacements so that convergence can be reached. A detailed description of the Line Search option is available in the Theory and Modeling

Guide (ADINA, 2006). Modifying the model with these options resulted in a converged solution.

The response at the top of the wall due to different soil moduli was compared over the construction sequence, after the anchor was applied, Figure 4.2-18. The trend is the same for both soil types and the deflections for all moduli show deflections away from the retained soil during excavation, and tipping back to the soil when the massive concrete cap is poured at time step 1.8 seconds. The displacements increase with decreasing stiffness, but differences are less significant when the modulus increases past 72 MPa. The WH soils deform less for all moduli value because the WH soils have a large Poisson's ratio and cohesion value. The larger Poisson's ratio means the soil is less compressible so it does not deform as much in one direction due to load in an orthogonal direction. The larger cohesion values means there will be less plastic deformations.

Changes to the earth pressures as a result of the soil stiffness are shown in Figure 4.2-19. The earth pressures in the top 2 m are controlled by both lateral and vertical movement of the soil; there is a small amount of differences between the soil stiffness. However, decreases in earth pressure for loose soils are a result of soil settling away from the pile.

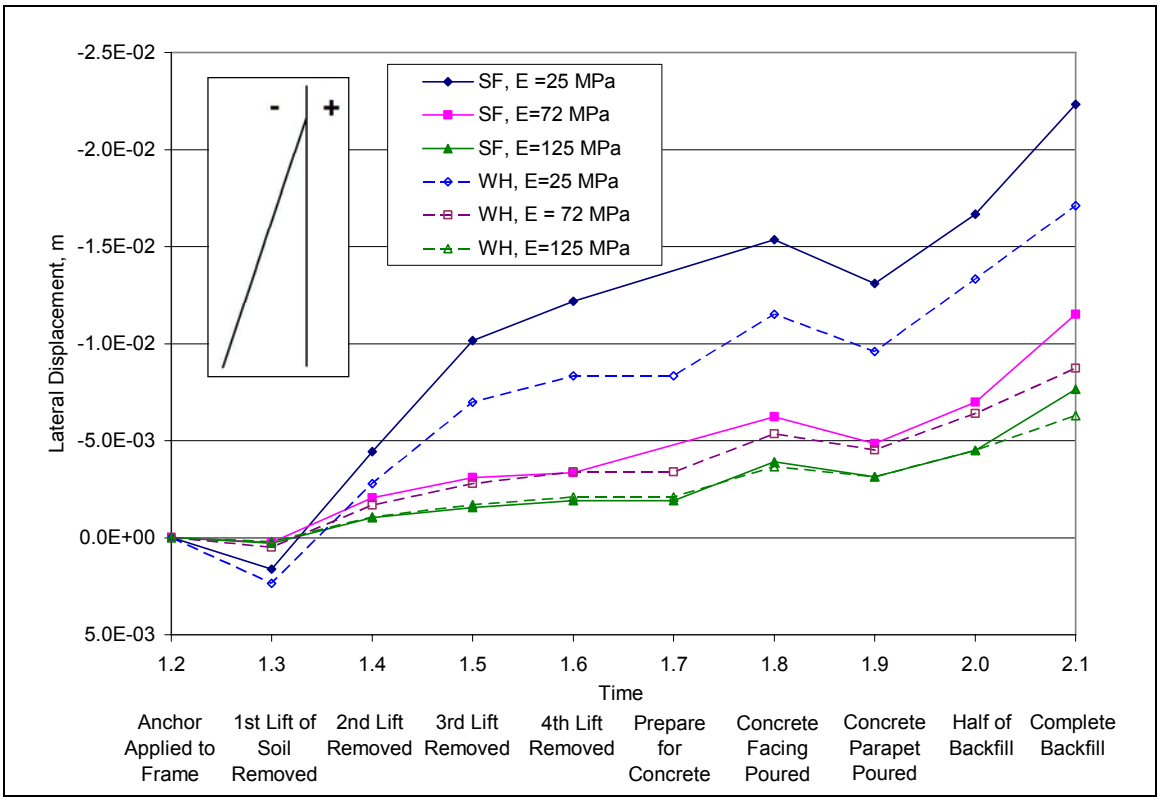

Figure 4.2-18 Effect of Soil Stiffness on Wall Deflection during Construction

Along the lower two-thirds of the wall, earth pressure decrease as the soil stiffness increases, because as the wall deforms, the stiffer soil deforms less possibly separating from the wall, which is similar to active conditions. For very loose soils, the soil remains in contact with the wall which is closer to at-rest conditions which produce larger pressures than active conditions. The same explanation describes the increase in pressure with stiffness near the base of the wall. Near the base, the wall exhibits yielding into the soil. As the stiffness of the soil increases so does it's resistance to wall yielding which is manifested in the form of larger lateral pressures from stiff soils. The earth pressure resultants decrease with increasing soil stiffness.

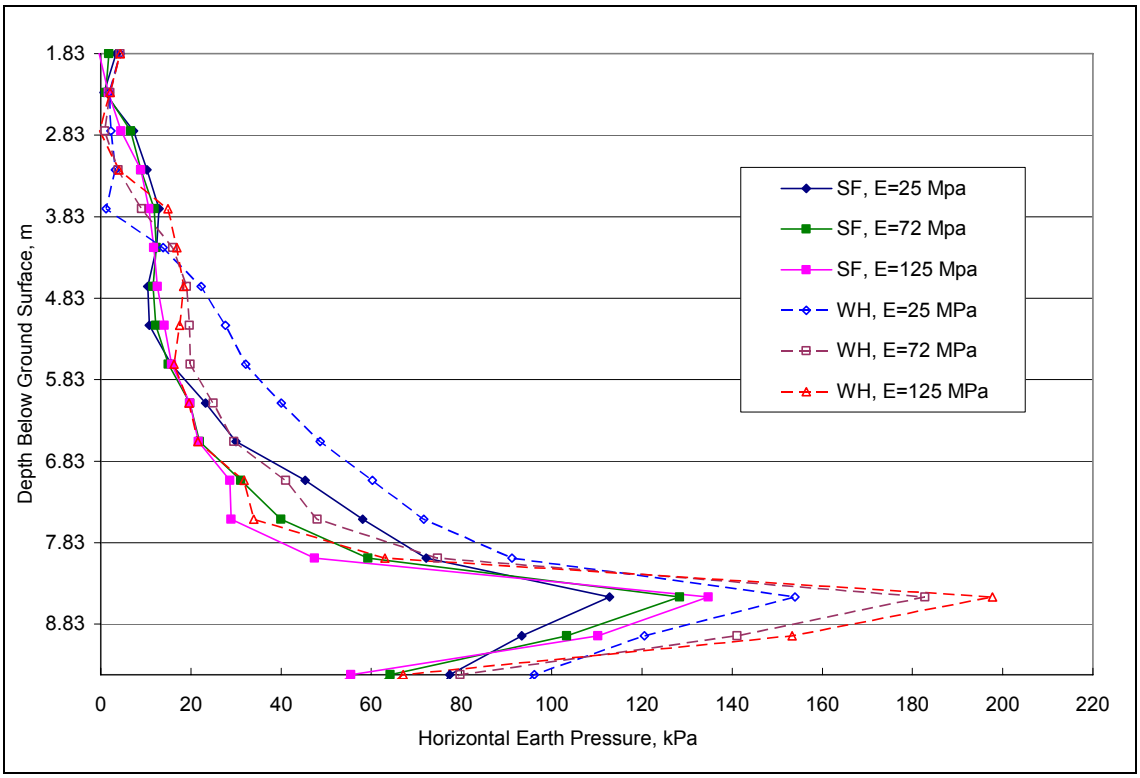

Figure 4.2-19 Effect of Soil Stiffness on Earth Pressures

The effect of the soil stiffness on the moment diagram in the pile is shown in Figure 4.2-20. The trend is the same for WH soils; it is evident that the positive bending moments in the wall increases with soil stiffness, while the negative moments in the pile are practically zero. This is possibly due to the fact that the earth pressures are higher for weak soils in the top two-thirds of the wall thus increasing the height above the grade of the location of the earth pressure resultant which would create larger overturning moments in the pile. In addition, the deflections were greater for lower stiffness values, because increased displacements cause increases bending stresses in the members.

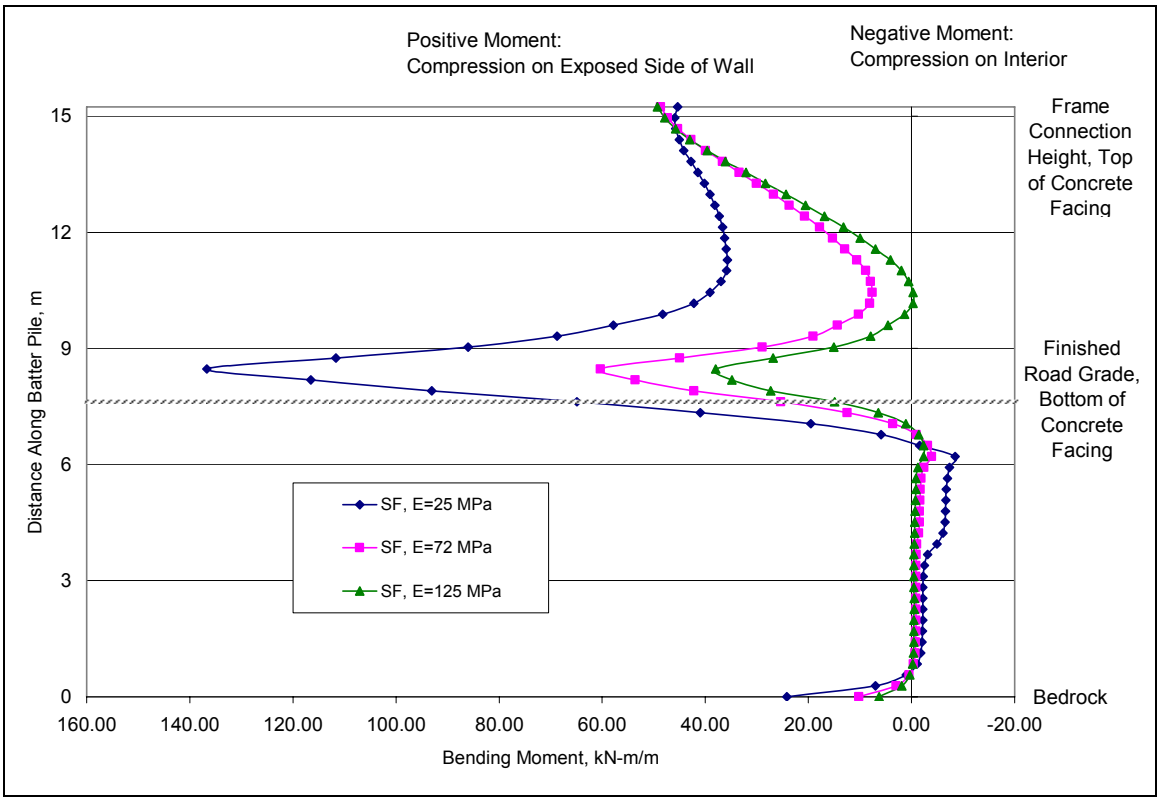

Figure 4.2-20 Effect of SF Soil Stiffness on Bending Moment in Batter Pile

Additional plots of the effects of soil stiffness on the maximum positive moments and shears in the wall are provided in Figure 4.2-21 and Figure 4.2-22 respectively. These plots reveal the importance of site conditions on the forces developed in the wall. Decreasing the soil stiffness from 72 MPa to 25 MPA increased the maximum moments for the models with SF soil and WH soil, 126% and 112% respectively. In addition, the low value stiffness increased the maximum shear 67% with SF soil and 51 % with WH soil. Increasing the soil stiffness from 72 MPa to 125 MPa decreased the maximum moments for the models with SF soil and WH soil, 58% and 55% respectively and decreased the maximum shear 35% and 38% respectively.

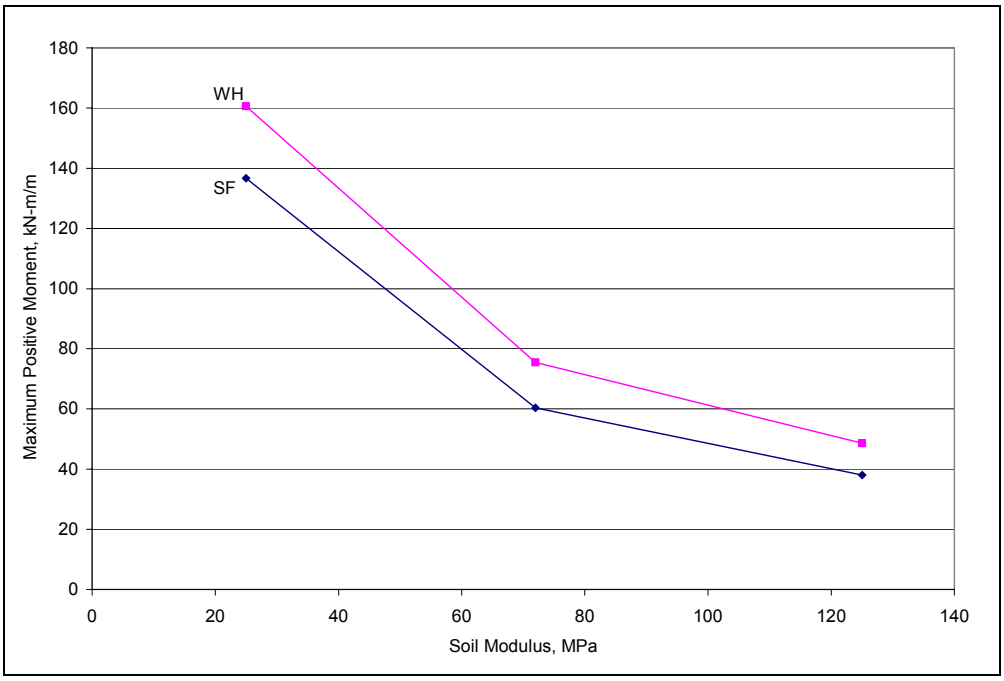

Figure 4.2-21 Effect of Soil Modulus on Maximum Positive Moment

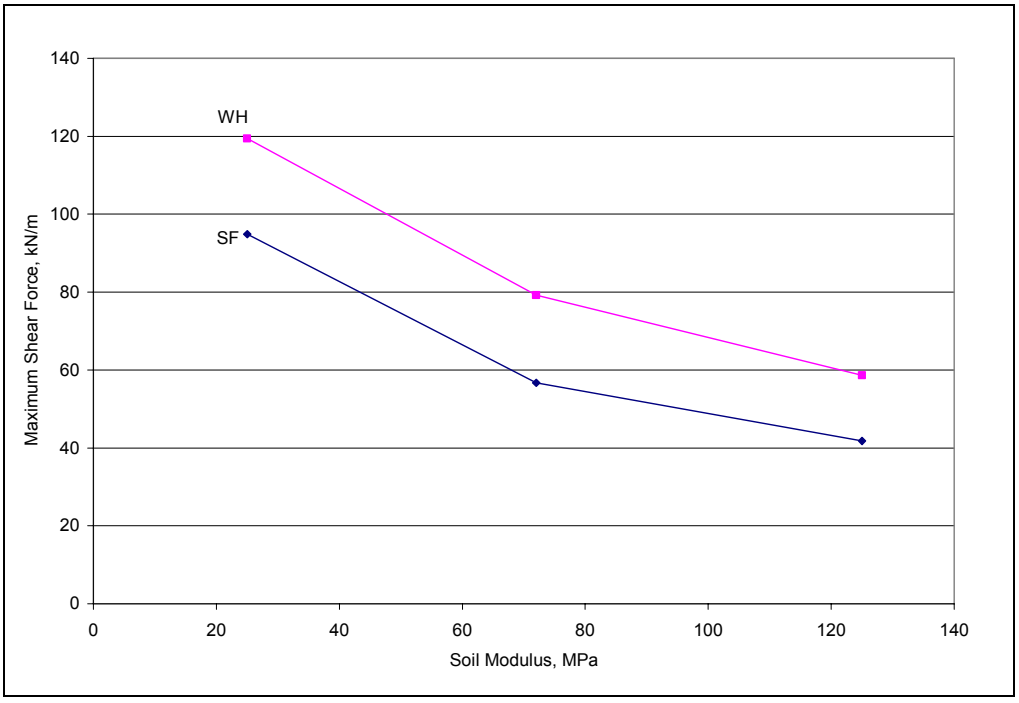

Figure 4.2-22 Effect of Soil Modulus on Maximum Shear Force

4.2.5 Effect of Wall Rigidity

The rigidity of the wall was varied by changing the moment of inertia, I_g, of the steel-concrete composite sections; the concrete facing-batter pile composite and the concrete cap-vertical pile composite. To represent cracked composite sections, 10% of Ig was evaluated, and to represent a very rigid section, values of Ig were increased orders of magnitude. The effect of wall rigidity on displacements along the pile is shown in Figure 4.2-23. Based on this result, the rigidity of the concrete composite sections have very little effect on the behavior of the wall and the original TDOT design is very stiff. This could be because the frame is sufficiently rigid and the self weight of the concrete combined with the anchor loads are the most important contributors to the wall stiffness.

Figure 4.2-24 shows the variation of earth pressures behind the concrete facing as a function of wall rigidity. Increasing wall rigidity has little effect on the earth pressures, however decreasing the wall rigidity results in some changes to the earth pressures distribution. The lateral pressures increased in the top third of the wall and decreased in the middle third compared to the other values of wall rigidity. This variation corresponds with the deflected shape of the wall with the reduced rigidity, in which there was less lateral yielding in the top third and more yielding in the middle third of the wall. Considering the entire distribution of earth pressures behind the wall, the earth pressure resultants are not affected by the rigidity of the concrete facing.

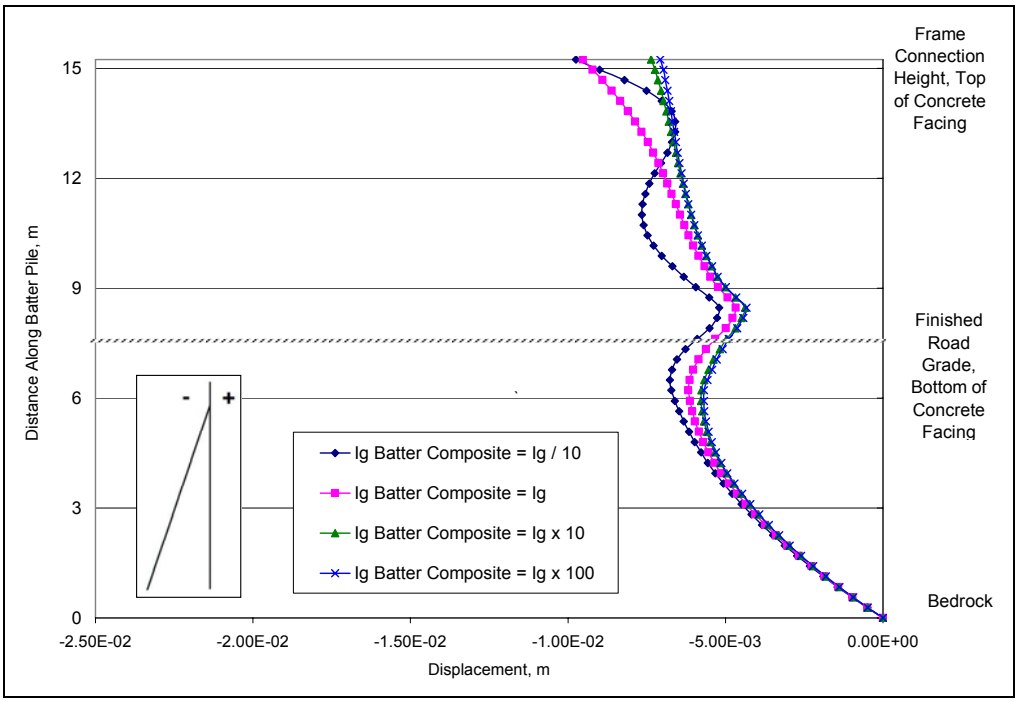

Figure 4.2-23 Effect of Wall Rigidity on Lateral Displacement of Batter Pile

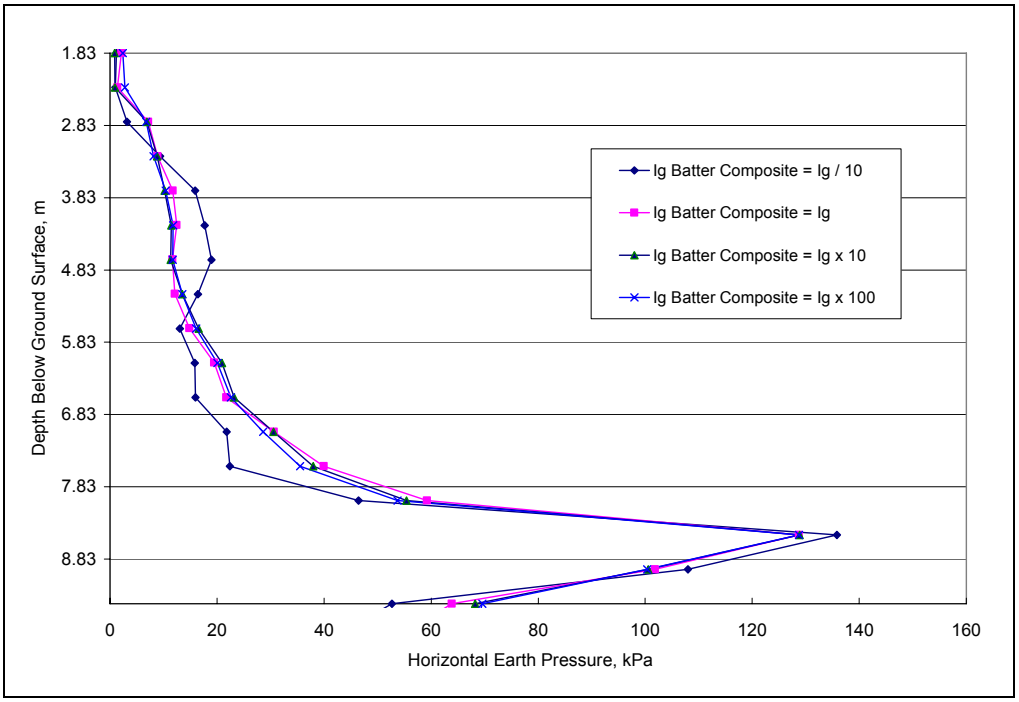

Figure 4.2-24 Effect of Wall Rigidity on Earth Pressures

4.2.6 Effect of Soil-Wall Interface Friction

The interface between the retained soil and the back of the concrete facing was model with contact elements in ADINA. All previous models have assumed frictionless contact; this study investigates the effect of the choice of a coefficient of friction, μ, when defining the soil-wall contact in ADINA. Two values of the frictional coefficient, 0.25 and 0.75, were selected to evaluate any significance it has in the FE model. The friction coefficient had to be defined in both the input and restart files.

According to Figure 4.2-25, the choice of friction coefficient does have an influence on the wall behavior. Increasing friction leads to additional restraint of the soil against sliding, reducing the overall displacements of the wall. Thus the choice of frictionless contact is most conservative since it predicts the largest displacements. The effect of friction on earth pressures is shown in Figure 4.2-26. It can be seen that the earth pressures are not highly dependent on the choice of the coefficient of friction. In general, the results of ADINA models with contact are sensitive to the FE mesh and amount of contact elements used, especially for frictional contact. The irregularity of the earth pressure distributions for the high friction value may just be a result of the number contact elements used for the soil elements which was small compared to the steel elements. Nonetheless, the irregularities are not significant enough to impact the earth pressure resultants, so the conclusion that frictional contact does not affect the earth pressure resultant is valid.

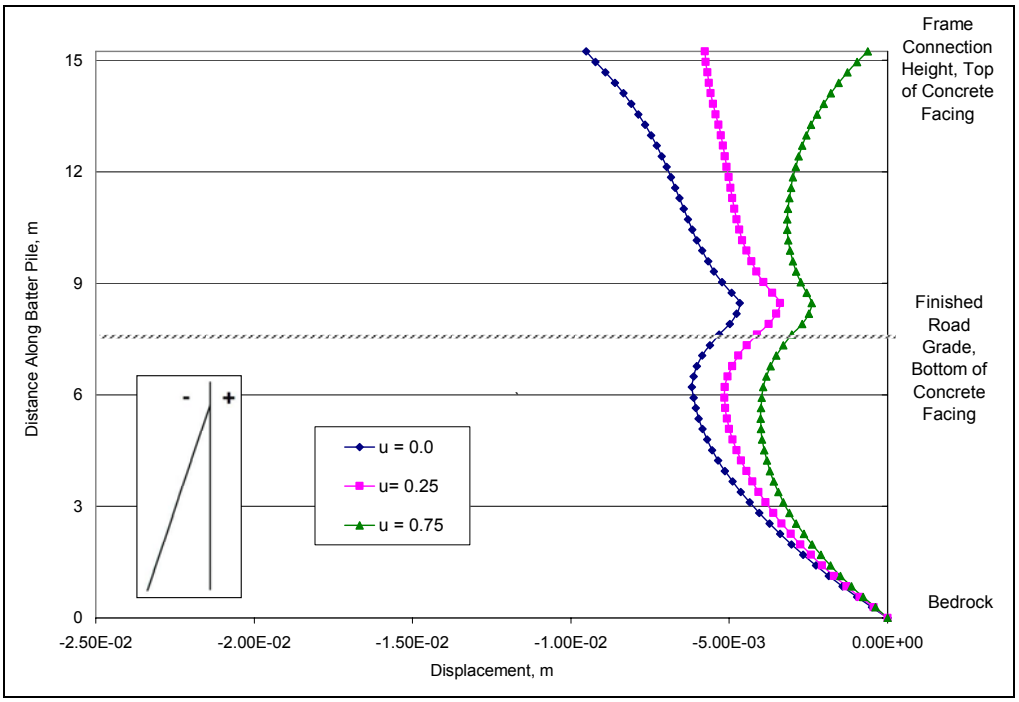

Figure 4.2-25 Effect of Interface Friction on Lateral Displacement of Batter Pile

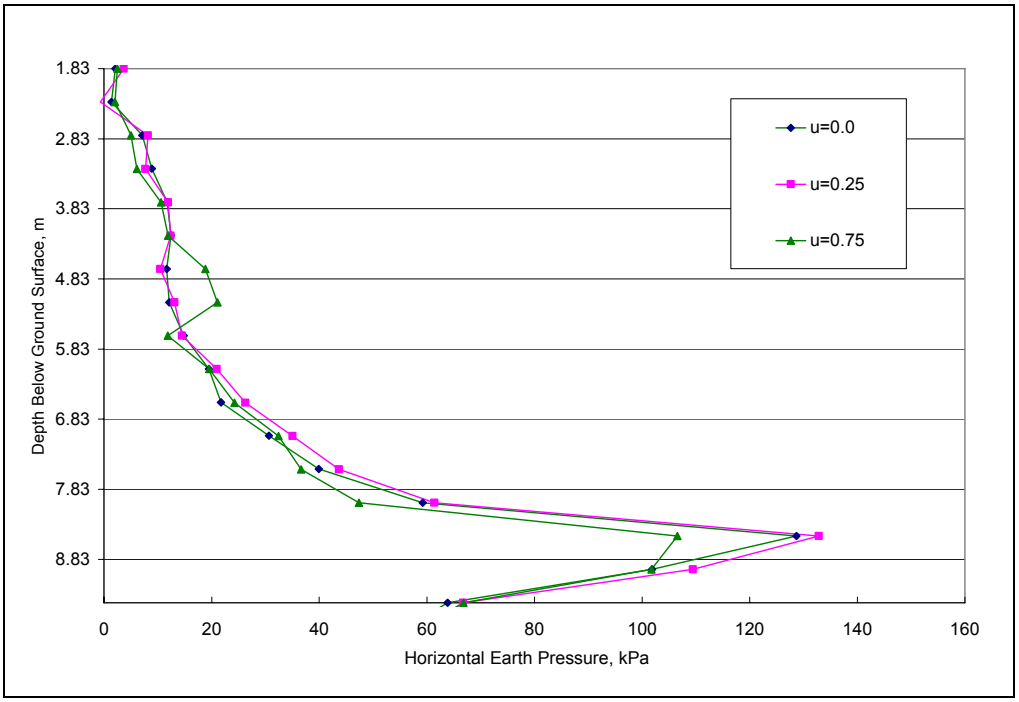

Figure 4.2-26 Effect of Interface Friction on Earth Pressures

4.3 Ultimate Capacity

To evaluate the capacity of the wall in terms of allowable surcharge, as well as how the wall might fail, the standard model of the typical pile-framed wall was loaded up to failure by applying a surcharge pressure to the top of the soil after all construction stages were complete. Since the beam elements were modeled linear elastic, which has no yield limit, the solution in ADINA may exceed the surcharge that would induce failure of the structural materials. The system would stop only when failure in the soil occurred since it was modeled with the Mohr coulomb (MC) model. This provided an evaluation of the ultimate capacity of the soil alone since it will limit overall capacity of the wall if the strength of the structural members is increased significantly.

To determine the limiting surcharge pressure for failure of the frame elements, the capacities of the sections were set as the upper limits of results from the model. The maximum bending and shear forces computed at the time steps were compared to the capacity and when one of the design capacities was exceeded the corresponding time step and surcharge was taken as the ultimate capacity. This was carried out for both soil types and three tie-down anchor forces for the 7.62m wall.

4.3.1 Ultimate Capacity of Wall System Based on Soil

Table 15 summarizes the ultimate surcharge capacity that creates failure in the soil based on Mohr-Coulomb criterion. It can be seen that a very large surcharge pressure can be applied if failure of the structural members is ignored. Thus the capacity of the can be

significantly increased if the structural members are strengthened. The SF soil with a smaller K_o, had a greater ultimate capacity since less horizontal pressure is developed from vertical stress. Significant zones of yielding occurred behind the top of the wall and at the toe of the wall as shown in Figure 4.3-1 for the two soil types and three anchor forces. The angle of the failure plane behind the wall corresponds closely with the active failure planes which are oriented at angles of 45 degrees minus half of the friction angle counterclockwise from horizontal. The magnitude of the pressure applied to the top surface in the figures is the combination of the surcharge and the backfill pressure applied during construction which was 31.6 kPa.

Table 15 Ultimate Capacity Based on Soil Failure

Soil Type	Force Per Anchor	Ultimate Surcharge
Units	kN (lb)	kPa (psf)
SF	0	765 (15,980)
	245 (55,000)	763 (15,940)
	445 (110,000)	600 (12,530)
WH	0	406 (8,480)
	245 (55,000)	397 (8,292)
	445 (110,000)	395 (8,250)

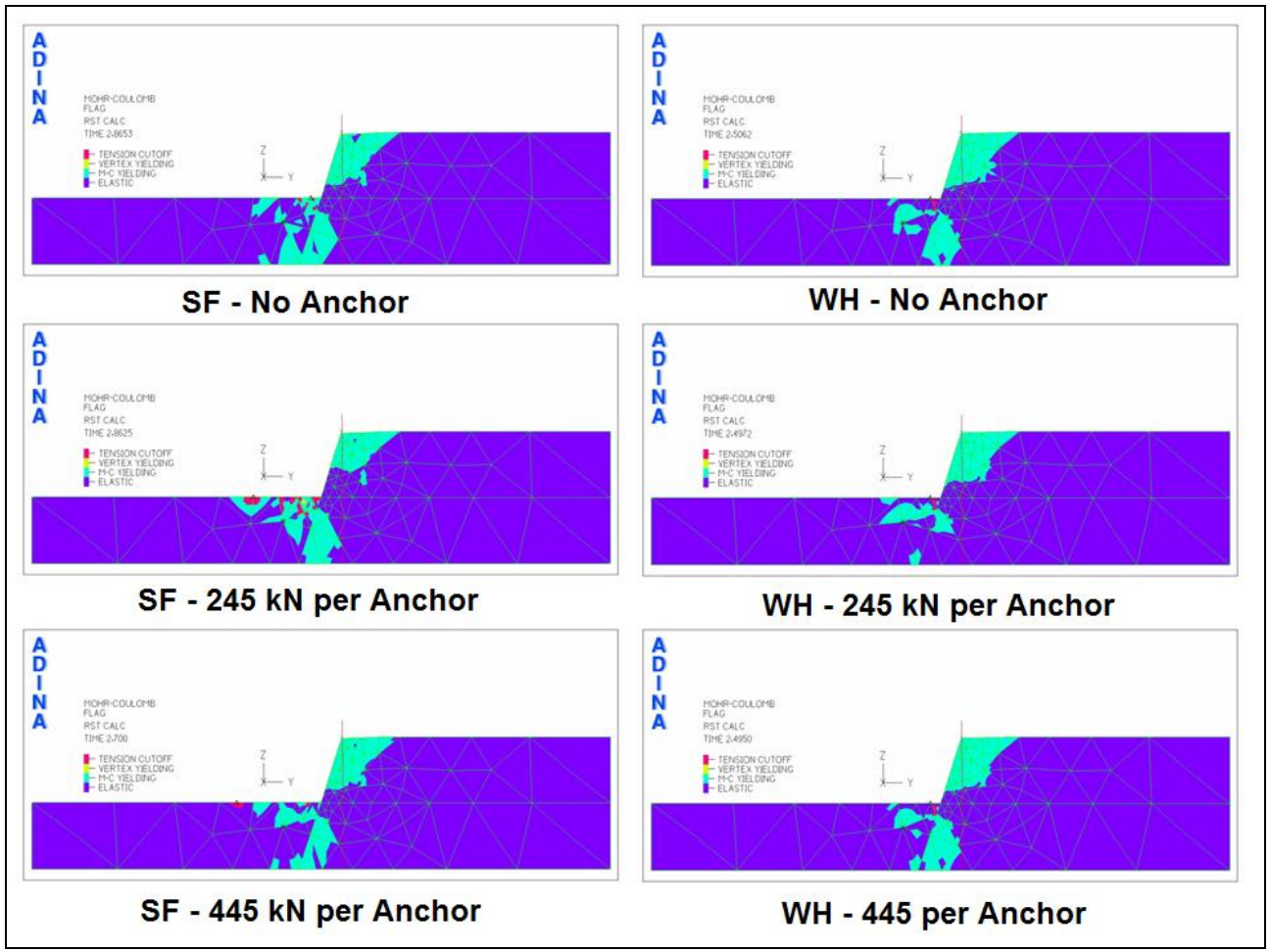

Figure 4.3-1Mohr Coulomb yielding at Ultimate Failure of Soil

4.3.2 Ultimate Capacity of Wall system Based on Structural Members

Table 16 summarizes the determined ultimate capacities as a function of anchor force and soil type. The governing failure mode in most cases was shear failure near the base of the composite batter section. Again, The SF soil had a greater ultimate capacity since it has a smaller K_o. The SF soil had capacity of about 150 kPa (3,133 psf) whereas the WH soil's capacity was 100 kPa (2,090 psf).

4.3.3 Location of Yielding in Structural Members

The bending and shear diagrams for the different anchor force and soil type combinations are shown below in Figures 4.3-2 and 4.3-3. The capacities of the composite sections are

Table 16 Summary of Ultimate Capacity of Pile Framed Retaining Wall

Soil Type	Force Per Anchor	Ultimate Surcharge	Max. (+) Moment	Max. (-) Moment	Max. Shear
Units	kN (lb)	kPa (psf)	kN-m/m (ft-lb/ft)	kN-m/m (ft-lb/ft)	kN/m (lb/ft)
SF	0	120 (2,506)	257 (57,770)	77.7 (17,470)	170 (11,660)
	245 (55,000)	150 (3,133)	269 (60,540)	70.0 (15,730)	174 (11,880)
	445 (110,000)	160 (3,342)	260 (58,420)	77.0 (17,310)	176 (12,030)
WH	0	90 (1,880)	203 (45,620)	38.5 (8,645)	176 (12,030)
	245 (55,000)	100 (2,090)	201 (45092)	40.0 (8,981)	180 (12,330)
	445 (110,000)	100 (2,090)	183 (41140)	39.4 (8,863)	175 (12,000)

plotted along with the diagrams to show where yielding occurs. The maximum negative moment in the batter pile developed in the top half of the wall. The positive moment in the batter pile occurred just above grade. The maximum shear for all cases occurred at grade or the base of the concrete facing. With any increase in surcharge the shear capacity would be exceeded before the moment capacities were reached.

4.3.4 Yielding in the Soil at Ultimate Conditions

Complete failure of the soil was not the limiting factor in the ultimate capacity analysis; however a significant zone of yielding developed under the ultimate surcharge applied to the soil. Figure 4.3-4 illustrates yielding in the soil in terms of the MC failure criterion for the model with SF soils and 245 kN per anchor. Figure 4.3-5 is a plot of the smoothed yield function which illustrates how close elements are to yielding, which occurs when difference between the shear stress of the soil and shear strength of the soil equals zero. This surcharge pressure is equivalent to placing backfilling and an additional 8.6 m of soil along the top surface of the soil behind the wall, thus the wall is very strong with a high factor of safety.

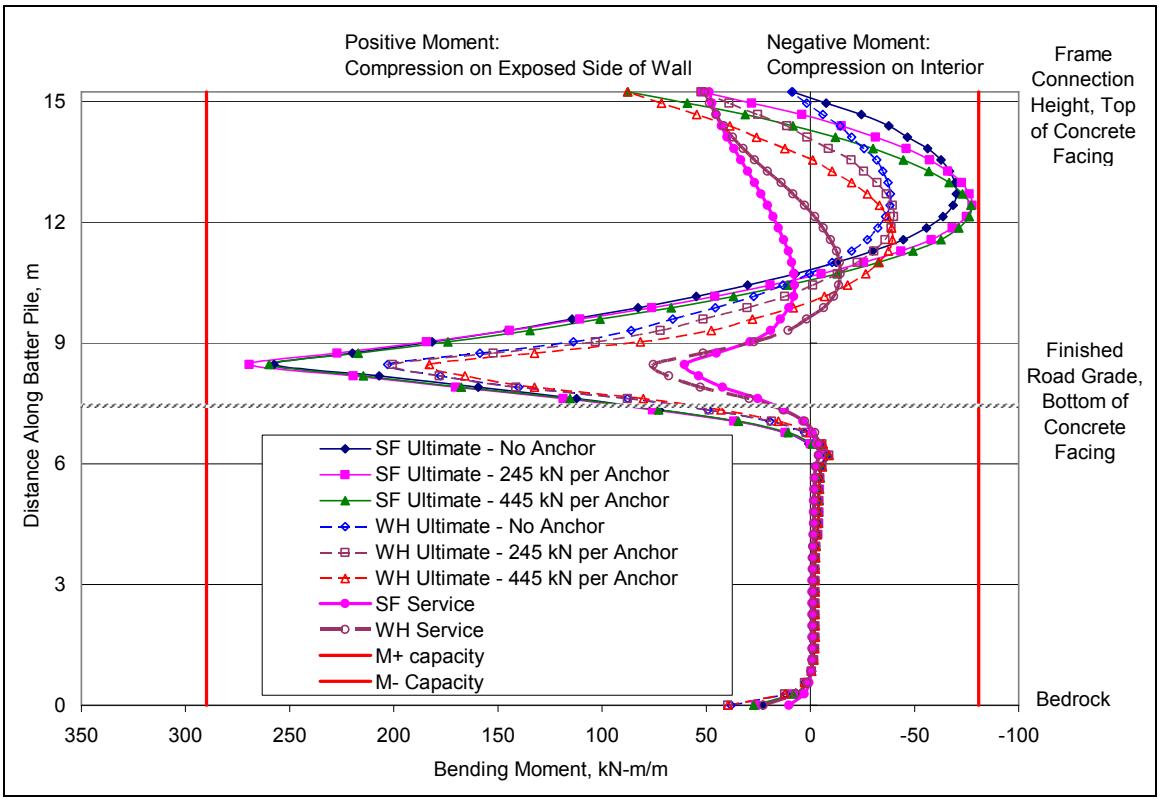

Figure 4.3-2 Moment Diagrams in Batter Pile at Ultimate Conditions

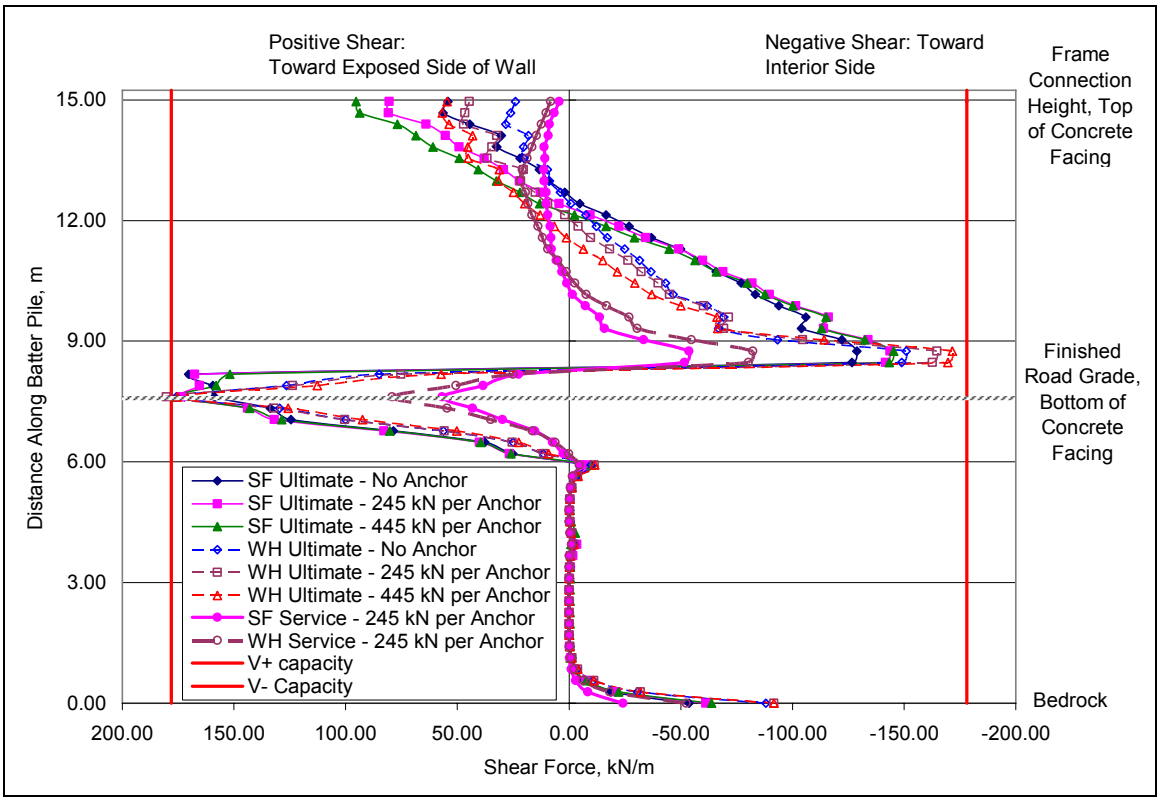

Figure 4.3-3 Shear Diagrams in Batter Pile at Ultimate Conditions

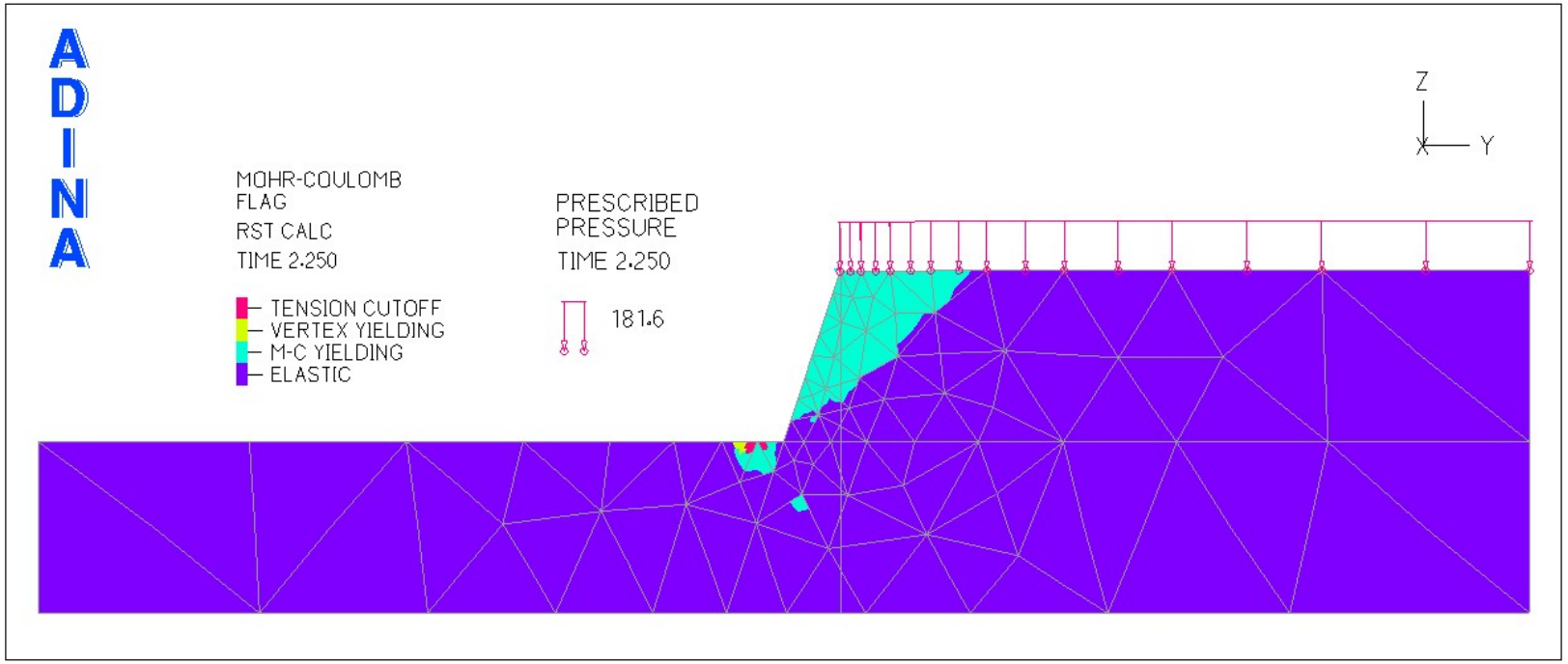

Figure 4.3-4 Mohr-Coulomb Failure at Ultimate Conditions

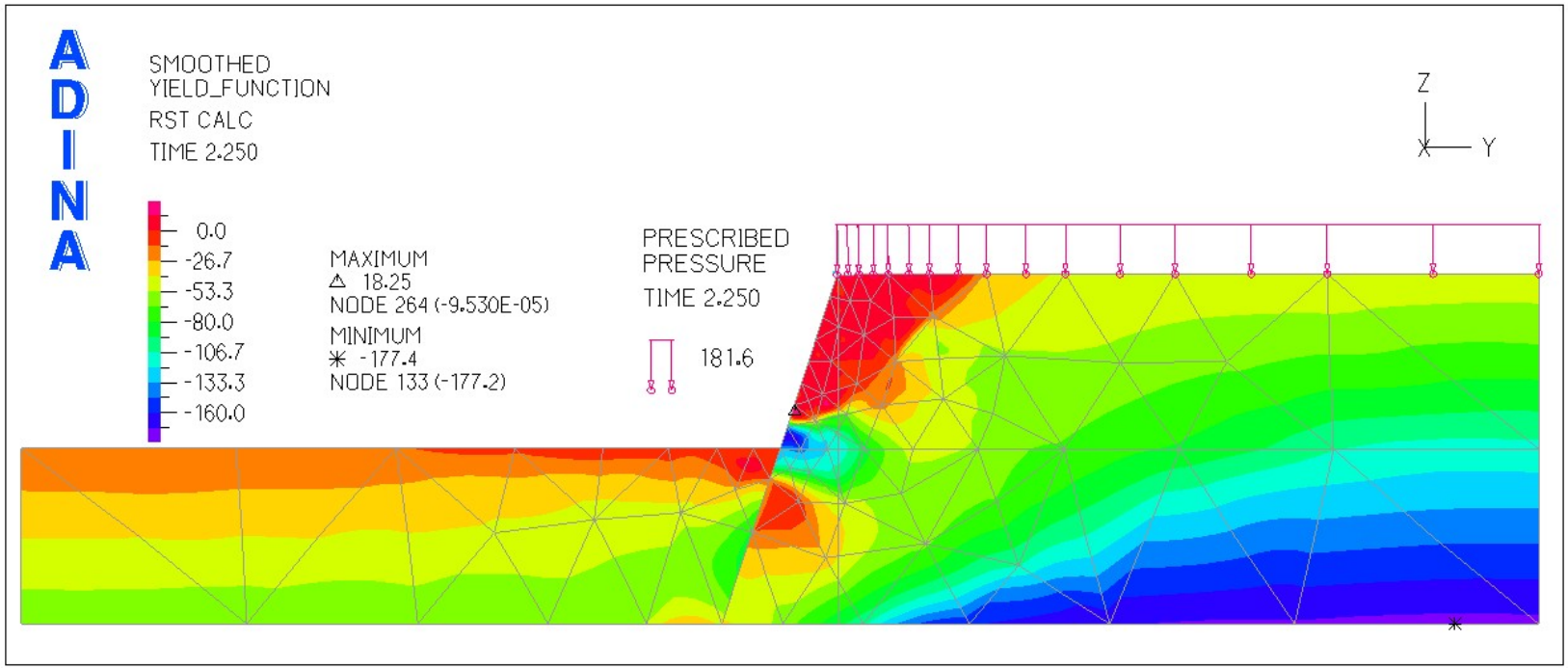

Figure 4.3-5 Smoothed Yield Function Plot at Ultimate Condition

CHAPTER V

CONCLUSIONS AND RECOMMENDATIONS

5.1 Summary

The construction of conventional retaining walls in urban settings is often limited to space constraints. The pile-framed retaining wall designed by TDOT is a novel design that unlike conventional retaining walls does not require wide construction easements because it is constructed from the top down. For the initial design, TDOT relied upon engineering judgment and educated assumptions, resulting in a wall that performs as intended. TDOT plans to use the pile-framed wall system in the future for various soil conditions and wall heights. There has been no previous research on this type of system, so a design approach based on analytical and experimental data is necessary.

The goal of this thesis was to provide an introductory analysis of the pile-framed system and to evaluate the design assumptions. A 2D plane-strain model of the wall system was created with the 900 nodes version of ADINA and analyzed using energy-tolerance convergence criteria. The initial height of the wall analyzed was based on typical sections of the wall, and studies were carried out to determine the optimal model boundary distances. Contact elements were utilized to incorporate the soil-structure interaction effects. The linear elastic material model was used for the steel and concrete

members, whereas the elasto-plastic Mohr Coulomb (MC) model proved necessary for the soil.

The construction sequence of the wall system was simulated with some simplifications for modeling purposes. The geostatic stresses in the soil were developed by applying gravity to the soil prior to any construction stages. The analysis was restarted with the geostatic stresses as initial conditions, and then construction loading and excavation commenced. The removal of soil was simulated with the element death option in ADINA. The results of the model with construction sequencing were validated with a simplified analysis of the pile-frame. The number of nodes used for the model was found sufficient because an increase in nodes did not affect results significantly. The predicted earth pressures behind the concrete face compared well with classical earth pressure methods, verifying the accuracy of the model.

Next, a parametric study was conducted for two soil types to evaluate the behavior of effects of design assumptions, design features, modeling assumptions and material properties for a range of site conditions that may be encountered for future walls. One soil type represented materials with high cohesion and low friction angle such as the soil encountered at the West Hills (WH) site. The second soil represents cohesionless materials with a high friction angle that was encountered at the SmartFix (SF) site. The effects of the parametric study were evaluated in terms of the deflections of wall-system, internal forces in the pile members, and earth pressures along the concrete facing.

Graphs were created to illustrate the relative effects of the various parameters on predicted results.

Finally, the ultimate capacity of the wall design was evaluated for two soil types by applying a surcharge load to the top surface of soil in the model. Failure of the wall was reached when the predicted internal forces exceeded the strength capacity of the piles as determined by standard methods for flexure and shear in steel and concrete. Yielding of the soil in terms of the MC failure criterion occurred in significant zones behind the wall at ultimate conditions.

The conclusions of the study are summarized by the following:

- The predicted deformations and internal forces of the frame in this study reveal what has already been evident by the performance of the first wall built: the wall design is rigid under service loads and performs very well.
- The TDOT assumption of Rankine's active conditions for the estimation of design earth pressures was adequate. However, analysis results suggest that the resultant earth pressure may be as much as 20% higher for low wall heights with the current design anchor force.
- In terms of modeling the pile-frame, assuming pile bases are fixed or pinned makes negligible difference on internal forces in the span of the wall, the displacements, and earth pressures. Decreasing the depth of fixity below the grade reduces the maximum positive moment and the shear in the piles, but

increases the maximum negative value. However, the maximum negative moment is still much less than the pile's capacity. Decreasing the depth of fixity reduced the earth pressures behind the wall and the predicted displacements. Thus, the TDOT assumed fixity predicts lesser internal forces and displacements, and should not be used because it won't provide the most conservative results.

- The effects of the soil types evaluated are based mainly on the Poisson's ratio, ν, of the soil and consequently can be scaled if the soil remains elastic. The earth pressure coefficient of the soil increases with ν; thus the clay type WH soil with larger ν produced great earth pressures, and greater forces in the frame. However, the material is less compressible as ν increases, thus the deformations of the wall model with WH soil are generally less than sandy-silty SF soil.
- As the wall height increases, the lateral movement of the wall away from the soil increases and the top of the wall experiences the greatest displacement. However, for walls over 10m, the top deflections are less than the deflections in the middle of the wall.
- Increases in wall height increase the maximum internal forces in the wall.
- Increases in the force per anchor decreases the displacements of the wall.
- Increases in the force per anchor decreases the maximum moments in the span of the wall but increases the moment at the connection point.
- The benefits of increased anchor loads have a limit, because the anchor loads induce forces and stresses in the piles that, when combined with stresses from the earth pressures, may cause the pile to yield prematurely.

- The deformations of the soil and subsequently the wall decrease with increasing soil stiffness, but differences are less significant when the modulus increases past 72 MPa.
- In general, the soil modulus has only a small effect on the earth pressures, with the low modulus values creating greater earth pressures. Thus, the bending internal forces decrease as the stiffness of the soil increases. Therefore, walls built at sites with loose soils should be designed more conservatively.
- Increasing rigidity of the concrete composite section does not result in significant reductions in wall displacement or earth pressures. This suggests that the thickness of the concrete facing does not contribute much to the overall stiffness of the wall.
- When modeling the soil-wall interface, assuming frictionless contact will result in the largest predicted wall displacements, and the inclusion of friction does not impact the predicted earth pressures.
- For the cohesionless SF soil, the ultimate surcharge capacity was approximately 150 kPa (3,133 psf), whereas for the cohesive, WH soil, the capacity was 100 kPa (2,090 psf).
- In general the pile-frame system will fail in shear rupture of the concrete composite section at ultimate conditions.
- The failure planes of the soil behind the wall are oriented along active failure planes and extend the entire depth behind the concrete facing.

5.2 Recommendations

5.2.1 Design Forces

The results of the parametric studies have been used to propose design envelopes of the maximum internal forces as a function of wall height for use by engineers. The plots are developed by considering several anchor forces, the two soil types and a range of soil stiffness representing a wide range of soil properties. The case with no anchor produced the largest forces in the wall; however, the anchors are necessary, so the maximum moments from the initial anchor design force were adopted. The lowest soil stiffness values studied significantly increased maximum positive moments and shear forces compared to the median stiffness value of 72 MPa, at a wall height of 7.62 m. Therefore, the same amount of increase was applied to the forces predicted at other wall heights for the models with 245 kN per anchor. At a wall height of 4.57 m, the WH soil produced the greatest forces in the wall so the greatest values were modified to include the increase due to weak soil. At the tallest wall height of 10.67 m, the SF soil produced the largest positive moment and shear forces, whereas the WH soil produced the largest negative moment.

The design envelopes were created using the largest internal force values at the different heights with E_{sl}=72 MPa, then amplifying those values for the effect of loose soils. For very stiff soils, the design forces were less than forces for the medium stiff soil, so only one envelope was created for soils that are stiff compared to very loose soils. The design

envelope for maximum positive moment, negative moment, and shear are provided in Figures 5.2-1 through Figure 5.2-3. The shear force envelope for loose soils exceeds the shear capacity of the batter pile, thus the wall design must be modified or ground improvement methods must be performed when site conditions exhibit very loose soils.

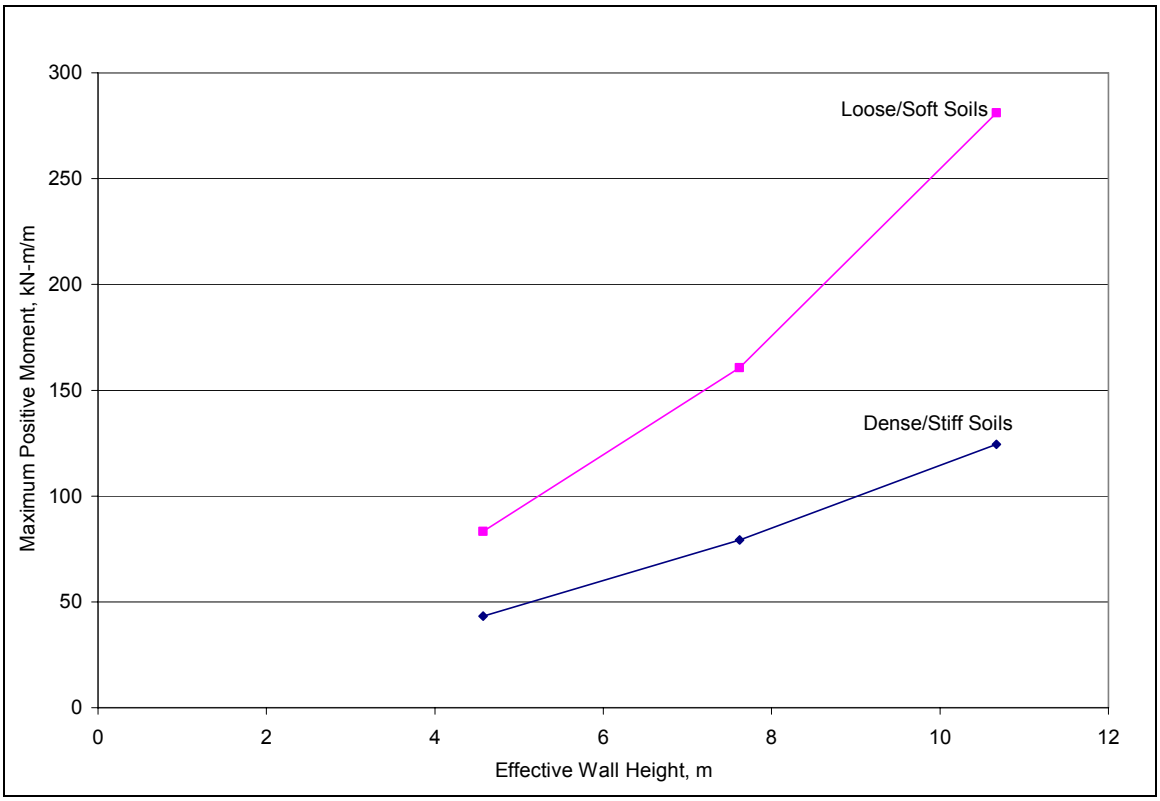

Figure 5.2-1 Design Envelope for Maximum Positive Moment

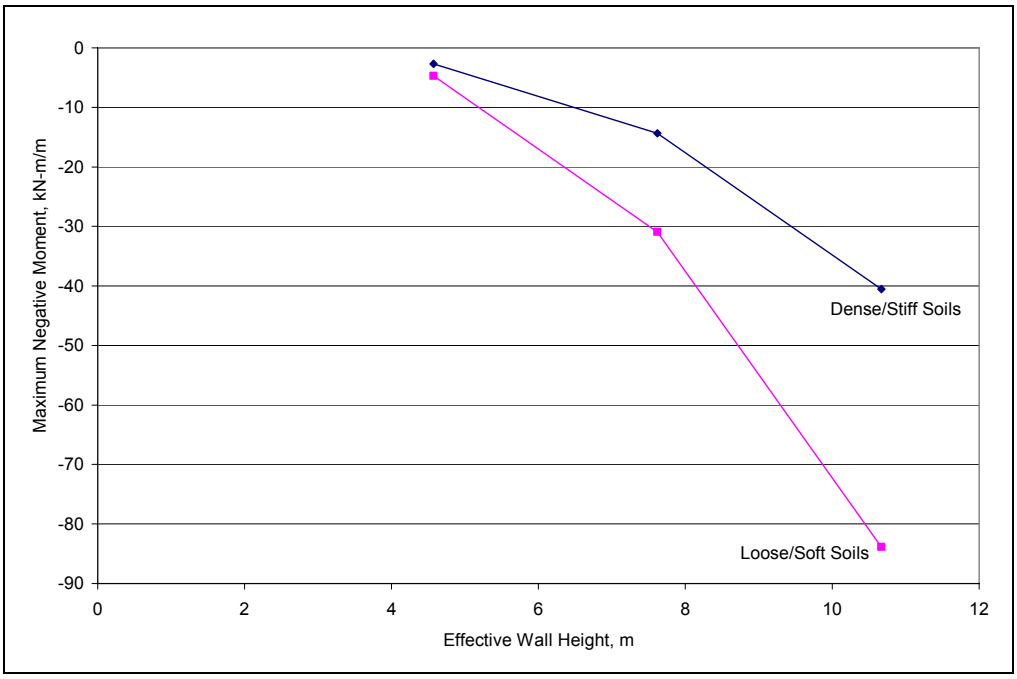

Figure 5.2-2 Design Envelope for Maximum Negative Moment

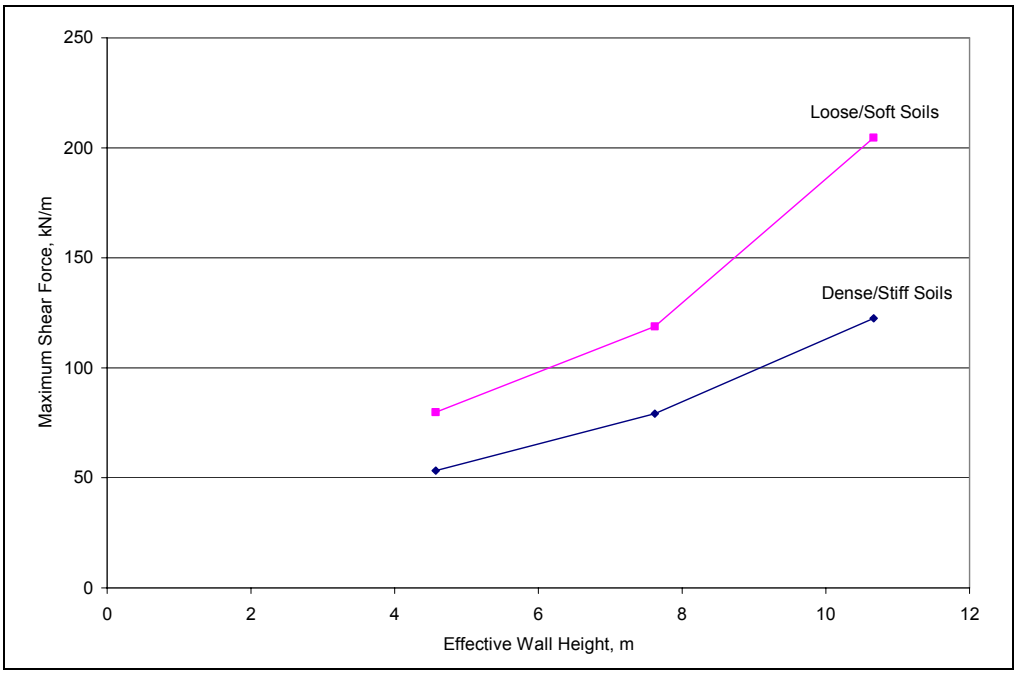

Figure 5.2-3 Design Envelope for Maximum Shear

5.2.2 System Modifications

The most difficult and costly feature of the pile-framed system construction was the tie-down anchors. The holes for the anchors had to be predrilled, cased and grouted, the whalers prepared, and finally the anchors load tested. The cost of the steel piles was most dependent on the pile-driving process that requires special equipment and time. The cost of the steel material is related to the weight per foot of the pile, which was very small relative to the construction cost per foot of piles driven. Therefore, using slightly larger materials will not significantly increase the cost per foot of the wall. Based on the results of the finite element analysis, the system can be modified by increasing the size of the pile members to reduce the number of anchors required by half to save construction costs and time.

Results show that the force of the tie-down anchor induces stresses in the batter pile, which become detrimental to the system capacity at large anchor forces; thus, there is a limit on the benefits of increased anchor loads. For the system analyzed, the design force per anchor was close to this upper limit, and although it may not be the optimal anchor force, the pile frame itself is sufficiently rigid to limit deflection and have a large ultimate capacity. Instead of using two anchors of 245 kN (55 kips) each, the system can be modified to have only one anchor in the center of the span between frames with a force larger than 245 kN and within a range of 490 kN (110 kips).

Change of the location along the whaler and magnitude of force in the anchor will induce different bending stresses in the whaler, which may cause failure in the whaler itself. The yielding and plastic capacity of the whaler was used to determine allowable loads. It was determined that an HP12x63 section used for the whaler would optimize the single load that can be applied without failing the whaler. Assuming the whalers are fixed at each end and there is no additional moment capacity from moment distribution to the frames, an anchor force of 333 kN (75 kips) can be applied without yielding and a force of 511 kN (115 kips) can be applied before plastic failure of the whaler. 333 kN is less than the total force of two anchors that was analyzed in the analysis; however, the size of the batter pile must be increased to make the modification possible. The flanges of the whaler and the batter piles are welded together so the two sections must have approximately the same depth; therefore, a HP 12x53 section, having the same depth, will have flanges that line up with the HP 12x63 section. The increased rigidity of the batter pile will counteract the decrease in wall stiffness from any reduction in anchor force.

5.2.3 Need for Further Research

To improve and extend the numerical model used in this thesis, a number of modifications could be made. The most obvious yet difficult to make would be to create a three-dimensional model of the system. The model was limited to 900-nodes, and a sufficient model would require much more than 900 nodes. It is possible, but much effort would be needed to mesh the complex geometries and interfaces of the 3-D system.

Secondly, this research assumed that the structural members would behave in the linear elastic range for service loads. As a result, nonlinear models for the steel and concrete were not employed in this model to evaluate wall behavior at ultimate conditions. An analysis incorporating the nonlinear behavior of the steel piles as well as the concrete facing can be included in future analyses to better understand the possible failure modes of the wall system.

The Mohr-Coulomb elasto-plastic model for soil was used for this thesis because of its wide acceptance and the fact that it requires only a few input parameters. There are several other models for soil available in ADINA, which require more inputs to define the soil. With the correct information about a soil from lab testing, these other soil models can be utilized in future models to evaluate the importance of material model selection on soil and wall behavior.

For simplicity the soil in the model was analyzed in terms of effective stress parameters, excluding the effect of pore pressures from this thesis. Groundwater may be encountered at wall sites in the future and conducting an analysis based on undrained strength parameters is necessary. With the correct soil parameters from lab testing, an analysis with pore pressures could be done with ADINA in the future.

In this thesis, contact between the soil and vertical pile was neglected because soil forces on the contact face were of interest. In future, models of the wall system should include contact on either side of the vertical pile to evaluate its effect on wall behavior. This may produce a more realistic model that includes all soil-structure interaction effects.

The construction sequence that was followed to build the first wall was simulated in this study. TDOT provided two options for construction, so the effects of the two construction sequence could be compared if both sequences are simulated. In addition, alternative construction methods could be evaluated through further modeling of construction sequence options.

Further study of the commands within ADINA is needed to develop a more efficient way to develop geostatic stresses in the soil without deforming the soil elements. Much time was given to finding a simple method to analyze the wall with initial stress, but one was not found. Possibly, with ADINA or with a different FE program, this issue can be resolved with further research.

Finally, the results of this thesis have been used to provide possible modifications to the pile-framed wall design. Any modification accepted or put forth by TDOT can be incorporated into ADINA as a check of the updated design procedure against the initial design analyzed in this thesis.

LIST OF REFERENCES

LIST OF REFERENCES

ACI Committee 318. Building Code Requirements for Structural Concrete (ACI 318-05). American Concrete Institute, Farmington Hills, MI; 2005.

ADINA R&D Inc. (2006)., *Theory and Modeling Guide, Report ARD 06-7*, vol. I, Watertown, Massachusetts

AISC. (2006). Steel Construction Manual, American Institute of Steel Construction; 13th Edition, Chicago, Illinois

Alawneh, A. S. (2005). Modeling Load-Displacement Response of Driven Piles in Cohesionless Soils Under Tensile Loads, Computers and Geotechnics, Volume 32, 578–586, Elsevier

Amde, A. M., Chini, S. A., Mafi, M. (1997). Model study of H-piles Subjected to Combined Loading, Geotechnical and Geological Engineering, Volume 15, Number 4, 343-355, Springer, Netherlands

Bathe. K.J. (1996). *Finite Element Procedures*, Prentice Hall, Englewood Cliffs, NJ.

Bentler J. G., Labuz, J. F. (2006). Performance of a Cantilever Retaining Wall, Journal of Geotechnical and Geoenvironmental Engineering, Volume 132, Issue 8, 1062-1070, ASCE

Borja, R.I., Lee, S.R., Seed, R. B. (1989). Numerical Simulation of Excavation in Elastoplastic Soils, International Journal for Numerical and Analytical Methods in Geomechanics, Volume 13, 231-249, John Wiley & Sons, Ltd.

Bowles, J.E., (1995). *Foundation Analysis and Design*, McGraw-Hill Science, New York, New York

CGS (1992). *Canadian Foundation Engineering Manual, Third Edition*., Canadian Geotechnical Society, BiTech, Vancouver, British Columbia

Coduto, D.P. (2001). *Foundation Design: Principles and Practices*, Prentice Hall, Englewood Cliffs, New Jersey

Dysli, M. (1983). Use of ADINA in Soil Mechanics With Case Studies for Excavations, Computers and Structures, Vol. 17, No. 5-6, 635-642, Pergamon Press Ltd.

Franzius, J. N., Potts, D. M. (2005). Influence of Mesh Geometry on Three-Dimensional Finite-Element Analysis of Tunnel Excavation. International Journal of Geomechanics, Vol. 5, Issue 3, 256-266, ASCE

Hegedus, E., Khosla, V. (1984). Pullout Resistance of H piles. Journal of Geotechnical Engineering, Vol. 110, No. 9, 1274-1290, ASCE

Hunt, C.E., Pestana, J.M., Bray, J.D., Riemer, M. (2002). Effect of Pile Driving on Static and Dynamic Properties of Soft Clay. Journal of Geotechnical and Geoenvironmental Engineering, Volume 128, Issue 1, 13-24, ASCE

Goh, A. T., (1993). Behavior of Cantilever Retaining Walls. Journal of Geotechnical. Engineering. Vol. 119, No. 11, 1751-1769, November, 1993

Lambe, W. W., Whitman, R. (1968). *Soil Mechanics*, John Wiley and Sons, New York, New York

Macnab, A. (2002). *Earth Retention Systems,* Mcgraw-Hill, New York, New York

McCormac. J.C. (2003). *Structural Steel Design: LRFD Method, Third Edition*, Prentice-Hall, Englewood Cliffs, New Jersey

Pate, H., Haddad, S. (2007). Piling Framed Tie Down Concrete Retaining Wall, Deep Foundations Institute, Spring 2007, Hawthorne, New Jersey

Potts, D.M., Zdravkovic L. (1999). *Finite Element Analysis in Geotechnical Engineering Theory*, Thomas Telford, London

Rajashree, S. S., Sitharam, T. G. (2001). Nonlinear Finite-Element Modeling of Batter Piles under Lateral Load. Journal of Geotechnical and Geoenvironmental Engineering, Volume 127, Issue 7, 604-612, ASCE

Simmonds, S. H., Playdon D.K. (1988). Modeling Soil-Structure Interaction Construction, Computers & Structures, Vol. 28, No. 2. 283-288, Pergamon Journals Ltd

Skirrow, R.K., Tenove, R.S., Sengupta, S. (1991). Impact of Voids Created During Driving of Piles. Proceedings of the 44th Canadian Geotechnical Conference, September 29 – October 2, Volume 44 Issue 2, Paper No. 87, 1-5

Sumino, K., Noguchi, H., Hyodo, K., Sekimoto, H. (1985). Application of ADINA in Analysis of a Soil Structure, Computers & Structures. Vol. 21, No. l/2, 51-61, Pergamon/Elsevier

Wilbur Smith and Associates, (2002). Noise Barrier Wall No. 1, I-40/I-75 West Hills Widening Project, Knoxville, TN. WSA Project No. 359601

Wilbur Smith and Associates, (2006). Phase II of I-40 Broadway Widening, Knoxville, TN. WSA Project No. 367102

VITA

Eli Lawrence Branch IV was born September 9, 1983, to Eli Branch III and Barbara Branch in Oakland, California. His family moved to Oak Park, Illinois, in 1994 where he graduated from Oak Park River Forest High School in 2001. In 2006 he received his bachelor degree in Civil Engineering at Iowa State University, in Ames, Iowa. In August 2006 he then pursued his Master of Science degree in Civil Engineering at the University Of Tennessee, Knoxville. Upon graduation, Eli will pursue his career at Mueser Rutledge Consulting Engineers in New York, New York.